Cost effective, automated portable high performance liquid chromatograph for on-site analysis of organic pollutants in river and ground water systems.

Patrick Roche, BEng

Thesis submitted in fulfilment of the requirements for the degree of

MASTER OF SCIENCE (MSc)

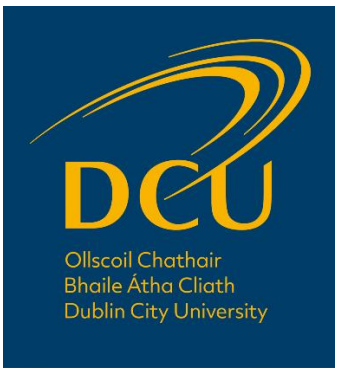

DUBLIN CITY UNIVERSITY

October 2023

Supervisor: Dr David Collins

School of Biotechnology

Declaration

I hereby certify that this material, which I now submit for assessment on the programme of study leading to the award of Master of Science is entirely my own work, and that I have exercised reasonable care to ensure that the work is original, and does not to the best of my knowledge breach any law of copyright, and has not been taken from the work of others save and to the extent that such work has been cited and acknowledged within the text of my work.

Signed: Patrick Roche

Patrick Roche

(Candidate) ID No.: 20215054

Date: 30/08/23

Acknowledgements

Firstly, I wish to thank T.E. Laboratories Ltd. for providing the opportunity to carry out this MSc as well as their flexibility and support. I also acknowledge the Employment-Based Scholarship received from the Irish Research Council for which I am grateful. I also wish to acknowledge the help and support from my friends and colleagues in T.E. Laboratories Ltd. who always kept me pointing in the right direction.

I am grateful for the immeasurable guidance and support given by both my academic supervisor Dr. David Collins and my employment mentor Dr. Eoin Murray. David's guidance has expanded my knowledge greatly, not just in engineering or chromatography, but in life itself. I am appreciative of Eoin's encouragement, insight and knowledge which has guided me throughout.

The journey taken from start to finish of this research has seen existing friendships grow, lifelong friends gained and a new addition to the family. To Samantha, your support throughout the years has made me who I am today, and I am immensely grateful for everything you have done and continue do.

Table of contents

Abbreviations

ADC	Analogue to digital converter
ASTM	American Society for Testing and Materials
AU	Absorbance unit
CAD	Computer aided design
CSV	Comma separated value
DC	Direct current
DI	Deionised
EOP	Electroosmotic Pump
FEA	Finite Element Analysis
FDM	Fused deposition modelling
FPLC	Fast protein liquid chromatography
HMI	Human machine interface
HPLC	High performance liquid chromatography
LC	Liquid chromatography
LED	Light emitting diode
LOD	Limit of detection
LOQ	Limit of quantitation
MS	Mass spectrometry
PAHs	Polycyclic aromatic hydrocarbons
PEEK	Poly(ether ether ketone)
PFAS	Per- and polyfluoroalkyl substances
PID	Proportional integral derivative
PTFE	Polytetrafluoroethylene
RPLC	Reverse phase liquid chromatography
RSD	Relative standard deviation
UHMW-PE	Ultra high molecular weight polyethylene
UV	Ultraviolet

List of tables

List of figures

Abstract

Patrick Roche

Cost effective, automated portable high performance liquid chromatograph for on-site analysis of organic pollutants in river and ground water systems.

There is a growing requirement for the real-time monitoring of our waterways in order to protect water quality, and the environment as a whole. The past decade has seen a rapid increase in research into portable liquid chromatography systems for the detection of organic compounds which can cause harm to the planet's water systems. Real-time field analysis provides major advantages over costly and time-consuming grab sampling. Thus, there is a requirement for portable, rapid analysis techniques to be employed in order to detect priority contaminants which complement existing laboratory methods in order to minimise workflows and reduce costs. In order to achieve rapid, in-situ analysis of labile organic analytes, standard laboratory based analytical techniques must be brought out to the field. However, with most research based systems requiring specialist knowledge to develop analytical methods, a robust portable system capable of performing laboratory methods must be developed.

By focusing on the development of novel pump technology, a portable High Performance Liquid Chromatograph has been realised. The pump has been characterised through the assessment of power consumption, flow rate accuracy, drift and precision, and the monitoring of pressure pulsations. An assessment of its capability has been conducted with over 120 repeated separations of a column performance check standard. The development of a UVC photometric detector along with an automated injector is presented along with the integration of the developed pump to create the portable HPLC system. Along with the assessment of the custom detector, the developed portable system has been compared to a laboratory based HPLC through the separation of a paraben mixture. The limitations of both the pump and portable HPLC system are discussed and potential areas for improvement are presented.

Chapter 1 Introduction

While much work has been done to regulate the quality of our water, European legislation relating to wastewater treatment, surface and groundwater quality is not enough to prevent the growing issues around the health of our water systems. For the past two decades, the European Water Framework Directive has played an important role in placing limits on harmful organic and inorganic pollutants. However, the monitoring of such pollutants is only carried out at the minimum intervals as set out by the directive [1]. With over 66% of Ireland's surface and groundwater sites monitored under the programme [1], minimising sampling based on seasonal trends [1] and the high associated costs result in unseasonal changes or pollution incidents being potentially missed. Fish kills such as those in Rathdowney Co. Laois [2] and the Ballinagh river in Co. Cavan [3] along with a swimming ban at Dublin beaches due to wastewater treatment plant overflow [4] highlight the need for real time, in-situ monitoring. However, issues such as low technological readiness levels, the expense of rolling out new technologies and maintaining these systems are potential barriers for uptake in portable analytical systems. Therefore, it is important to address these issues through the research and development of novel technologies, to bring robust portable analytical instrumentation into the field.

One such technology which has been improved upon and which has been further developed through this research is a compact, lightweight high-pressure pump. By developing a robust apparatus to deliver mobile phase at high pressures to a separation column, the pump's capabilities have been demonstrated and compared to a traditional laboratory-based benchtop system. Additional work has been conducted to develop a simple portable system which utilises this pump to demonstrate isocratic HPLC separation methods in a portable unit. By doing so, the aim is to create a portable analytical platform with a performance envelope similar (or better) than those of benchtop instruments used in the laboratory testing environment.

1.1 Organic pollutants and their environmental impact

Recent reports regarding climate change have delivered stark warnings about the impact of the human race's past and current behaviours on the overall health of our planet. However, while most of the emphasis in media is fixated on temperature increases and the impact of severe weather events, other serious issues such as levels of micro plastics, forever chemicals, domestic and industrial wastewater discharge are of major concern also. Therefore, easily deployable, and robust sensor systems should be made available for high spatial and temporal resolution measurements of environmental parameters to ensure we

can gather as much data about the world around us. One such area of concern is around the introduction of priority pollutants into the environment.

Article 16(2) of the European water framework directive states that the list of priority substances "*which present a significant risk to or via the aquatic environment*" will be targeted for reduction and phasing out of discharge into the environment. Presently there are 45 priority substances identified, with 21 identified as priority hazardous substances [5]. The water framework directive describes hazardous substances as those that are toxic and liable to bioaccumulate. A recent publication has theorised that our ability to monitor the release of chemicals into the environment cannot keep pace with environmental release [6] and that the level of PFAS in rainwater are higher than drinking water limits [7]. These stark findings reinforce the need to develop monitoring technologies. To fully characterise the levels of priority contaminants in our waterways, we need to increase monitoring frequency and reduce the sample to result time associated with grab and lab practices. This time lag can only be significantly reduced by placing analytical technology *in-situ.* While many sensing technologies including colorimetric and electrochemical exist, chromatographic separation techniques present a potential robust and effective way to perform analysis in the field. In this research High Performance Liquid Chromatography (HPLC) is the technique of choice.

1.2 Liquid chromatography

According to the Oxford English Dictionary chromatography is *"a process of separating and purifying the substances dissolved in a mixed solution by slow passage through a tube or over a surface of adsorbing material, making use of differences of partition, adsorption, ion-exchange, etc."* An article from Nature published in 1951 credits Friedrich Goppelsroeder with the real start of chromatographic analysis through his work on analysing petroleum products and plant pigments on strips of paper and textile materials [8]. While Mikhail Tsvet is credited with the invention of adsorption chromatography, Lester Reed is credited with the first mention of separating compounds using a porous media packed into a tube by allowing a solution to soak downwards through the tube, 13 years before Mikhail Tsvet. [8][9]. Work presented in 1903 by Tsvet described the filtration of leaf extract with ligroin through a tube filled with inulin powder, which details the formation of bright green and yellow rings [10]. In his work, he describes how the rings widened and moved down the column with subsequent washings. When Tsvet published his work in 1906, he described the column with rings as a chromatogram [10]. However, it was over two decades later before Tsvet's work was investigated further.

Between the 1930s and 1940s most separations were conducted using similar techniques to Tsvet with apparatus consisting of 150 - 200 mm glass tubes of 10-30 mm diameter packed with adsorbent [11]. During these early years of column chromatography, further innovations such as the use of fluorescence to see colourless substances on the column was utilised and the continued flushing of columns with solvent to remove the separate compounds was realised [11]. Figure 1.1 describes this chromatographic separation technique.

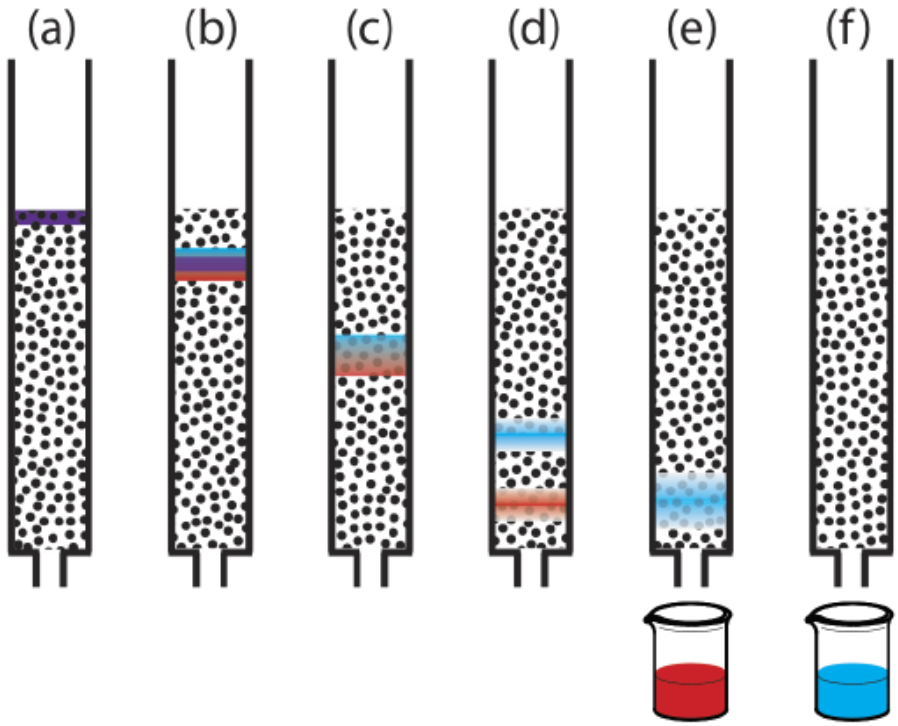

Figure 1.1 - Chromatographic separation of a two component sample in a hydrophobic resin-packed glass column [12].

A sample solution is added to the top of the column. When a solvent is introduced into the top of the column, the sample begins to separate into individual components as it moves downwards through the adsorbent or stationary phase. The speed at which the individual components move downwards is dependent on how they interact with the stationary phase. This process is known as adsorption and desorption which affects the migration rate of each compound as it moves through the adsorbent. A stronger affinity to the packing material in the column means the compound will take longer to reach the outlet. A stronger affinity to the solvent used to wash the column will result in the compound moving quickly down the column.

1.3 High performance liquid chromatography

High performance liquid chromatography (HPLC) can trace its roots back as far as 1941 when it was predicted by Martin and Synge, that small particles and high column pressures would lead to more efficient separations [13]. It was over two decades before this prediction came to reality as reported by Horvath *et al* in 1967 when describing a fast method for separating non-volatile organic compounds using a high-pressure liquid chromatographic system coupled with ultraviolet (UV) detection [14]. Through the following decades, advances in stationary phase development, detection technologies and the rise of computing power, transformed liquid chromatography into a powerful analysis technique, used in laboratories across the world. Today, HPLC is described as a gold standard of analytical techniques [13]. The advantages of only requiring small sample sizes, repeatability of separations, coupled with the ability to analyse any sample that can be dissolved in a liquid have led to the mass adoption of the technology. Modern HPLC systems such as shown in figure 1.2 are often modular with most basic systems offering a solvent rack, a pump, a heated column compartment, sample injection module and a detector unit.

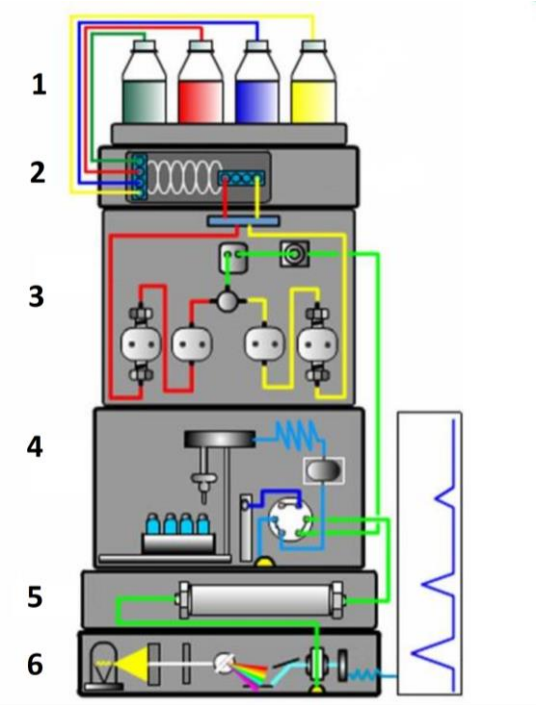

Figure 1.2 - Modular HPLC system

With respect to figure 1.2 above, the solvent rack (1) is simply a secure location to store multiple containers of solvents required for the mobile phase. Some solvent racks offer built-in degassing systems (2) such as the Dionex SRD-3x00 series, while other systems require a separate degasser like the Agilent 1260 Infinity High Performance Degasser. Other pumps like the Waters 1525 Binary HPLC pump have built-in degassers.

In most cases these work as in-line degassers, where the mobile phase flows through a tubular gas-permeable membrane which is housed in a vacuum chamber. The vacuum causes the gas to be drawn out of the liquid as it flows through the membrane and into the pump. Degassers are employed to remove the gas from the mobile phase before it can form bubbles which can cause issues in pumps and detectors.

The pump (3) is one of the most important components within any liquid chromatography system. The pump must continuously deliver mobile phase at a fixed flow rate, regardless of back pressure. The pursuit of pulse free, repeatable flow has led to the development of highly complex electro-mechanical devices which can compensate for mobile phase compressibility, mix multiple solvents to precise ratios and last for many years with the proper maintenance. Section 1.4 below discusses pump technology in more detail.

The role of the autosampler and sample injection unit (4) is to deliver a known volume of sample into a flow of high-pressure mobile phase. In simple terms, an auto sampler contains a storage rack for sample vials and a moving syringe with a needle to draw sample from the vials. The automated system can load the syringe with precise amounts of sample and keep track of each vial from which it has drawn. Coupled with chromatography data software (CDS), sample chain of custody can be easily managed. The syringe can then load loop with precise amounts of sample solution. Once loaded, the injection valve must operate in a quick and smooth manner to minimise interruption to flow or back pressure. Figure 1.3 shows the fluidic pathways of an injection valve. Once the sample loop is filled the valve switches from the load position to the inject position. Mobile phase then flows through the sample loop, pushing the sample out of the loop and onto the separation column.

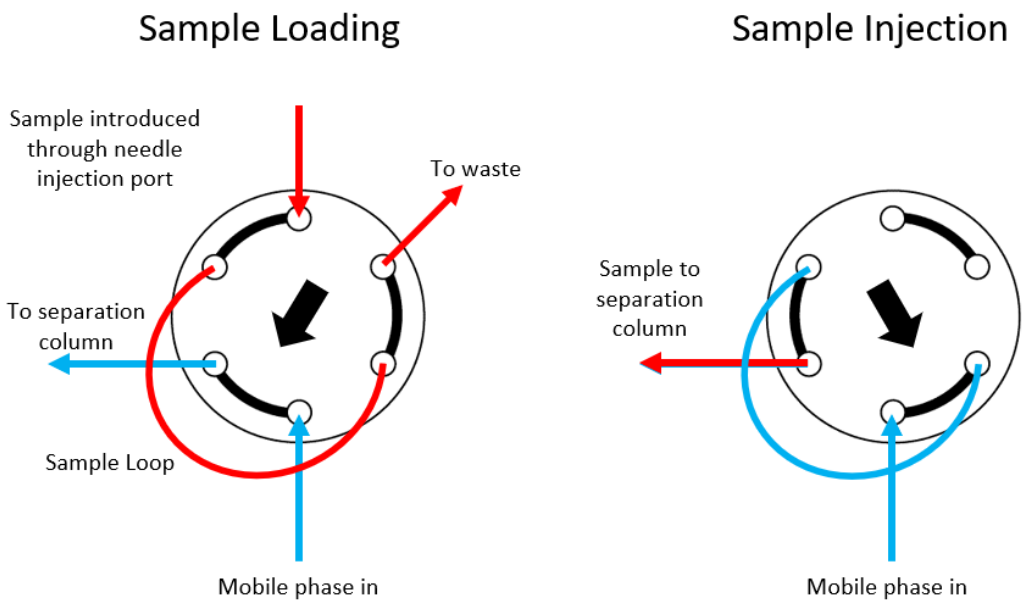

Figure 1.3 - Continuous flow injection valve diagram.

The column compartment (5) plays a critical role in the repeatability of results from the HPLC system and the transfer of methods between different HPLC systems. Changes in temperature can influence retention time, selectivity, and peak shape [15]. A 1°C increase in temperature can reduce the retention time of an analyte by 1-2% in an isocratic separation [16]. The preferred method of column temperature control is with a block heater, where the column wall is directly temperature regulated. This has the advantage over convection through forced air heated column compartments as the temperature can be swiftly increased or decreased to match the temperature of the mobile phase entering the column. Mobile phase pre-heating is also offered as an option, particularly on still air heated compartments because a difference in temperature between the column and mobile phase can cause a temperature gradient [17] within the column itself which has a negative effect on separation parameters.

The detector (6) is the final major component in the fluidic path of a HPLC system. There are many different detection techniques used in HPLC systems from refractive index to charged aerosol detection. Each method of detection relies on detecting a physiochemical property of an analyte. One of the most common techniques is photometric detection in the UV-visible range due to its sensitivity, broad linear range and compatibility with most solvents used in HPLC separations [18]. The Dionex VWD 3400-RS detector which is being used for comparative purposes in this project for example, can operate in a range from 190 to 900 nm. This wide range is achievable due to the use of a deuterium and tungsten lamp.

The wavelength at which a molecule absorbs light depends on the structure of that molecule, as the absorption of UV and visible light is associated with the excitation of electrons [19]. The amount of energy required to make the electrons transition to a higher energy level determines the wavelength absorbed. As the irradiated light interacts with the electrons, the energy is used to transition the electron to a higher level. This results in the light being absorbed. The larger the gap an electron must jump, the higher the energy required. Shorter wavelengths such as those in the UV range have more energy and are therefore easily absorbed. The measurement of the absorbance of light at a specific wavelength is what enables UV-visible detectors to perform quantitative analysis. According to the Beer-Lambert law, a linear relationship exists between the concentration and absorbance of a solution. A calibration curve for an analyte can be generated by measuring the absorbance of known concentrations of that analyte. This is then used to quantify an unknown concentration of the analyte in question. As the analyte passes through the detector, the response is plotted against time which is known as a

chromatogram such as that shown in figure 1.4. Chromatograms are used to both identify analytes based on their retention time and quantify them based on the area under the peak.

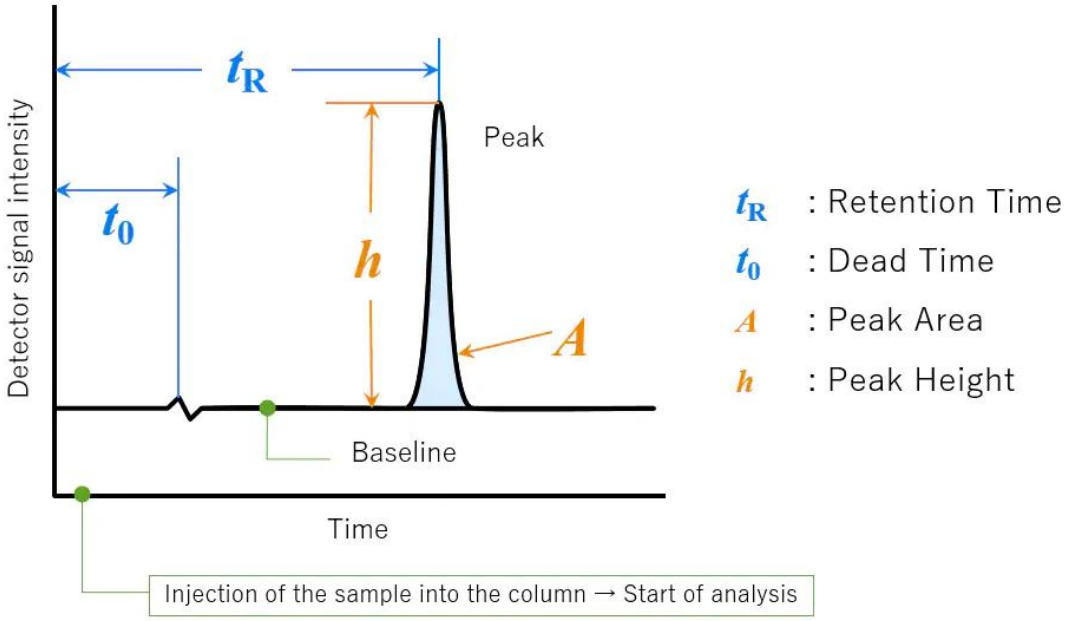

Figure 1.4 - Chromatogram and important features [20].

The aim of any HPLC method is to achieve the ideal resolution in the shortest time possible. That is, good separation between analytes in the sample while ensuring the most retained analyte elutes as quickly as possible. Chromatographic resolution is represented by the following:

$$Resolution = \frac{t_{R2} - t_{R1}}{(w_{B1} + w_{B2}) \times 0.5} \tag{1.1}$$

In equation 1.1, t_{R1} and t_{R2} are the retention times of two closely eluting peaks, while w_{B1} and w_{B2} represent their width at the baseline. A resolution value of 1.5 or greater enables two peaks to be accurately measured. Resolution is dependent on three key parameters, retention factor, selectivity, and efficiency.

As seen in figure 1.4, the peaks that are retained are approximately gaussian. The dead time t_0 is the amount of time it takes non retained compounds to reach the detector after injection. These compounds have no interaction with the stationary phase inside the separation column and move through the column at the same rate as the mobile phase. The dead time is useful for troubleshooting issues with the HPLC system and for the calculation of retention factors and system void volume (volume from injector to detector).

The retention time t_R is used as a qualitative aspect of the chromatogram. It is the amount of time an analyte spends in the column, interacting with both the mobile and stationary phases. Under ideal chromatographic conditions, the retention time of an analyte should be the same across different HPLC systems using the same separation method conditions. The retention factor is the measurement of the amount of time the analyte spends interacting with the stationary phase of the column. To calculate the retention factor (k) of an analyte, equation 1.2 with respect to figure 1.4 is used:

$$k = \frac{t_R - t_0}{t_0} \tag{1.2}$$

A high retention factor indicates that the analyte has spent a considerable amount of time interacting with the stationary phase. A retention factor between 1 and 5 is ideal for separations of a few analytes. Mixtures with larger amounts of analytes, a retention factor of between 1 and 10 is sufficient. Under ideal chromatographic conditions, the retention factor of an analyte should be the same across different HPLC systems using the same separation method conditions. The retention factor is independent of small flow rate changes and column dimensions.

Selectivity (α) is simply the ratio between the retention factors of two peaks. Its value must always be greater than 1. If the selectivity factor is equal to 1, then the peaks are coeluting and are not separated. The higher the selectivity factor, the stronger the separating power of the method used.

Finally, column efficiency (N) is a measurement of the diffusion of an analyte band as it passes through the separation column. A separation column can be separated into small sections known as theoretical plates. The higher the number of plates, the more separating power the column has.

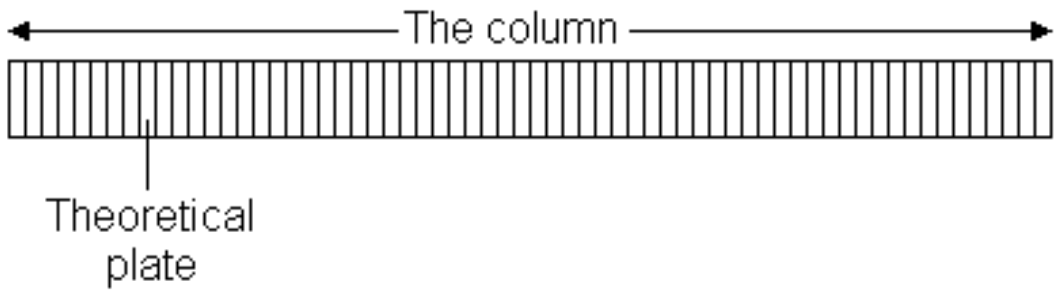

Figure 1.5 - Separation column efficiency represented by the division of the column into theoretical plates.

As mentioned previously, chromatographic resolution is dependent upon retention factor, selectivity, and efficiency. Alterations to any of these parameters will affect the resolution. Table 1.1 summarises how each of these parameters can be altered to improve resolution.

Table 1.1 - Modification of chromatographic parameters to optimise resolution.

Parameter	***Modification***
Retention Factor	Solvent strength - % Organic modifier
Selectivity	Mobile phase pH Temperature Chemical composition of mobile phase (ACN vs MeOH *etc*.) Stationary phase chemistry
Efficiency	Separation column - Stationary phase Injection volume Flow rate

The separation mode used in a HPLC system depends on the type of compounds to be analysed. Table 1.2 summarises some common modes of chromatography and the compounds suitable for separation. The mode of chromatography is defined by the mechanism of interaction between the analyte and the stationary phase [21].

Table 1.2 - Chromatography modes and suitable compounds for analysis

Mode	***Compound***
Reverse Phase	Neutrals, weak acids, weak bases
Ion Pair	Ionics, Acids, Bases
Normal Phase	Compounds not soluble in water
Ion Exchange	Ionics, Inorganic ions
Size exclusion	Compounds with high molecular weight

This research has utilised the reverse phase mode of chromatography. Reverse phase liquid chromatography (RPLC) is the most widely used mode of separation. RPLC can be used in many industries where there are strict requirements for quality control and regulatory bodies. Areas such as environmental monitoring, food production, clinical trials, pharmaceutical quality control and manufacture are some of the applications that rely on RPLC [22]. Reverse phase chromatography can be described as combining a non-polar stationary phase with a polar mobile phase.

1.4 Liquid chromatography pumping technologies

As column particle sizes decreased in the pursuit of increased separation speed and efficiency, pump development had to keep up with the increasing back pressures. Modern HPLC pumps are complex pieces of equipment which are designed to deliver the user's requirements under all conditions. Because of this, they have evolved to become precision instruments designed to overcome high back pressures and deliver precise compositions of mobile phase at stable flow rates. In more simple terms, the pump is required to deliver a constant, reproducible supply of mobile phase to the column [23].

In the early days of liquid chromatography, analytical systems employed single piston pumps to deliver the mobile phase. These early pumps could deliver at pressures up to 35 bar [24]. The relatively simple mechanical setup as seen in figure 1.6(a) below, enabled low-cost compact designs. These pumps offered the advantage of continuous flow over their syringe pump counterparts in use at the time, but at the cost of pulsed flow. Due to the single piston design, during the piston aspirate stroke, no mobile phase would be delivered to the column. The use of pulse dampeners helped to reduce the pressure pulsations, however the large internal volume of these dampeners caused issues for gradient elution.

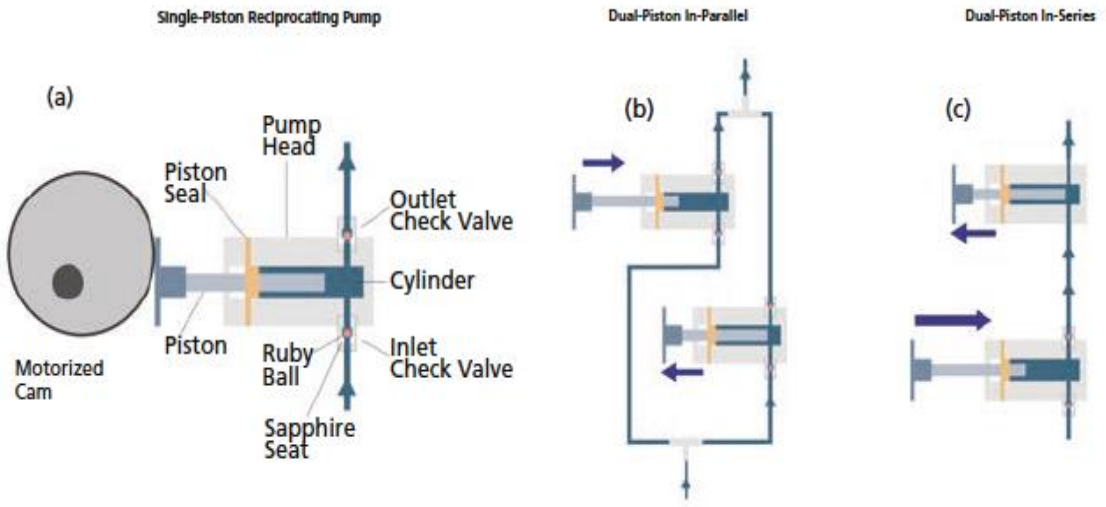

Figure 1.6 - HPLC pump configurations in which the mechanism of a single-piston reciprocating pump (a); a dual-piston in parallel (b); dual-piston in series (c) are graphically shown [25].

The single piston pump was eventually phased out in favour of a dual-piston design. By driving two pistons 180° out of phase, a near pulseless flow of liquid could be achieved. While one piston is delivering fluid, the other is filling. There are two variations of a dual-piston pump, in-parallel and in-series. Figure 1.6(b) illustrates the layout of a dual-piston

in-parallel pump. Both pump heads work independently drawing fluid from a reservoir and delivering it to a column. The outlet from each pump head is connected *via* a tee connector or manifold. Special motorised cam designs can be used to reduce pressure pulsations by allowing a small overlap between the end of a delivery stroke. Figure 1.6(c) is a diagram of a dual-piston in-series pump. The in-series pump is mechanically the same as the parallel, however the outlet of the first pump head is connected to the second pump head's inlet. Generally, as the first piston known as the primary is dispensing, it primes the second piston as well as delivers fluid out of the pump. When the secondary piston, known as the accumulator, dispenses the primary piston fills. Variations on this design involve either different piston diameters or different piston speeds. The major advantage of the in-series arrangement is the reduction of check valves required, but at the expense of control complexity to reduce pulsations. The early gold standard of dual piston pump was the Waters M6000 which was specifically designed for HPLC applications with a maximum pressure of 6000 psi achievable [26].

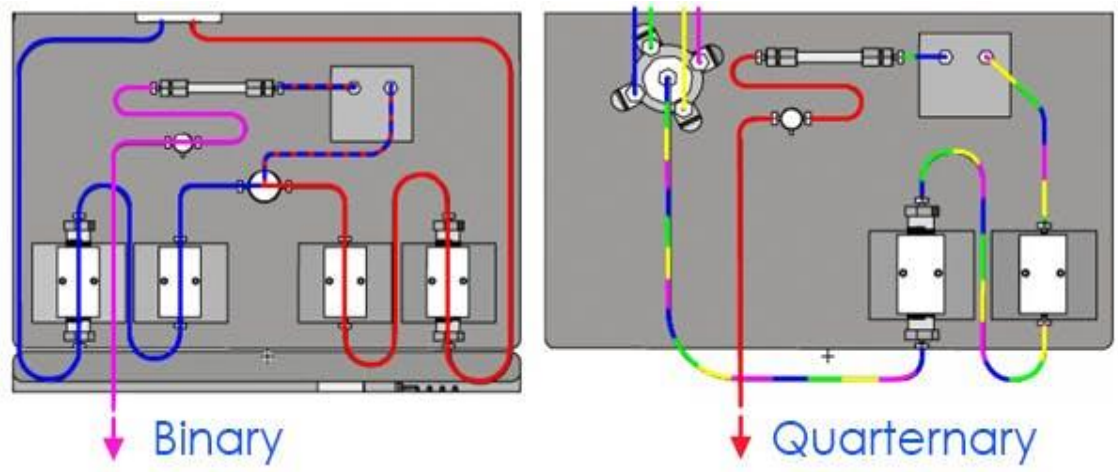

Figure 1.7 - Binary and gradient fluidic pathways [27].

Another feature of modern HPLC pumps is the ability to combine multiple mobile phase solvents to create a fixed known ratio that remains stable (isocratic) or a solvent ratio that changes (gradient) over the course of the analysis of a sample. Two approaches to mixing the solvents are available as seen in figure 1.7, high-pressure found in binary pumps and low pressure found in quaternary pumps. Binary pumps combine two dual-piston in series pumps which each draw a different solvent. Mixing occurs on the high-pressure side with the aid of a mixer unit to ensure the mobile phase composition reaching the column is homogeneous. The advantage of binary pumps is the dwell volume, which is the volume between the point of mixing and the head of the separation column, is minimised and highly accurate gradients are achievable. However, because of combining two pumps into one unit, costs are higher. An alternative can be found in quaternary pumps. Modern quaternary

pumps use a solvent proportioning valve placed before the inlet of a single dual-piston in series pump. The proportioning valve can rapidly switch between four solvent channels, synchronised with the flow rate of the pump. Mixing occurs in the primary head of the pump. A mixer may also be incorporated into the fluidic circuit after the pump. The quaternary pump usually has a higher dwell volume which decreases gradient accuracy but is a more cost-effective solution.

LC pump characteristics such as noise, flow drift and accuracy can cause issues depending on the type of separation and analysis being implemented. For quantitative and qualitative analysis, stable flow rates with low drift are important to ensure peak areas and retention times are stable over repeated separations. Pulsations in flow can cause issues with trace analysis [23] as a fluctuating flow can increase noise in detector baselines, increasing the limit of detection. Pumping systems that can reliably perform with high precision, accuracy and low pulsation are required for efficient and repeatable separations. This is important not only for laboratory-based systems, but for portable analysers too.

1.5 Portable analytical systems

The push for miniaturisation is prevalent across many industries with the benefit of placing technology in the hands of those who can utilise it best. This is of a huge benefit to those working in areas where the analysis of samples in real-time can cut costs and reduce decision making time to almost zero. Analytical chemistry is one of the fields where miniaturisation is yielding huge benefits. With Sharma *et al*. defining the weight of a portable LC system as less than 7 kg [28], a clear picture of the technological progress of portable analysers can be described. One of the earliest lab portable systems developed was reported by Baram *et al*. in 1983 weighed in at 42 kg [29] followed by the same author in 1996 reporting a system weighing in at 14 kg [30]. More recent developments have seen overall system weights decrease further to 4.5 kg reported by Sharma *et al*. in 2015 [31] and 2.7 kg Lam *et al*. in 2020 [32].

However while weight is a key factor, analytical performance is paramount. The keystone to any separation method is a reliable flow of mobile phase. One of the reasons that the weights of portable systems have decreased dramatically over the years, has been due to the development of portable pumps suitable for use in these systems. Portable liquid chromatography systems require a compact, power efficient pumping systems. Desirable traits for portable pumps include low weight, ability to deliver fluid at high pressures, stable flow rates independent of back pressure, and compatibility with various solvents. Finding a suitable solution that fits all the criteria can be challenging as different pumping technologies bring different advantages and disadvantages.

In 1986, Otagawa *et al*. reported the first portable LC. The system was also described in a patent filed in 1989 as suitable under field conditions [33]. An isocratic separation method coupled with electrochemical detection was applied to the analysis of coal derived products. The system utilised an off the shelf pump described as a dual-piston isocratic pump [34]. However performance of the system was limited by the self-described low-pressure configuration [35]. A maximum system operating pressure of 10.34 bar [33] lead to poor separation resolution. This was further impacted by the pressure pulsations seen at flow rates above 0.7 ml/min, reducing operating pressure to 4.14 bar and flow rate to 0.6 ml/min [35].

Baram published work in 1996 regarding a portable liquid chromatograph for mobile laboratories. The system provided good resolution on separations of polynuclear aromatic hydrocarbons, phenols, and pesticides amongst others. The pumping system comprised of a dual-syringe high pressure gradient metering pump with a reported flow rate range of 5 to 999 µL/min. Flow rate accuracy of ±1 % and precision of ±0.3 % were reported at 100 µL/min. The high precision value reported is expected for a syringe type pump as flow is achieved through displacement rather than a reciprocating plunger which can cause pulsations. The maximum pressure of the pump is 70 bar [30].

In 1998 a practical portable HPLC was described by Tulchinsky and St. Angelo [36]. While no operating results were reported regarding pump performance, specifications of 350 bar maximum pressure and a flow rate range of 0.1 to 2.5 ml/min were presented in relation to a pumping system that consisted of two dual piston reciprocating pumps. However despite the advances in pump performance over previous systems reported, analytical performance of phenols in lake water showed poor resolution.

The year 2015 saw three systems reported which used an electroosmotic pump (EOP)[37], a dual nanoflow pump configuration [31] and a syringe pump system [38]. Pressures reported an operating pressure of less than 10 bar for the EOP with a flow rate range of 0 to 10 µL/min. Flow precision was measured at 0.17% at a flow rate of 5 µL/min, while accuracy was reported through peak retention times with a maximum deviation of 0.44% RSD reported [37]. The nanoflow pumping system constructed by VICI can operate at pressures up to 550 bar at flow rates of 10 nL/min up to 90 µL/min, with a reported error of less than 0.1%. Typical flow rates of 350 nL/min gave peak retention precision of less than 1.42% RSD [31]. The syringe pump system published by Li *et al*. is described as a medium pressure LC. Using a 5 µL syringe an operating pressure of approximately 114 bar was reported with isocratic peak retention RSD of 0.7 to 1.4% given. It was also reported that fluctuations at low flow rates were generated by the stepper motor of the syringe pump

when using syringes with volumes larger than 5 µL. The combination of four syringe pumps gave a combined flow rate range of 0.04 to 5600 µL/min.

Research in 2017 presented by Lynch *et al*. described an EOP capable of pressures up to 140 bar [39] but no clear information is provided on its performance. In 2019 a new method of pumping mobile phase was introduced by Chatzimichail *et al*. A pressurised gas reservoir was used to force the mobile phase through the fluidic system at flow rates of 50 nL/min to 1 µL/min. A reported backpressure of 150 bar and flow precision of less than 0.2% [40]. Again in 2021, Chatzimichail *et al* reported an updated system with operating pressure up to 300 bar and an even lower variation in flow rate of 0.097% RSD at 152 µL/min [41].

Commercial portable LC systems are few and far between. The only system reported so far that was commercially available was the system reported by Baram in 1996, known as the MiLiChrom-4. More recent systems such as the Axcend Focus LC and the Aquamontrix Nitrite and Nitrate analyser were presented in peer-reviewed publications. The Axcend Focus LC launched in 2018 is built upon work published by Sharma *et al*. [31][42] and Zhao *et al*. [43]. The system is described as a nanoflow liquid chromatograph and has been demonstrated through the separation of pharmaceuticals and illicit drugs [44] as well as PAHs and BTEX compounds [45]. System performance specifications are reported with up to 689 bar operating pressure at flow rates of 0.5 to 10 µL/min [46]. In a similar vein to the Axcend system, the Aquamonitrix was built upon research [47][48]. Work published by Murray *et al*. describes a fully automated, low-cost ion chromatography system. While the Aquamonitrix analyser is focused on the analysis of Nitrite and Nitrate, it merits recognition amongst the portable systems available due to zero intervention required when operating. This is because of an automated sample intake system which draws in sample from a water source and automatically fills the sample loop on the injection valve [48]. Further work published has utilised modified versions of the platform for the analysis of nitrite and nitrate in saline waters [49] as well as the detection of phosphate in effluent and natural waters [50]. The system is also in line to become the first commercial portable analyser to receive certification under the ISO13034:2016 Environmental Technology Verification standard. Other portable LC systems are available are marketed for specific analysis such as the LightLab3 cannabis analyser from Orange Photonics and the SmartLifeLC from PolyLC for the screening of diabetes marker $A1_C$ and blood disorders [51].

The portable LC systems presented above cover a wide range of compounds analysed, including pesticides, pharmaceuticals, phenols, proteins, and amino acids. Applications ranged from analysis of coal derived products, surface water samples to forensics. Most systems from 2015 onwards use UV LEDs for detection, with earlier systems relying on UV lamps or electrochemical detection. Reverse phase separation methods are common across

all systems with a wide range of columns used. These range from capillary scale (0.3 - 0.5 mm inner diameter) and at the analytical scale, micro bore columns (1 – 3 mm i.d.) and standard bore columns (3 – 7 mm i.d.) [52] as well as using monolithic and packed stationary phases. A summary of research based, and commercial systems and their specifications follows in table 1.3.

Table 1.3 - Summary of research based and commercial portable LC systems.

LC System	*Year*	*Analysis of*	*Column*	*Mobile Phase*	*Detection*	*Pump*	*Flow Rate*	*Pressure (bar)*	*Weight (kg)*
Otagawa *et al.*	1986	Primary aromatic amines	10 µm 3x4.6 mm	Isocratic	Electrochemical	Dual piston isocratic	0.22 - 0.58 ml/min	< 10	-
Baram *et al.*	1996	Pesticides & phenols	6-8x2 mm	Gradient	UV-Deuterium lamp	Dual syringe	5-1000 µl/min	-	14
Tulchinsky, St. Angelo	1998	Phenolic pollutants	4.6mm	Gradient	Fixed-wave UV	2 dual piston	0.2 - 2.5 ml/min	Up to 350	9.5 (no lead acid battery)
Ishida *et al.*	2015	Alkylphenols & catecholamine	3x0.8 mm	Gradient	Electrochemical	EOP	0 - 10 µl/min	< 10	2 (no laptop)
Sharma *et al.*	2015	Pesticides & phenols	Monolith (13 cm x 150 µm)	Gradient	UV-LED	VICI nanoflow	nl/min range	550	4.5 (no battery)
Li *et al.*	2015	Parabens	Monolith (18 cm x 100 µm)	Gradient	UV-LED	Syringe	0.0036 - 141 µl/min	100	1.3 (no power or data acq.)
Lynch *et al.*	2017	BSA & myoglobin	Monolithic (100x75 mm)	Gradient	Separate UV-MS	EOP	nl/min range	140	3
Chatzimichail *et al.*	2019	Amino acids	Capillary, standard	Isocratic	UV-LED	Gas pressure	50 nl - 1 µl/min	150	6.7
Lam *et al.*	2020	Pharmaceuticals & Parabens	Capillary	Gradient	UV-LED	Syringe	µl/min range	26	2.7
Foster *et al.*	2020	Pharmaceuticals & Forensic	Capillary	Gradient	UV-LED	Syringe	0.8-50 µl/min	689	7.82
Chatzimichail *et al.*	2021	PAH	Microbore (2.1 mm)	Isocratic	UV-VIS	Gas pressure	0.22 - 0.58 ml/min	300	4.2
Axcend	-	Pharmaceuticals & Forensic	Capillary	Gradient	UV-LED	Syringe	0.5-10 µl/min	689	7.98
Aquamonitrix	-	Nitrate & Nitrite	Standard	Isocratic	UV-LED	Syringe	-	-	12
Orange Photonics	-	Cannabinoids	-	-	-	-	-	-	6.12
PolyLC	-	$A1_C$ Testing (Diabetes)	-	Gradient	LED – 415 nm	Binary Pumps	0.001 – 5 ml/min	206	11.3

Most systems reported the use of monolithic or capillary separation columns. The pumping system and separation method are complimentary, with most systems only capable of operating within the ranges reported. Capillary separation columns require specialised pumping systems that produce little to no pulsation that can affect peak retentions at low flow rates. For example, the Axcend system uses cartridges for changing the capillary column and detection wavelength, and for a system that starts at $35,000 [53] high costs and proprietary components are prohibitive to wide adoption. Non-commercial portable analysers such as the Hand-Portable system reported by Chatzimichail *et al*. [41] which reported low pulsation, requires a 4500 psi (310 bar) gas reservoir to drive the mobile phase through the system. Pressurised non-flammable gas is regarded as a potential safety hazard and would face strict regulations regarding its handing and transport.

While there are valid arguments for the use of capillary and microbore columns in portable analysers such as reduced mobile phase usage and sharper peaks, these separation techniques require a higher level of expertise to exploit the advantages they provide. Due to reduced internal column volumes, tubing connections, unions, injections and any extracolumn effect will cause issues with separation efficiency [54]. Another disadvantage of capillary and narrow bore columns lies with their reduced capacity. Due to the smaller internal diameter, there is less room for the stationary phase particles, which in turn means less room for functional sites for analytes to be attracted to. When analysing samples of unknown concentrations, overloading of the column could occur [55]. While diluting the sample or using a smaller injection volume are valid ways to avoid column overloading, this can potentially reduce the peak height, negating the advantage of sharper peaks [55].

Therefore, to address the potential issues outlined above regarding column sizes, weight, cost, battery run time and pump performance, this work is focused on the development of a novel pumping solution which can provide stable flow rates with low pulsations, while maintaining low power consumption and high operating pressures in a compact and lightweight from factor. A simple but effective approach, with the help of a novel reciprocating pump technology, is to stick to a portable system that uses analytical scale columns, where well established methods can be implemented with the simple change of a column and mobile phase. While many of the systems outlined above give comparable results to laboratory equipment, the legality of results generated by non-standardised methods may come into question. Laboratory based equipment is operated under ideal conditions and using certified workflows and procedures. By developing a system that has the potential to run certified methods, results could be generated at the source that are comparable to laboratory results that may take hours to days to be reported.

The following chapters describe the development of the pump, as well as a simple portable system that is demonstrates the pump's capabilities using isocratic, reverse phase separations.

Chapter 2 Pump development

Chapter one gave a brief insight into the HPLC and the importance of a stable pump. This chapter introduces the novel swash plate high pressure pump. The mark one pump was a proof-of-concept prototype which laid the foundation to the mark two pump developed in this research.

2.1 Novel swashplate high pressure pump

Through this research, the aim is to improve upon and showcase the robustness of novel pumping technology and how this enables the use of analytical scale benchtop HPLC columns in a portable system.

2.1.1 Mark one pump - Original swashplate high pressure pump

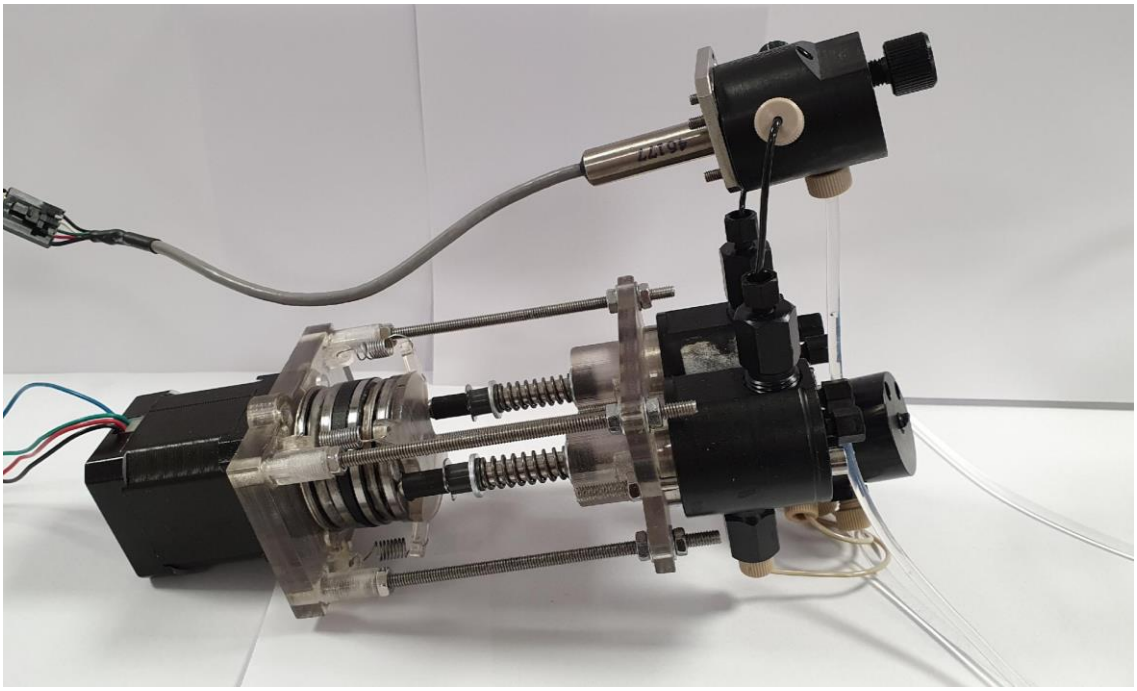

Figure 2.1 – Replicated mark one swashplate pump prototype, built using leftover parts.

As part of research funded under SFI TIDA (14/TIDA/2406) a novel pump design was conceived to address the need for a compact, lightweight, high pressure, low pulsation pump for use in portable systems. This pump design sought to overcome the fact that most portable liquid chromatography systems are designed for specific analytes, usually opting for low pressure stationary phases or low flow rates. By utilising a pump capable of delivering mobile phase at high back pressures in a portable system, certified analytical methods could be used as they are in more expensive laboratory-based equipment. This development work led to the short stroke oscillating swashplate axial piston pump with low

dead volume and low noise as shown in figure 2.1. Figure 2.2 illustrates the layout of a typical axial piston pump.

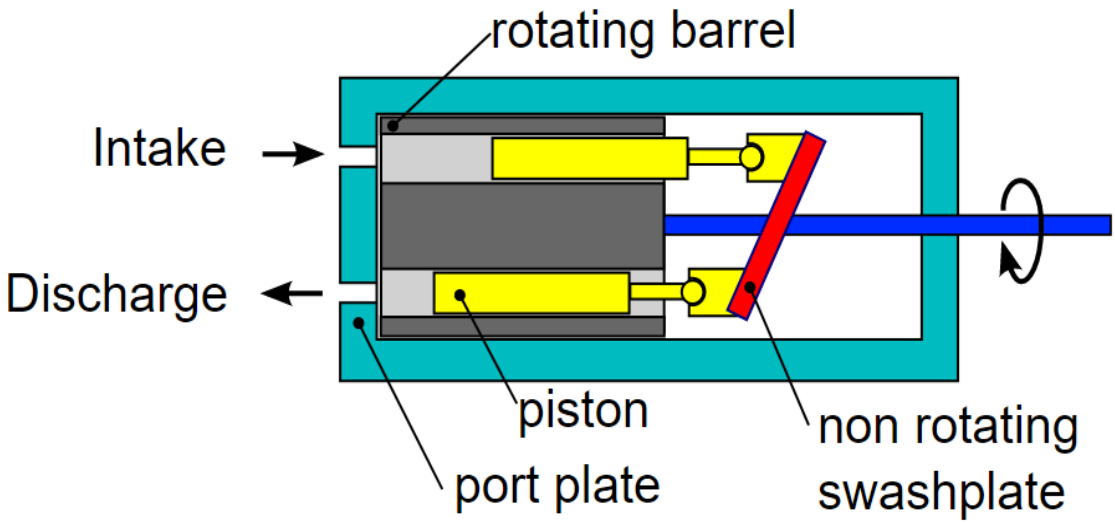

Figure 2.2 - Axial swashplate pump layout [55].

As the driveshaft (blue) rotates the barrel, the pistons are reciprocated back and forth by maintaining contact with the stationary swash plate. This causes the pistons to fill and empty as they rotate through 360°. Multiple pistons are utilised to reduce pressure pulsations from the output port by overlapping the discharge phases. Axial piston pumps are typically used in high pressure applications such as hydraulic systems of aircraft or heavy machinery or air conditioning systems [57]. In terms of design, this means pump size and weight is not of major concern. Even more complex designs exist where the swash plate angle can be altered to change the piston displacement. Although micro axial piston pump designs do exist, they are usually designed to pump mineral oil and are not suitable for use in analytical applications. In contrast, figure 2.3 shows the relatively simple mechanical setup of the novel piston pump.

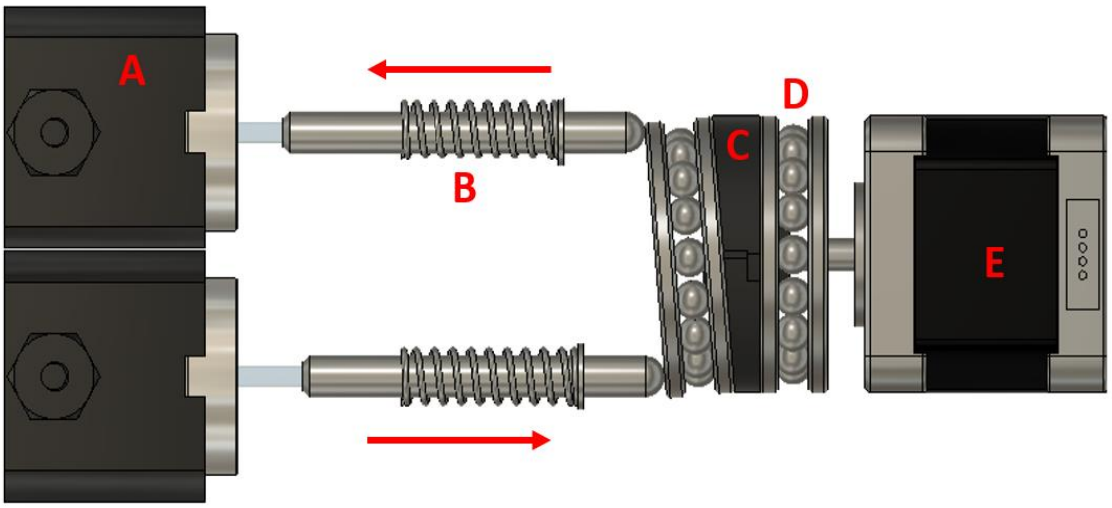

Figure 2.3 - Mechanical setup of the swashplate pump. Legend: (A) Pump Heads; (B) Pistons; (C) Swash Plate; (D) Thrust Bearing; (E) Stepper Motor.

The pump uses a swashplate mechanism like that described in figure 2.2 above. However, by rotating the swashplate rather than a housing with the pistons mounted within, the entire design is simplified. Looking at figure 2.3, a motor (E) turns the swash plate (C) which is mounted on a thrust bearing (D). A second thrust bearing is mounted on top of the swash plate. Two pistons (B) which are 180° out of phase are held against the plate of the thrust bearing with compression springs. The rotation of the swash plate causes the pistons to reciprocate in and out of the pump heads (A). The novelty of the pump was in replicating the piston movements of a typical cam driven pump with a compact, low angle swashplate. There are many advantages to a low angle swashplate. A low angle results in a short piston stroke which equates to a low pump volume which is important in systems where mobile phase gradients are altered. It also has the effect of reducing pressure pulsations and reduces the torque requirement of the drive system. Further reducing the stopping torque on the motor is the use of only two pistons, compared to 3 or 5 in a typical axial piston pump.

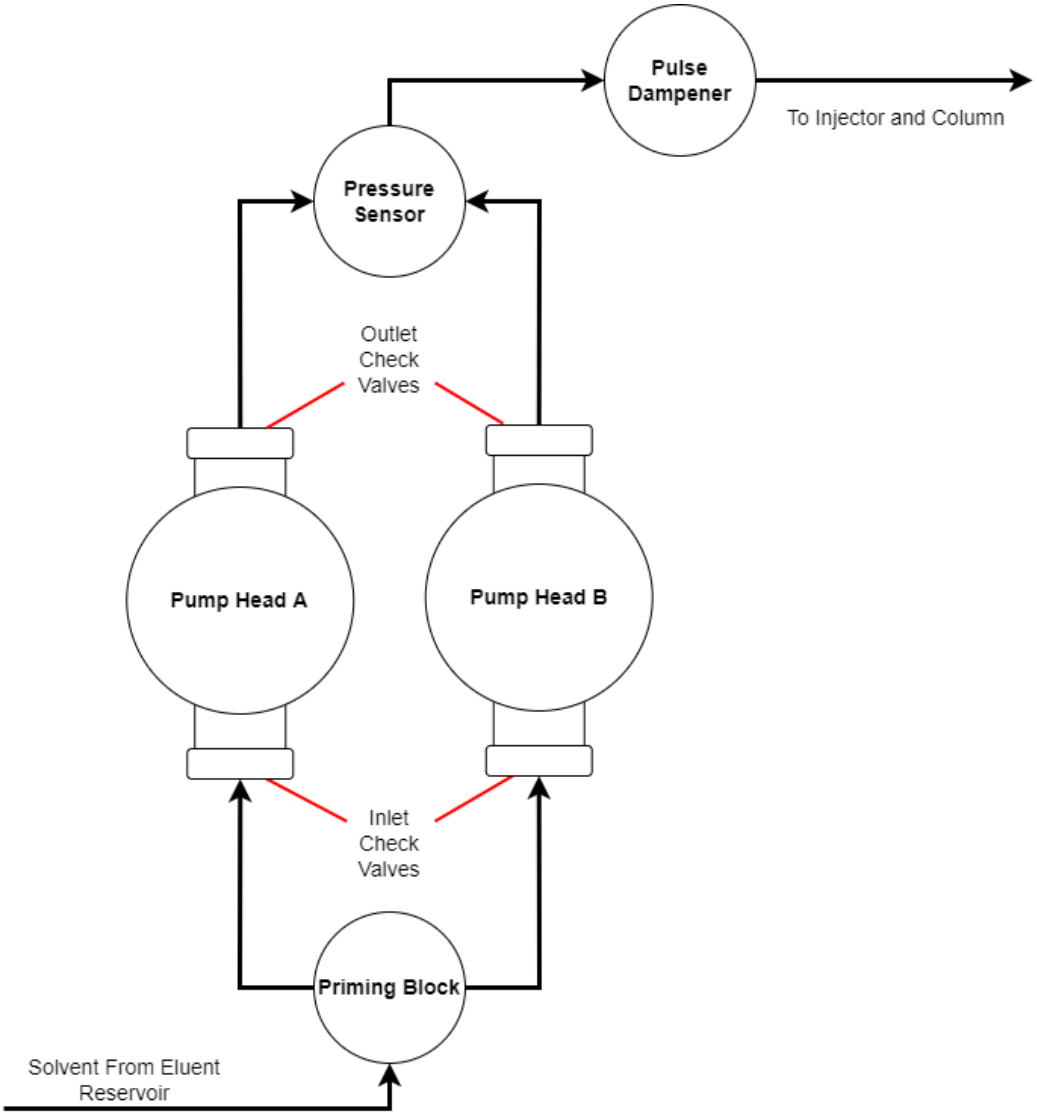

Figure 2.4 - Swash plate pump fluidic diagram.

The fluidic setup of the pump in figure 2.4 is a dual piston in parallel configuration. This setup was chosen over dual piston in series as it simplified the control algorithm. Using an in-series setup would either have required the primary piston to travel faster than the accumulator piston for pistons of the same size or require the use of a larger diameter piston which would have created load imbalances on the swash plate.

One drawback in choosing the in parallel configuration is the issue of minor pressure pulsations during changeover of fluid delivery to the system from pump head A to pump head B. These pulsations are caused by the opening and closing of the inlet and outlet check valves as the flow direction changes. A pulse dampener is utilised to minimise pulsations. A pulse dampener provides a diaphragm that expands to compensate for any increases in pressure, greatly reducing pulsations downstream of the dampener. The RESTEK MiniPulse pulse dampener used in this configuration was selected for its low internal volume of 160 µL.

The wetted materials within the flow path determine the separation modes a HPLC pump can be used for. Mobile phases for ion chromatography for example, are incompatible with stainless steel. The wetted materials of the swash plate pump consist of the thermoplastic polymer PTFE, the high-performance thermoplastic PEEK, sapphire, ruby and ultra-high-molecular-weight polyethylene (UHMW-PE). The pump heads, check valve housings, interior of the pulse dampener and all high-pressure tubing used consists of PEEK. The piston plunger tips are made from sapphire while the check valve ball is made from ruby. The piston plunger seals are manufactured from UHMW-PE. All tubing on the intake side of the pump is made of PTFE. This selection of materials makes the swash plate pump suitable for use with normal and reverse phase separation modes as well as ion-exchange and ion-pair separation modes up to pressures of 344 bar which is limited by the piston seal design.

2.1.2 Piston displacement and velocity profiles

The swashplate design used in the novel pump, is essentially a cylinder that has been cut at an angle. A cylinder that is cut obliquely will produce a sinusoidal pattern when laid out in one dimension. Figure 2.5 illustrates this concept in a simple manner. A paint roller dipped into paint at an angle will create a sinusoidal pattern when rolled on a flat surface. As the swashplate rotates this translates to a sinusoidal displacement profile for the pistons.

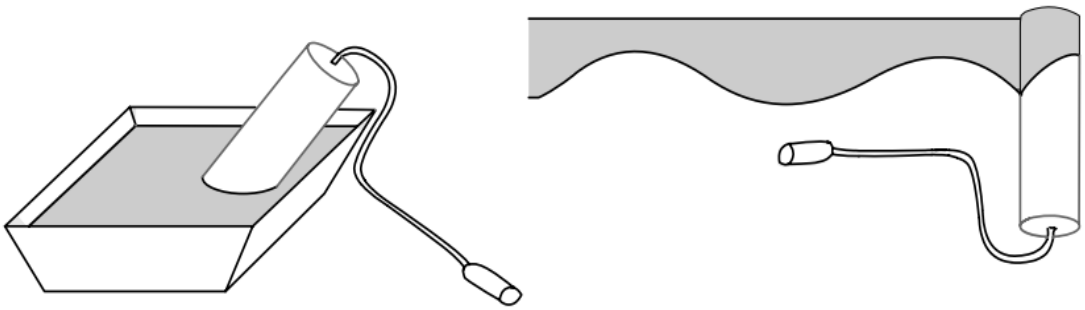

Figure 2.5 - Creating sinusoidal patterns on a flat surface [58].

The first derivative of this sinusoidal displacement, the velocity, is a cosine wave. The sinusoidal velocity of the piston as it moves with the swashplate during the delivery stroke, can lead to increased back pressure pulsations in the output flow of the pump. This is because the piston speeds up and slows down during the delivery stroke. Figure 2.6 below visualises the displacement and delivery velocity profile with respect to the angle of rotation of the swashplate. The displacement profile of piston A (black) and piston B (grey) is illustrated with the delivery stroke as a solid line and the intake stroke as a dotted line.

As the swash plate rotates and piston A moves forwards as shown by the black trace, the black velocity trace increases during the first 90° of rotation and decreases during the second 90°. It is this change in velocity over the delivery stroke that causes pulsations in the pump output.

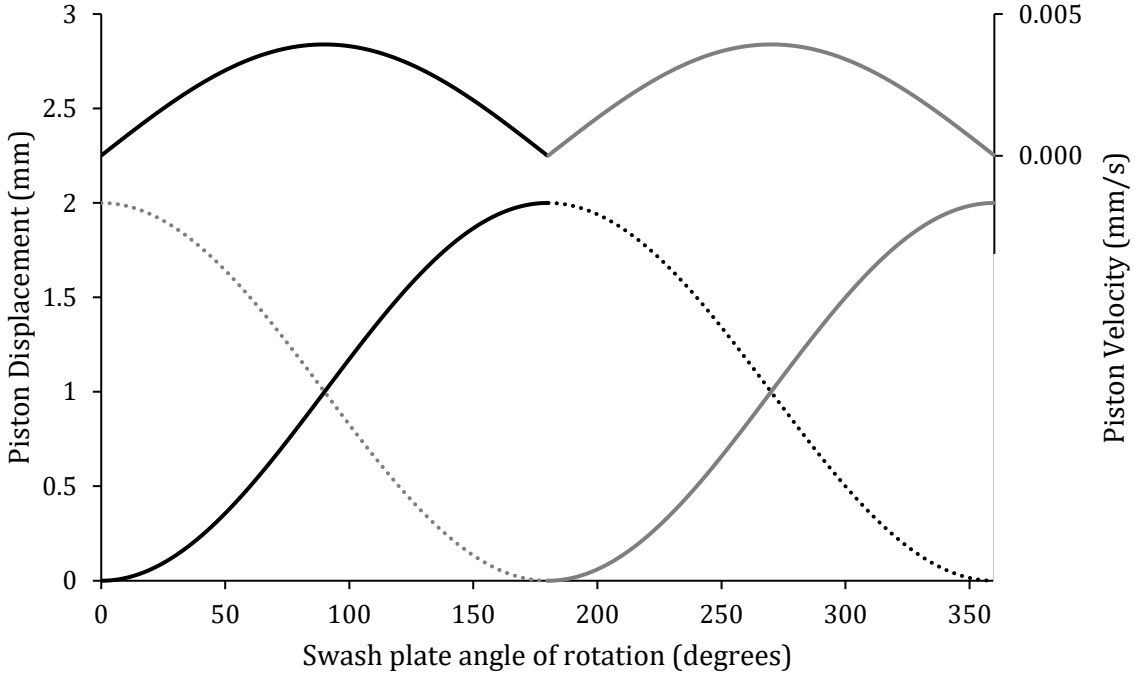

Figure 2.6 - Piston displacement and velocity profiles.

Large pressure pulses can cause issues with sensitive LC columns such as those with crosslinked copolymer phases or FPLC columns [59]. In most cases, modern LC instruments are not affected by small pulsations in flow. However, issues with peak area variance at low concentrations can be traced back to pump pulsations. Therefore it is important to reduce pressure pulsations to an absolute minimum. To reduce these pulsations, variances in the piston velocity must be eliminated. The ideal piston displacement profile is a triangle wave. For each unit of time that passes, the piston moves the same distance. This equates to a constant velocity. The following two sections discuss methods of achieving as near as constant piston velocity during the delivery stroke.

2.1.3 Swash plate oscillation

The mark one pump relied on oscillating the swashplate forwards and backwards along the most linear part of the sinusoidal curve, stopping and reversing every 150°. The advantages of this approach included simple control algorithms and a close to ideal piston displacement profile. Figure 2.7 illustrates the swashplate oscillation concept. By working within the

angular limits of the actual piston displacement profile, the piston velocity fluctuations and output pulsations were reduced.

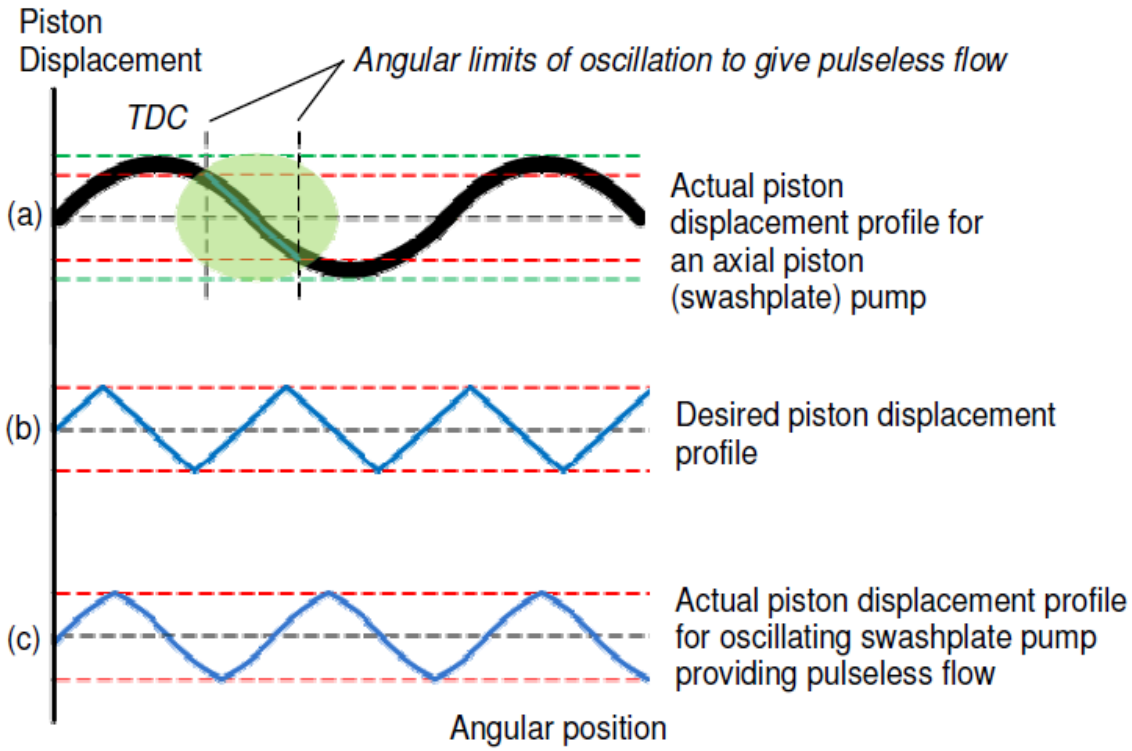

Figure 2.7 – Replicating a desired displacement profile by swash plate oscillation.

The swash plate oscillation frequency was simply dictated by the piston stroke rate needed to deliver the required flow rate. However, even though the actual displacement profile was much closer to the ideal, variances in piston velocity were still present although drastically reduced. To overcome these variances in piston velocity, another approach is required.

2.1.4 Swash plate velocity modulation

The idea of swash plate velocity modulation is based on the concept of wave interference, specifically destructive interference. As shown in figure 2.8, the sum of amplitudes is zero for two waves of equal frequency and amplitude but 180° out of phase. This is because when one wave is at its maximum, the other is at its minimum.

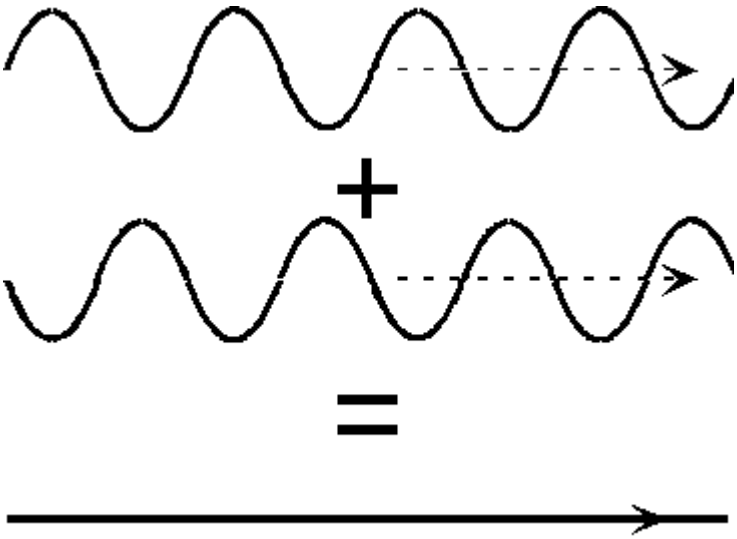

Figure 2.8 - Destructive interference example [60].

As seen in figure 2.6 previously, when the swash plate rotates at a constant velocity, the piston displacement profile is sinusoidal and consequently the velocity is sinusoidal. Because velocity is the first derivative of displacement, the first derivative of a sine wave is a cosine wave, which is 90° out of phase from the original sine wave. This means the velocity profile of a piston is 90° out of phase from the displacement profile. By altering the velocity of the swash plate in a sinusoidal manner as illustrated in figure 2.9, as it rotates through 360° the piston velocity can be kept constant due to destructive interference which in turn reduces pressure pulsations to an absolute minimum.

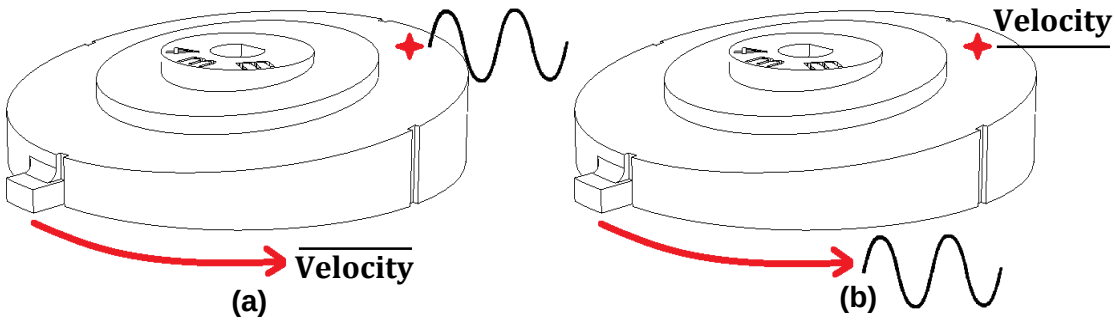

Figure 2.9 - Swashplate constant *versus* sinusoidal velocity.

When the swashplate rotates at a constant velocity (a) the velocity of a point on the surface as it rises and falls with the slope of the swash plate is sinusoidal. When the swash plate rotates with a sinusoidal velocity (b), the velocity of the fixed point is constant as it rises and falls with the face of the swash plate.

Therefore by applying a sinusoidal velocity profile to the swash plate, which matches the piston velocity profile of a piston that is filling, the resulting velocity profile of the piston that is delivering will in effect be cancelled out.

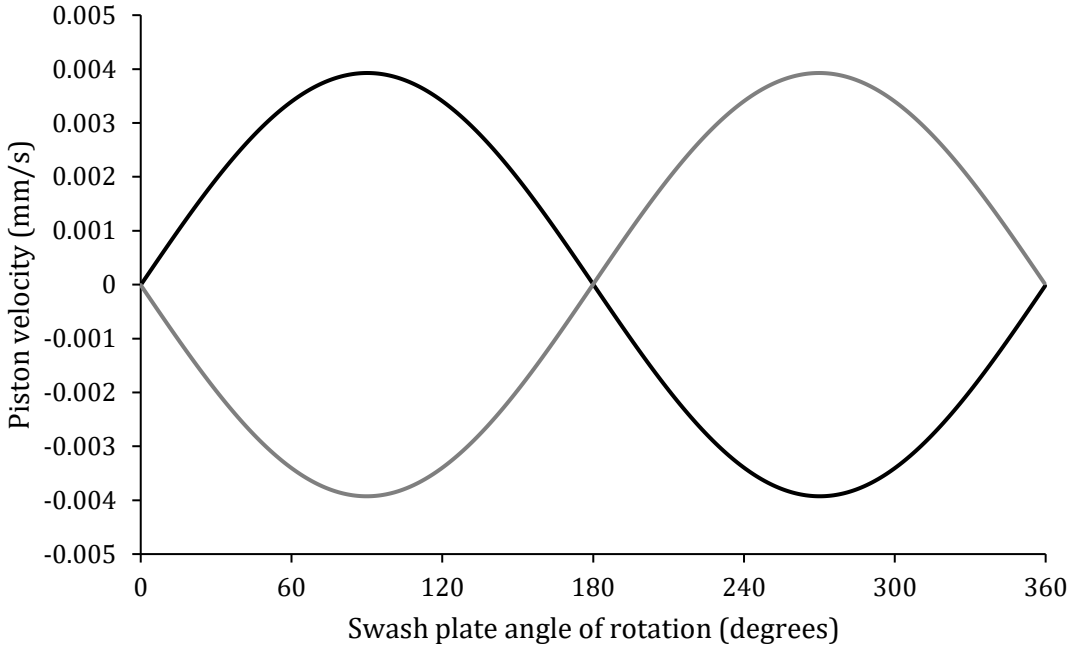

Figure 2.10 - Piston velocities with respect to swash plate angle of rotation.

Looking at figure 2.10, because velocity is a vector quantity, when the piston is in the delivery phase, the velocity is in the positive half cycle of the sine wave. When the direction of the piston reverses, the velocity is represented in the negative half cycle of the sine wave. When piston A (black trace) is delivering fluid out of the pump head, the swash plate velocity must replicate the velocity profile of piston B (grey trace). This in cancels out the sinusoidal profile. Because the pistons are 180° out of phase, the velocity modulation is reset at the delivery stroke for each piston. Therefore, the ideal swash plate velocity profile is a repeating negative half cycle.

2.2 Mark two pump development

The path of development of the mark two pump within this project would focus on the velocity modulation of the swash plate, the development of the firmware and electronics to achieve this and upgrades to the pump chassis.

2.2.1 Pump development path

Initial work focused on the development of the velocity modulation of the swash plate. The mark one design was assembled, and prototype electronics developed to control the stepper motor. During the initial testing it was found that the velocity modulation caused

significant wobble in the chassis when operating under load. Compared to oscillating the swash plate which operated in the linear area of the displacement profile, the full rotations caused the pistons to slide laterally with the slope of the swash plate, especially on larger angled plates. The first addition to the mark one pump was a plate to stabilise the pistons as shown in figure 2.11.

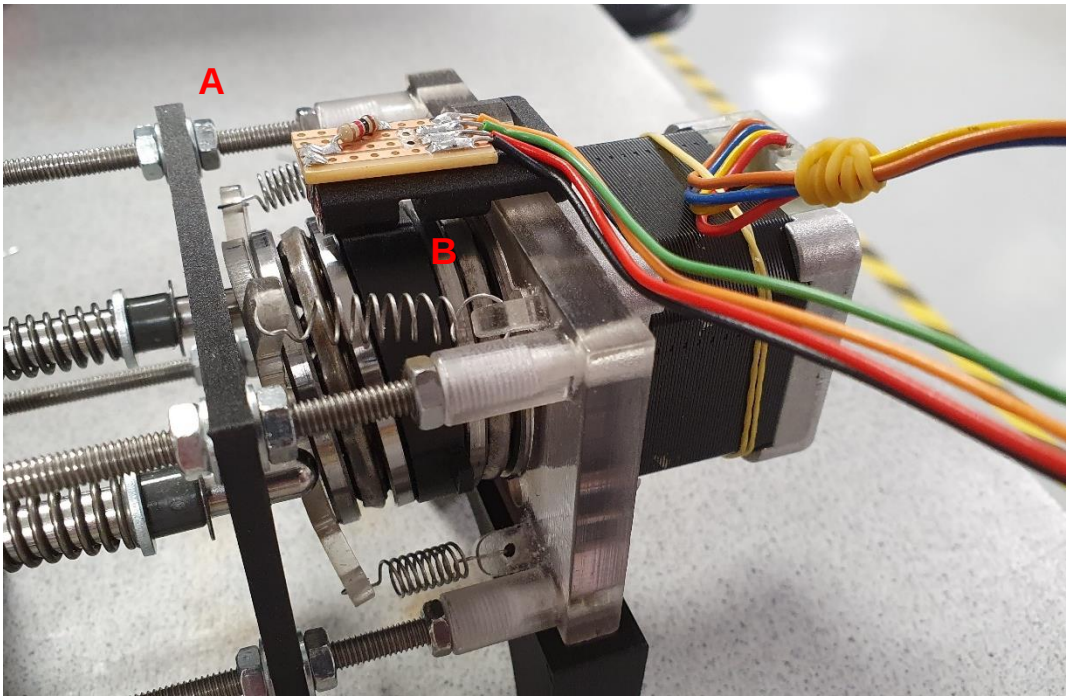

Figure 2.11 - Initial prototype for testing swash plate velocity modulation. Legend: (A) Piston Guide Plate; (B) Swash Plate.

Seen within figure 2.11 detail A, the piston guide plate used to keep the piston concentric to the plunger seal and detail B, the updated swash plate design with tabs that passed through a custom photo-interrupter. In addition to these changes, a custom electronics module was fabricated to control the stepper motor and monitor pressure.

To address the wobble seen under high loads, a new pump head plate was printed. This plate was based on the original design but incorporated steel plates onto which the pump heads were placed. However after a period of testing, it was seen that the pate was warping. An updated design was created with a thicker cross section to increase the part strength. This provided a significant improvement. However, because the pump heads were firmly secured to the pump head plate and the pistons could not move laterally, the problem of undesired movement was transferred to the motor plate. Therefore a full redesign of the pump chassis was required.

2.2.2 Pump design

All design work for the pump was carried out with Fusion 360 design software and parts 3D printed on a Markforged Mark Two FDM 3D printer. This printer was available for use in T.E. Laboratories and used a nylon based, carbon-fibre composite filament. The finish and strength of parts from this printer allow fully functional proof-of-concept designs to be realised. The combination of CAD software and 3D printing enabled rapid prototyping, where critical areas of the design such as interference fittings, mounting holes and clearances were tested with smaller prints to check tolerances before printing of the full part. This not only sped up the design process in the long-term but reduced the use of 3D printer filament used.

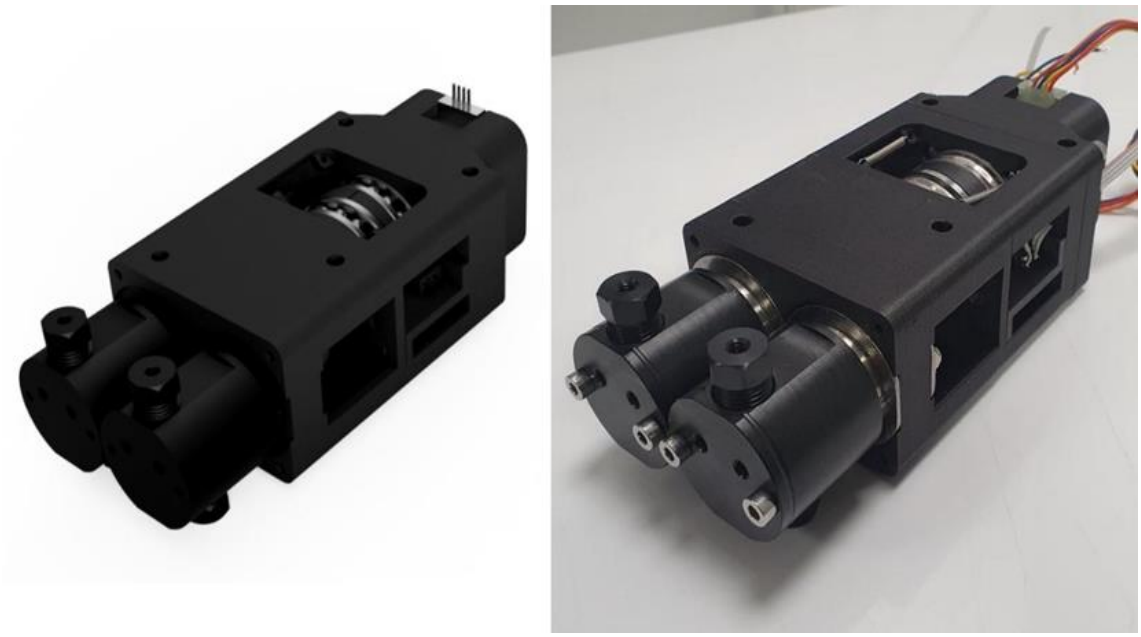

Figure 2.12 - Final swash plate pump design. (Left) Render of design, (Right) Photograph of assembled pump.

The final pump design as seen in figure 2.12, retains the critical dimensions of the mark one pump, but with a more robust frame. The pump heads were the limiting factor in terms of dimensional changes required. With the two pump heads placed side by side, the minimum distance between the two pistons was 37 mm. Therefore it was decided to retain the original 42 mm outer diameter thrust bearings. The pump chassis is made up of many separate elements which slot together to create a single robust assembly. The finished pump design comes in at 979 grams in weight, 175 mm in length, 74 mm in width and 50 mm in height. An exploded view of the pump assembly can be seen in appendix D.

The pump head plate shown in figure 2.13 features two steel plates on the outside and two on the inside faces. The pump heads are mounted onto the outer plates while the inner plates are used to distribute the load of the lock nuts that secure the pump heads in place. These lock nuts are tightened to the manufacturer's specification of 12 in-lb torque. These plates also help to distribute the load of the pump head backup washer to ensure a proper seal with the PEEK head is created. To secure the pistons in place and ensure smooth reciprocating motion, plain sleeve bearings were placed inside each plunger barrel of the pump head plate. A cap with a washer mounted within was used to locate the plunger correctly within the pump head. The washer was inset into the cap to create a solid surface for it to compress against and a lip to keep it aligned. A threaded rod was inserted into each corner of the pump head plate on to which the piston guide plate and motor plate were located.

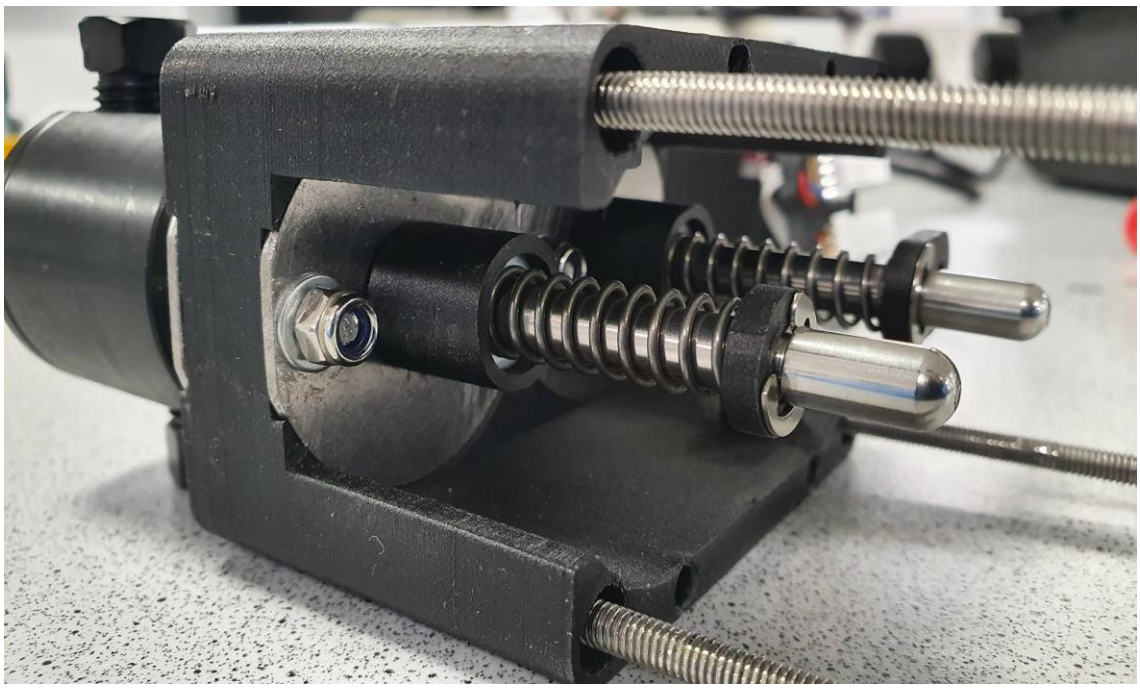

Figure 2.13 - Pump head plate.

Figure 2.14 details the piston guide plate which was introduced into the mark two pump design to minimise any movement of the pistons that is perpendicular to the axis of the pump. Plain sleeve bearings were placed into the holes through which the end of the piston would pass. This plate also served to support brackets which mounted electronic components used to monitor the pump during operation. The plate was located onto the pump head through four interference fittings.

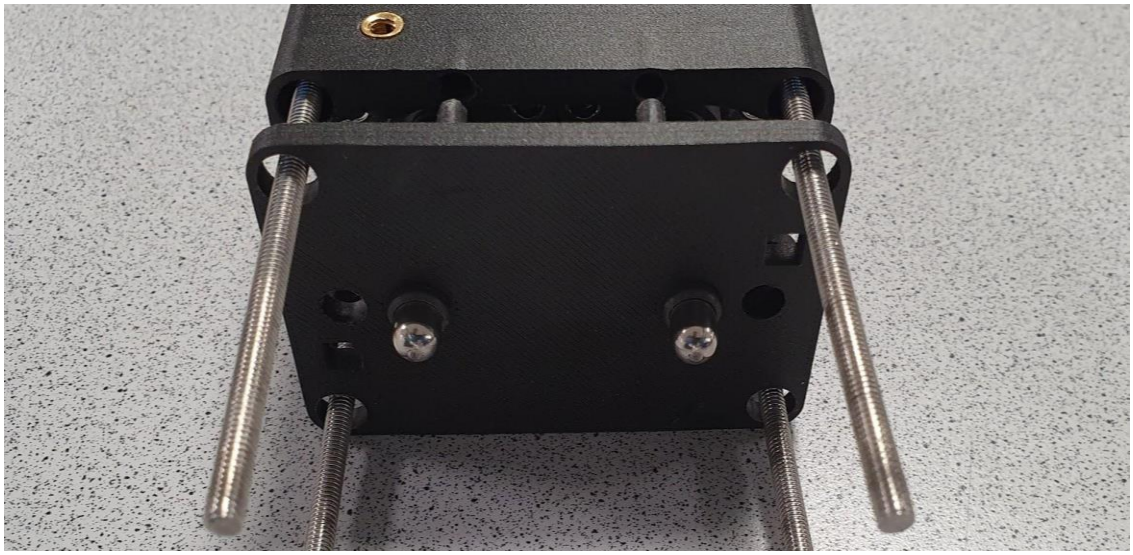

Figure 2.14 - Piston guide plate showing the plain sleeve bearings.

The swash plate assembly shown in figure 2.15, consists of the swashplate sandwiched between two thrust bearings. The upper thrust bearing sits on top of the swash plate and provides the surface on to which the pistons sit. A spring mounted retaining plate is used to hold the upper thrust bearing together and keep the top plate from sliding off. The lower thrust bearing sits underneath the swash plate and is held in place by compression between the swash plate and motor plate.

Figure 2.15 - Swash plate assembly.

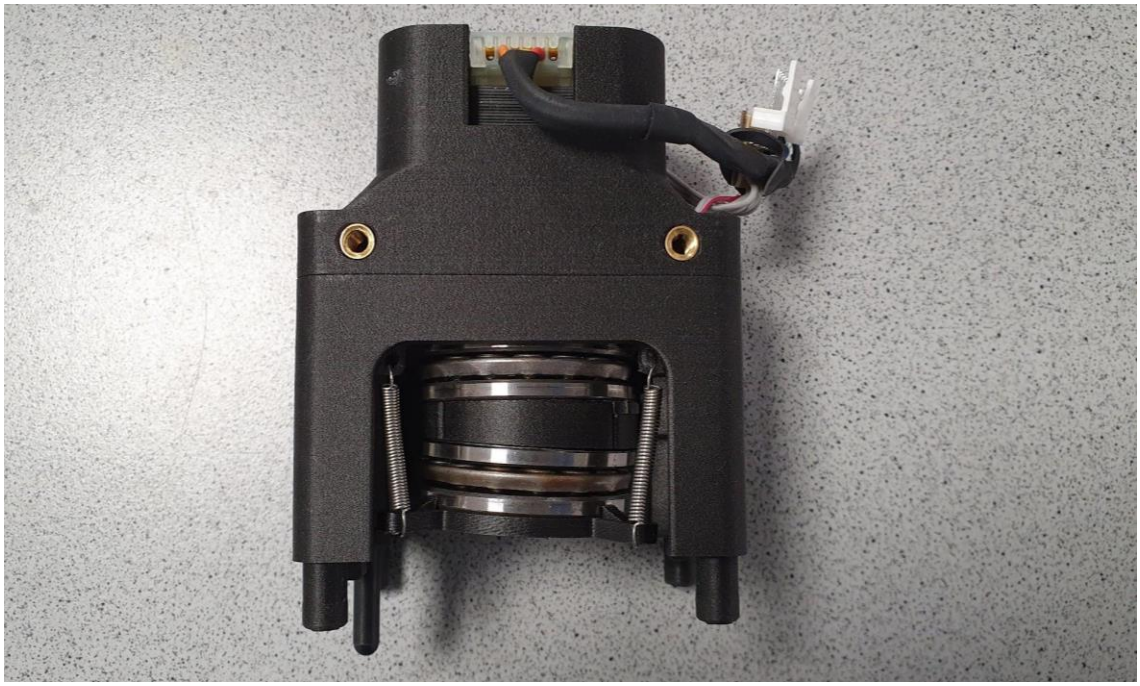

Figure 2.16 - Motor plate with swash plate assembly mounted inside.

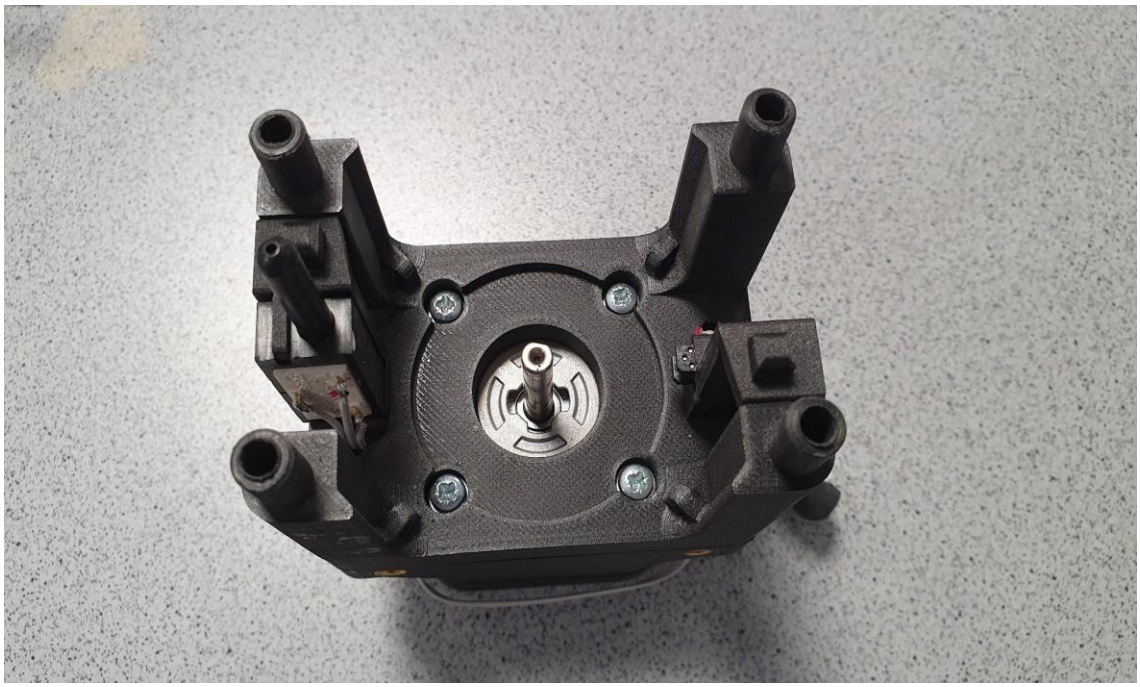

Figure 2.17 - Motor plate with swash plate assembly removed.

Figures 2.16 and 2.17 illustrate the motor plate which holds the swash plate assembly, the motor and brackets for the electronic components mentioned above. The primary features are on the inside face of this component and are located about the motor shaft axis. Four holes for a 42 x 42 mm stepper motor are located under a recessed feature for the swash plate assembly. The lower thrust bearing of the swash plate assembly sits into this recess to secure it into position. The motor shaft protrudes through the centre of the lower thrust bearing to provide enough length for the swash plate to be pressed onto. Four features are

provided to secure the extension springs of the swash plate assembly retaining plate. Features to mount brackets for a linear position sensor and a photo interrupter are included as well as holes through which the wiring can pass through. A motor cover was included to stabilise the motor during high-pressure operation due to some small flex in the motor plate. The motor cover is held onto the motor plate with lock nuts. These lock nuts compress the piston guide plate and the motor plate against the pump head plate, securing the entire assembly.

A second pump was built during this research project was handed over to the research and development team in T.E. Laboratories Ltd. for use in a portable ion chromatograph prototype. The pump followed the same design philosophy outlined above but used an older pump head, which resulted in larger dimensions. Figure 2.18 below shows the two pump designs side by side.

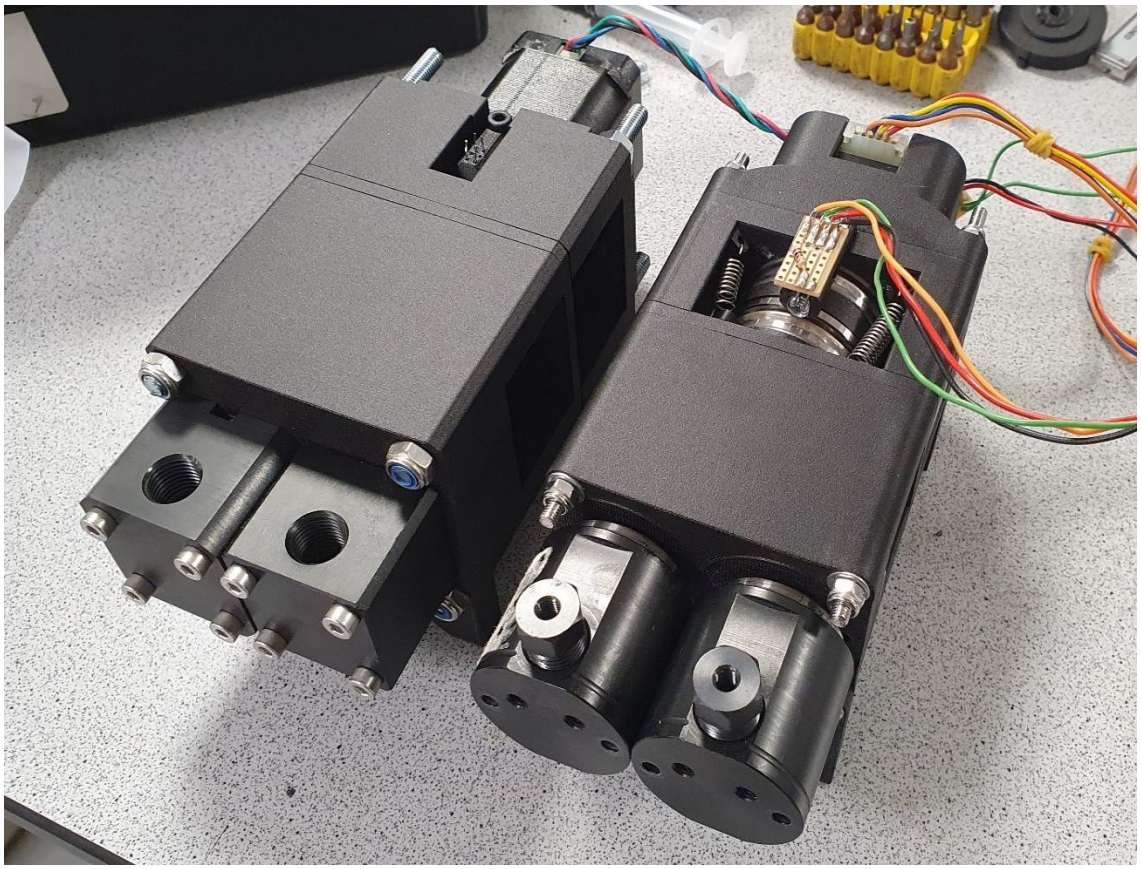

Figure 2.18 - Comparison of the DXP (left) and GP50 (right) swash plate pumps.

The names used to distinguish the two swash plate pumps are based on the LC pump model the pump heads are used on. The DXP pump heads are used on a Dionex DXP isocratic single piston pump, capable of operating up to 275 bar. The pump heads used on the swash plate pump reported in this thesis were sourced from a Dionex GP50, dual piston in parallel pump

with a maximum operating pressure of 345 bar. All results reported and any mention of swash plate pump refer to the GP50 pump design.

2.2.3 Selection of swashplate angle

The angle of the swash plate has a large influence on the operation of the pump. As the swash plate angle increases, motor torque must increase to overcome the backpressure within the fluidic circuit. For each step the motor takes, the piston is displaced forwards a set distance. This distance is dependent on the slope of the swash plate and can be approximated to either an inclined plane or a wedge. These simple machines give a mechanical advantage where the force required to move an object up the inclined face is less than lifting the object directly upwards. The steeper the angle, the closer the force is to the actual weight of the object. In this case the object is the piston, and the swash plate is the inclined plane. The forces acting against the swash plate are the back pressure generated as the piston moves forward during the delivery stroke as well as the force of the compression spring which keeps the piston pressed against the face of the plate. Friction forces can largely be ignored due to the inclusion of the thrust bearings. By keeping the swash plate angle to a minimum, the force required by the motor to turn the plate is minimised.

Piston displacement and velocity are two key factors determined by the swash plate angle. There is, however, a critical component within the pump head which can limit the maximum velocity and displacement of the sapphire plunger. The plunger seal plays a crucial role in the operation of the pump head by allowing the plunger to reciprocate in the pump head while keeping liquids inside the chamber at high pressures. To maintain the service life of the seal, the pump head pressure and plunger velocity must stay within the limits of the seal's capabilities. Further to this, the plunger must stay concentric to the seal. A phenomenon known as side loading [61] can occur when the piston is allowed to move off-axis and the load is transferred into the seal itself. This occurs during the delivery stroke as the pressure builds within the pump head. Reducing the plunger displacement will minimise the period during which the side loading may occur. However, the reduction of the displacement ultimately leads to an increase in velocity. The plunger velocity must not exceed the rating for the piston seal. A plunger size to stroke length of 1:1 is optimal to minimise issues with side loading and pulsations.

The plungers used in the mark two design are 3.175 mm in diameter, therefore a swash plate angle which translates to a displacement of 3.175 mm is optimal. Table 2.1 summarises the relationship between swash plate angle, motor torque, piston displacement and piston velocity for the mark two pump delivering a flow rate of 2.5 ml/min. With the pump heads connected in series, each pump head must deliver 1250 µL/min.

Table 2.1 - Swash plate angle comparison in relation to motor torque.

Piston Displacement (mm)	***Swash Plate Angle (°)***	***Peak Motor Torque (Nm)***
1	1.548	0.137
2	3.094	0.274
3	4.635	0.412
4	6.170	0.551
5	7.696	0.689

As seen in table 2.1, the peak motor torque increases as the piston displacement increases. The holding torque of the stepper motor used on the pump is 0.39 Nm. The pull-out torque or the maximum torque the motor can deliver without stalling or skipping steps stays above approximately 0.375 Nm up to 100 rpm. The incremental torque between each stepper motor micro step stays well below the calculated value.

Table 2.2 - Swash plate angle comparison in relation to motor and piston velocity.

Piston Displacement (mm)	***Swash Plate Angle (°)***	***Average Motor Speed (rpm)***	***Piston Velocity (mm/s)***
1	1.548	157.888	2.631
2	3.094	78.944	1.316
3	4.635	52.629	0.877
4	6.170	39.472	0.658
5	7.696	31.578	0.526

2.3 Control electronics and firmware

2.3.1 Embedded system overview

The embedded system was designed to control and monitor the pump to ensure the desired output flow was achieved and to minimise pressure pulsations. The pump relied on a 24 Volt DC supply for the Sanyo Denki 103H5208-5240 stepper motor which was stepped down to 5 Volts using a Murata OKI-78SR-5/1.5-W36-C DC-DC switching regulator for the embedded system. A Teensy 3.6 USB development board equipped with a 180 MHz Cortex-M4F processor provided the computing power to drive the stepper motor at a high frequency while simultaneously monitoring pressure, flow, and piston position. The stepper motor was actuated through a Texas Instruments DRV8825 stepper motor driver which was connected to the 24 Volt supply and controlled by 3.3 Volt signals from the microcontroller. Flow was monitored through a Sensirion SLF3S-0600F liquid flow sensor *via* I2C connection to the microcontroller while pressure was monitored using a Piezo-Metrics MP40A pressure transducer. The differential signals from the pressure transducer were fed into a Texas Instruments ADS1115 16-bit ADC. This ADC has a built-in programmable gain amplifier which gave sufficient resolution from the millivolt signals. The swash plate position was checked twice per revolution by a tab on the outside of the swash plate which passed through a Rohm RPI-352 slotted optical switch. This served to reset the time signals generated by the firmware to ensure the signal was synchronised with the swash plate. Piston position was monitored by Sensata 9605 linear position sensor. An overview of the embedded system can be seen in figure 2.19. A schematic of the pump control board is available in appendix E.

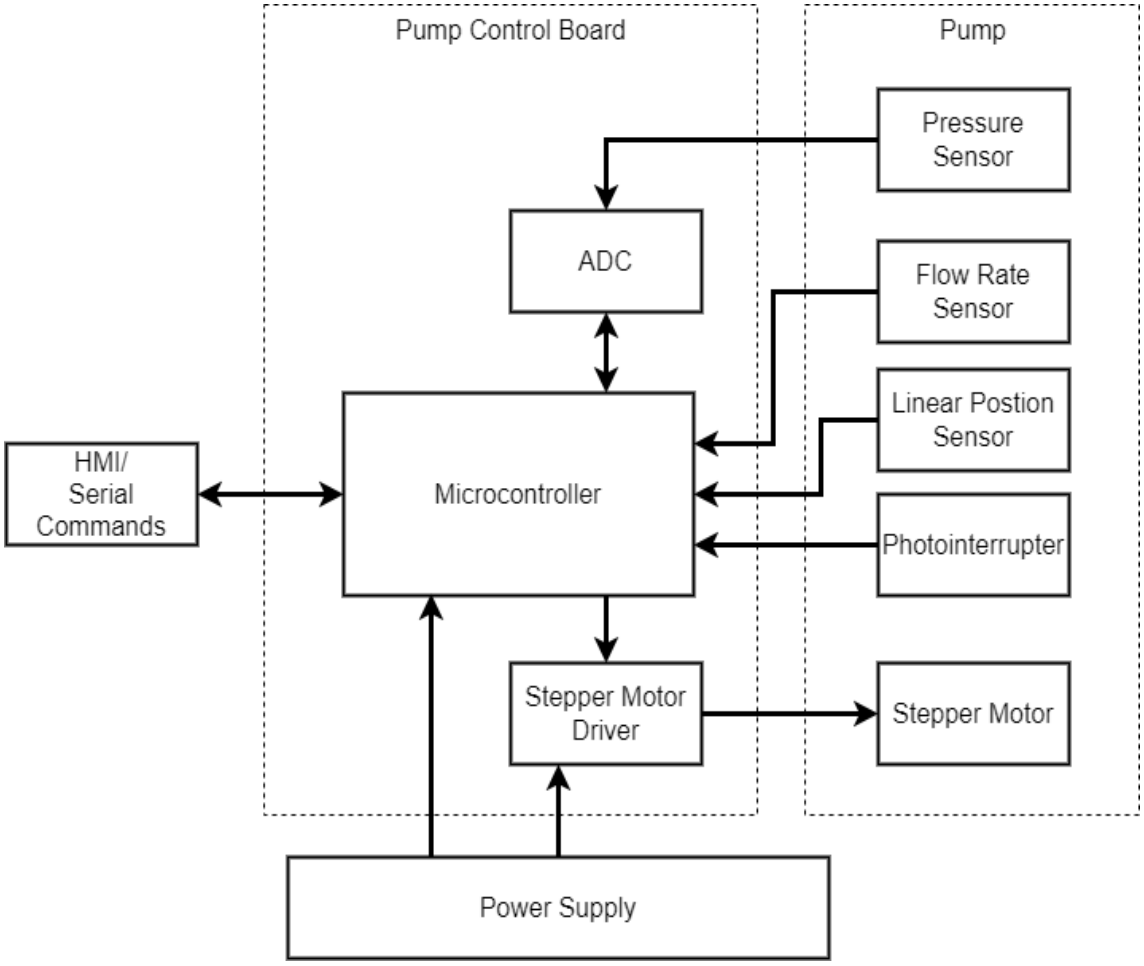

Figure 2.19 - Embedded system overview.

2.3.2 Stepper motor control

As previously mentioned, the stepper motor is driven through a DRV8825 stepper motor driver which is interfaced to the microcontroller. There are three key inputs required by the stepper motor driver in order to ensure correct operation of the motor. The first and most important input signal to the stepper driver is the step input. Each high pulse sent to this pin will move the stepper motor forward by a single step. The datasheet for the DRV8825 specifies a minimum high pulse time of 1.9 µs. However, there are limitations to how quickly a stepper motor can be run without any issues such as skipping steps, stalling, and overheating. Using equation 2.1 below, the minimum step time in milliseconds was calculated.

$$Minimum\ Step\ Time\ = \frac{2\,L\,I}{V} \tag{2.1}$$

Where L is the motor winding inductance per phase, I is the motor current per phase and V is the drive voltage. The values from the datasheet of the stepper motor used for the pump give an inductance value of 9.5 mH and a maximum current of 1 Amp. The supply voltage for the motor is 24 Volts. Placing these values into equation 2.1 we get the following:

$$Minimum\ Step\ Time\ = \frac{2 \times 9.5 \times 1}{24}$$

$$Minimum\ Step\ Time\ = 0.792\ milliseconds$$

Regarding the DRV8825 motor driver, this calculated value of 792 microseconds is the minimum time from the start of a high pulse to the start of the following high pulse. If a high pulse duration of 2 ms was used, the step pin would be pulled low for the remaining step time of 790 µs. This is illustrated in figure 2.20.

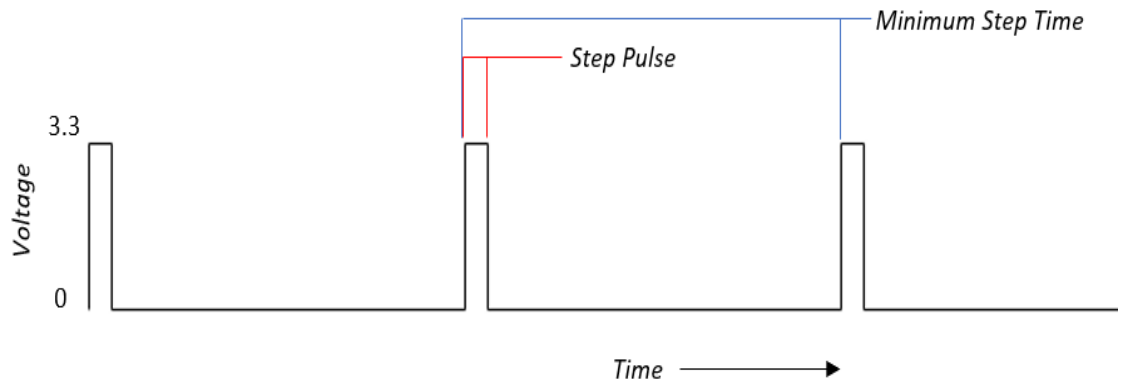

Figure 2.20 - Visualisation of signal sent to the stepper driver.

These considerations would go on to be used in the firmware for the calculations to generate a sinusoidal velocity signal for the stepper motor. The second key input required is the step size selection as represented in table 2.3. Due to the sinusoidal velocity profile required in this case, a 1/8 step size was selected to allow sufficient control at low motor velocities. This equates to 1600 steps per revolution when using the Sanyo Denki 103H5208-5240 stepper motor selected for this application.

Table 2.3 - Logic table for micro step selection with the selected configuration in italics.

M0	***M1***	***M2***	***Step Resolution***	***No. Steps per revolution***
Low	Low	Low	Full Step	200
High	Low	Low	Half Step	400
Low	High	Low	1/4 Step	800
High	*High*	*Low*	*1/8 Step*	*1600*
Low	Low	High	1/16 Step	3200
High	Low	High	1/32 Step	6400

The microcontroller firmware is configured to send the required signals to the ports outlined in table 2.1 above to set the stepper driver to 1600 steps per revolution. The third and final key input is the motor direction. While the direction the motor spins is not important, the direction must stay constant while the pump is operating. With frequency modulation, the motor is not oscillated in any fashion and the swashplate must turn through 360° to generate the correct displacement and velocity profiles.

2.3.3 Swash plate velocity control

Generating the velocity signal is not a complex task, however there are many steps to take before generating a signal and using it to control the speed of the pump. Two values are used in the firmware to control the signal sent to the step pin of the motor driver. The step-time-on value is the duration in microseconds of the high pulse used to step the motor forward one step. The step-time-on value is set manually and in this case a value of 75 µs was selected based on trial and error. Values outside the range of 50 to 150 µs began to negatively affect the piston displacement profile. The step-time-off value is the duration in microseconds between each high pulse. The number of rotations the swash plate must make per second, defines the step-time-off value. To calculate the time off period, the volume of liquid displaced by the pump for one full rotation of the swash plate must be known.

As shown by equation 2.2 and 2.3 below, this volume is calculated by combining the displacement volume of each piston. This value is referred to as the cycle volume.

$$V_{piston} = \pi r^2 h \tag{2.2}$$

In equation 2.2, r is the piston radius and h is the piston displacement due to the swash plate.

$$V_{cycle} = V_{piston} \times 2 \tag{2.3}$$

This cycle volume is then used to generate the number of cycles per second that are required to achieve the desired flow rate. This value is the frequency at which the swash plate must cycle at. In equation 2.4, for a known flow rate, the swash plate frequency can be calculated:

$$\nu_{swash} = \frac{V_{output/sec}}{V_{cycle}} \tag{2.4}$$

Where, ν_{swash} is the frequency of oscillation in hertz, $V_{output/sec}$ is the volume output required per second in microlitres and V_{cycle} is the combined volume displaced by the pistons from equation 2.3. The swash plate period is then calculated and used to generate an average step-time off-value. For example, a swash plate that displaces a 3.175 mm diameter piston by 2.105 mm for that piston's delivery stroke, the piston volume displaced is calculated using equation 2.2 and cycle volume using equation 2.3:

$$V_{piston} = \pi \times 1.5875^2 \times 2.105$$

$$V_{piston} = 16.67\ \mu L$$

$$V_{cycle} = 16.67 \times 2 = 33.34\ \mu L$$

For a flow rate of 1000 µL/min, we require the pump to deliver 16.67 µL per second. Placing these values into equation 2.4:

$$\nu_{swash} = \frac{16.67}{16.67 \times 2}$$

$$\nu_{swash} = 0.5\ Hz$$

If the swash plate is cycled at a frequency of 0.5 Hz, the period of rotation is 2 seconds. To convert this to a step-time-off value, the number of micro steps and the step-time-on value are required. Taking the values mentioned previously, 1600 steps per revolution and a step-time-on value of 75 µs, the step-time-off value in µs is calculated as follows:

$$Step\ time\ off = \frac{(Swash\ Period \times 10^6)}{No.Steps} - Step\ time\ on \tag{2.5}$$

The $Swash\ Period$ in equation 2.5 is converted to microseconds. The total step-time-on is subtracted from this value and divided by the number of steps per revolution. Using the figures presented in equation 2.5:

$$Step\ time\ off = \frac{(2 \times 10^6)}{1600} - 75$$

$$Step\ time\ off\ =\ 1175\ \mu s$$

If the stepper motor step pin is repeatedly sent a high signal with the step-time-on duration of 75 µs followed by the calculated step-time off value of 1175 µs, the motor will rotate at a constant velocity at the desired 2 second period.

Of course, the goal of the control system is to rotate the swash plate with a sinusoidal velocity. To achieve a sinusoidal velocity profile, the average value must be converted to a sine wave over the 1600 steps. This is achieved by generating a sine wave based on the angle of the rotation of the swash plate which is then multiplied by the step-time-off value.

$$Toff_{sinu} = Toff \times \sin(\theta_{swash} - 90) + Toff \tag{2.6}$$

Equation 2.6 is calculated for each step the stepper motor takes. $Toff$ is the step-time-off value calculated previously. At 1600 steps per revolution, the stepper motor angle advances by 0.225°. θ_{swash} is incremented for each step the motor takes. The sine value is shifted by 90° to cancel out the sinusoidal velocity profile of the pistons as discussed in section 2.1.4. and the step-time-off value is added to offset the calculated value and stop it becoming negative with the negative half of the sine wave. Section 2.4.1 details how this is applied through the control system firmware.

2.3.4 Piston displacement mapping

The displacement profile of the pistons as they move forwards and deliver fluid to the pump outlet is critical to reducing pressure and flow pulsations. Using a Sensata 9605 linear position sensor mounted to one of the pistons, the piston displacement profile was viewable in real-time while the pump was running.

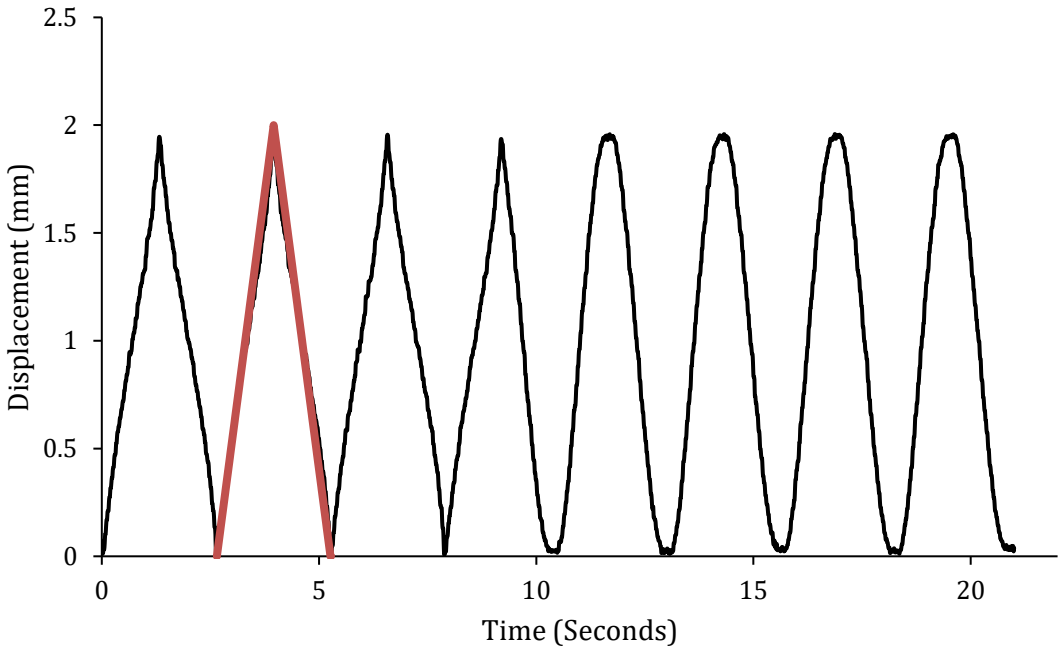

Figure 2.21 - Piston displacement profile from sinusoidal to constant swash plate velocity.

The voltage from the position sensor was read by the on-board ADC of the Teensy 3.6 development board. Using a feature known as Direct Memory Access, the linear position sensor signal could be sampled at a high frequency while the pump was operating, without any interference to the swash plate control algorithm. Figure 2.21 shows the transition from a sinusoidal swashplate velocity to a constant velocity. It is observed that the piston displacement profile changes from a triangle wave to a sinusoidal wave as expected. For reference, the desired piston displacement profile is highlighted in orange.

2.4 Control methodology

2.4.1 Velocity signal generation

Within the firmware, the step-time-off period for each step is calculated to generate a sinusoidal velocity profile for the swash plate. The calculations described in section 2.3.3 are performed in the following function found in the pump firmware:

```
void generateAverageTimeOff(double d_timeOn, double d_flowRate, double
d_pistonDisplacement, double d_checkValveDeadVol)
{
  double d_pistonVolume = (d_pistonDisplacement * PI * 2.52015625);
  double d_cycleVolume = (d_pistonVolume * 2) - d_checkValveDeadVol;
  double d_swashHz = (d_flowRate) / 60.00 / d_cycleVolume;
  double d_swashPeriod = 1 / d_swashHz;
  d_averageTimeOff = ((d_swashPeriod * 1000000.00) - (d_timeOn * 1600.00)) /
1600.00;
}
```

The input variables into the function include the step-time-on, the flow rate required and the piston displacement. The final variable, seen here as check valve dead volume, is used to account for any pumping losses and is a fixed value. This function updates a variable known as d_averageTimeOff, which is the required average step-time-off value to deliver the desired flow rate. Within the pump firmware, a function called IntervalTimer is used. This timer will repeatedly execute a custom interrupt function based on the period supplied to it. One of the features of this timer is the ability to update the timer with a new period, which will begin when the current period has ended. This simplified the application of the pulse frequency modulation required to drive the stepper motor with a sinusoidal velocity. Within the stepper start command function the following three lines are present:

```
digitalWrite(MOT_ENABLE, LOW);
digitalWrite(MOT_STEP, HIGH);
stepperTimer.begin(interruptFunction_2, d_stepTimeOn);
```

When the start command is given, the generateAverageTimeOff() function detailed previously as well as the code above is executed. The stepper driver enable pin is pulled low which energises the stepper motor. The motor step pin is set to high to move the stepper forward one step. The stepper interrupt timer then begins and will execute the interrupt code, seen above as interruptFunction2 when the period set to the step-time-on value ends. When this value is reached, the following interrupt code is executed:

```
void stepperTimerInterrupt()
{
  i_motorStep++;
  *portToggleRegister(MOT_STEP) = 1;
  if (c_opMode == 's')
  {
    if (i_motorStep % 2 == 1)
    {
      ato = d_averageTimeOff * arm_sin_f32((((i_motorStep * 0.225) * (PI / 180.00)) * 1) - (90.00 * (PI / 180.00))) + d_averageTimeOff;
      stepperTimer.update(ato);
      //stepperTimer.update(d_averageTimeOff * arm_sin_f32((((i_motorStep * 0.225) * (PI / 180.00)) * 1) - (90.00 * (PI / 180.00))) + d_averageTimeOff);
    }
    else
      stepperTimer.update(d_stepTimeOn);
  }

  if (c_opMode == 'c')
  {
    stepperTimer.update(d_stepTime[i_motorStep]);
  }
  if(i_motorStep >= 1599)
  {
    i_motorStep = 0;
  }
}
```

Within the stepperTimerInterrupt function, several tasks are executed. Starting from the top, the motor step value is incremented. Immediately after this the motor step pin is toggled. Because the previous value was high, the pin is now pulled low. Next, if the pump is set to operate in sinusoidal mode, the value of the motor step is checked. If the motor step value is odd, the average step-time-off value is used to generate the period for the time the pin will remain in the low state. This value is calculated based on the angle the swash plate has rotated in one step, which increases each time the interrupt function is executed.

If the step value is even, the stepper timer period is updated with the step-time-on value. This repeats for every step that the motor takes. Once the value of the motor step variable reaches 1600, it is reset to zero to keep the calculated angle correct. This value is also reset to zero when tabs on the swash plate pass through the photointerrupter described in section 2.3.1. Because the tabs are located at the highest and lowest point of the swash plate displacement, the velocity signal is reset at the start of each delivery stroke, ensuring the signal is synchronised with the swash plate angle of rotation.

2.4.2 Flow rate control

Generally, reciprocating pumps do not require closed-loop feedback systems to provide accurate flow and generally operate above 85% but commonly around 90% efficiency [62]. However due to a potential combination of fluid compressibility at high back pressures, coupled with the short stroke of the 2 mm swash plate used, discrepancies between the set point and the actual volume measured were enough to implement a closed loop system.

There are two basic types of control systems, an open loop system and a closed loop system. Systems such as domestic central heating are generally open-loop systems. The boiler is controlled by a timer that turns the system on and off based on a pre-programmed timer. However the boiler controller has no feedback on the air temperature of the room. If the system operated during the summer months, the room would become uncomfortably hot. During cold winter days, the heat from the radiators may not be enough to reach a comfortable room temperature. Closed loop control is a method of reducing the error between the desired output and the actual output of a system. Modern air conditioning systems such as those found in offices hotel rooms and even cars operate with closed-loop control. The user would set a desired temperature and as the system heats or cools the air, feedback is given to the controller by a signal from a temperature sensor. This is known as a feedback loop. The controller calculates the error between the desired temperature and the actual temperature, and it adjusts the output accordingly. Figure 2.22 illustrates the difference between an open loop and a closed-loop system.

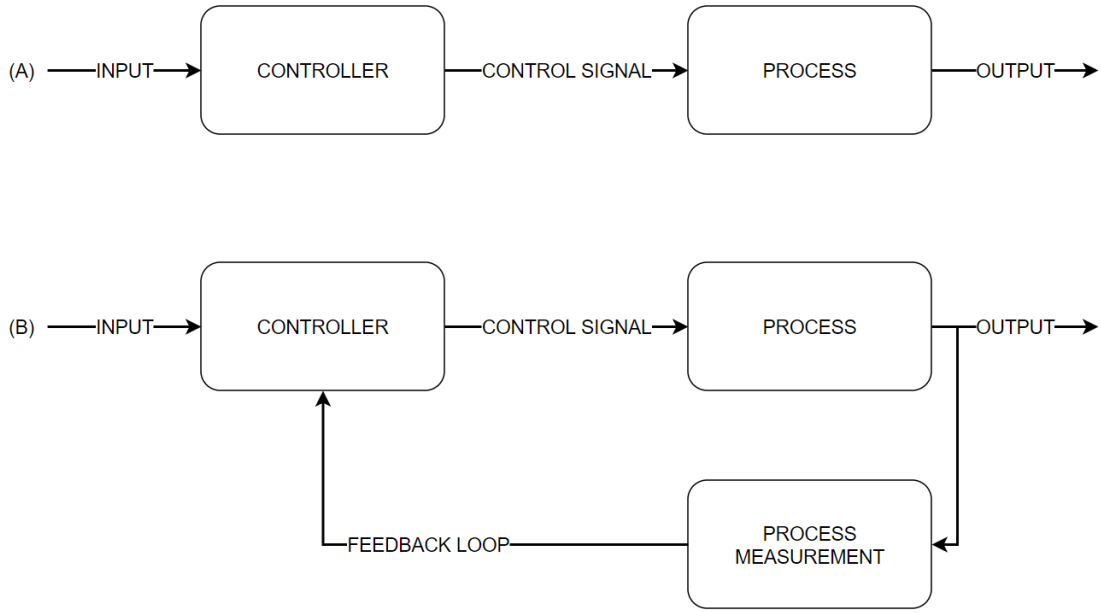

Figure 2.22 - Diagram of open-loop system (A) and a closed-loop system (B).

The function of the controller as seen in figure 2.22 is to reduce the error between the input and output. For example if the output value is above the input, the controller will reduce the

control signal. If the output is below the input value, the controller will increase the control signal. There are many different types of controllers, from simple on-off control such as a thermostat found in an oven, to more complex control algorithms such as fuzzy logic and proportional, integral, derivative (PID) control. Regardless of the type of controller used, the goal of closed loop control is to maintain a stable output signal at the desired output value, regardless of any external interferences. The closed loop control system developed for the swash plate pump was developed to control the flow of the pump over extended periods of operation and minimise the effects of drift due to ambient temperature. The addition of a flow sensor to the output of the pump which would provide feedback to a control algorithm implemented in the firmware.

PID control was selected for use. PID is a three-term controller where the error between the setpoint (desired output) and the measured output is manipulated by each of the three terms and the outputs summed together to become the control signal as illustrated in figure 2.23. The proportional term dictates the speed of the controls system response. A large proportional term will generate a fast system response. If the proportional term is too large however, the output may oscillate. The integral term sums the error over time and is used to drive the steady state error to zero. The derivative term looks at the rate of change of the error. It can be used to dampen any output overshoot. Each term has an associated gain. For the proportional term, the error is multiplied by the gain. For the integral term, the integral of the error is calculated and multiplied by the integral gain. And for the derivative term, the derivative of the error is calculated and multiplied by the derivative gain. The behaviour of the output signal can be changed by tuning these gains. Characteristics such as overshoot, oscillations and settling time can be adjusted, as necessary.

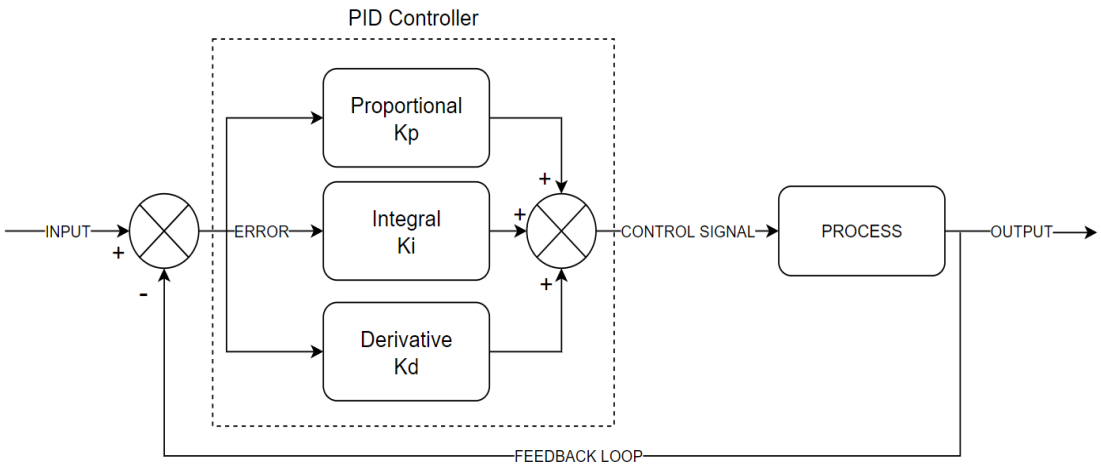

Figure 2.23 - PID controller diagram.

The task of sourcing a flow sensor for the feedback loop was challenging. Not only would it be subjected to high pressure flow, but there was a requirement to minimise the internal volume so it would not significantly add to the dwell volume of the pumping system. Off the shelf HPLC flow sensors [63][64] require computer software to record high resolution data and could not be directly integrated into the pump control electronics. Most industrial sensors were designed for high flow applications and not suitable. A relatively low-cost flow sensor that could be integrated was sourced from Sensirion, the SLF3S-0600F. However, compromises were made such that the flow rate would be restricted to a maximum of 2000 µL/min and the sensor would have to be placed after the HPLC detector as it has an operating pressure of 12 bar. By placing the sensor far away from the pump's outlet at the end of the fluidic system, a large lag was introduced to the control system.
As presented in sections 2.3.3 and 2.4.1. the speed of the swash plate is determined by the required flow rate. In open loop mode, this value is set by the user and the motor rotates at the calculated speed. In closed loop mode, the initial flow rate value provided by the user is used as the setpoint for the PID controller. The flow rate provided by the flow sensor is used to update the stepper motor step-time-off value, which adjusts the motor speed as required.

Tuning the controller was done by capturing the pump's open loop response to a step input. By characterising the pump's open loop response, the appropriate PID gain values could be applied to the system. This was carried out by recording the flow sensor value as a step input was applied to the pump. By setting the flow rate to 1000 µl/min and starting the pump, a graph was generated and a typical first order system response was observed as seen in the Open-Loop graph in figure 2.26. The time constant and the steady state values were extracted. The time constant is the time in seconds at which the system reaches 63.2% of the steady state value. This figure is based on the exponential decay of a first order system where after one unit of time the response is e^{-1}. However, in an increasing system it is subtracted from 1 which gives approximately 0.632. These values were applied to a first order transfer function which is the relationship between the input and output signal of a system shown in equation 2.7.

$$Y(s) = \frac{K}{\tau s + 1} \tag{2.7}$$

The output $Y(s)$ is the relationship between the steady state gain K and the denominator which includes the time constant τ. From the pump's response a steady state value of 986 µL/min was observed and a time constant of 4.71 seconds was calculated. These values

were used to model the system in Simulink software. The three terms of the PID controller could be applied to the model and a closed loop response modelled. The schematic of the model is shown in figure 2.24.

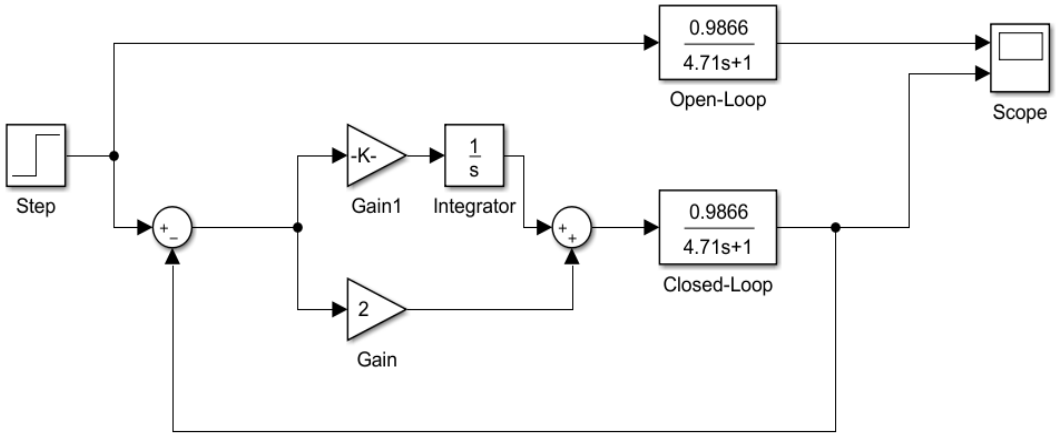

Figure 2.24 - Simulink model used to tune proportional and integral gain values.

In the figure above, the responses are modelled using transfer functions. A step input is directly applied the open loop response while the control signal sent to the closed loop transfer function is manipulated by proportional and integral terms. The derivative term was not included as the system is inherently stable, or at least any changes in output are slow. The proportional term was enough to increase the pump's responsiveness and the integral term eliminated steady-state error. The open-loop response of the pump to the step input was captured, the time constant and steady state values were extracted from the data and then applied to the transfer functions. Figures 2.25 and 2.26 show the modelled and real-world system responses respectfully.

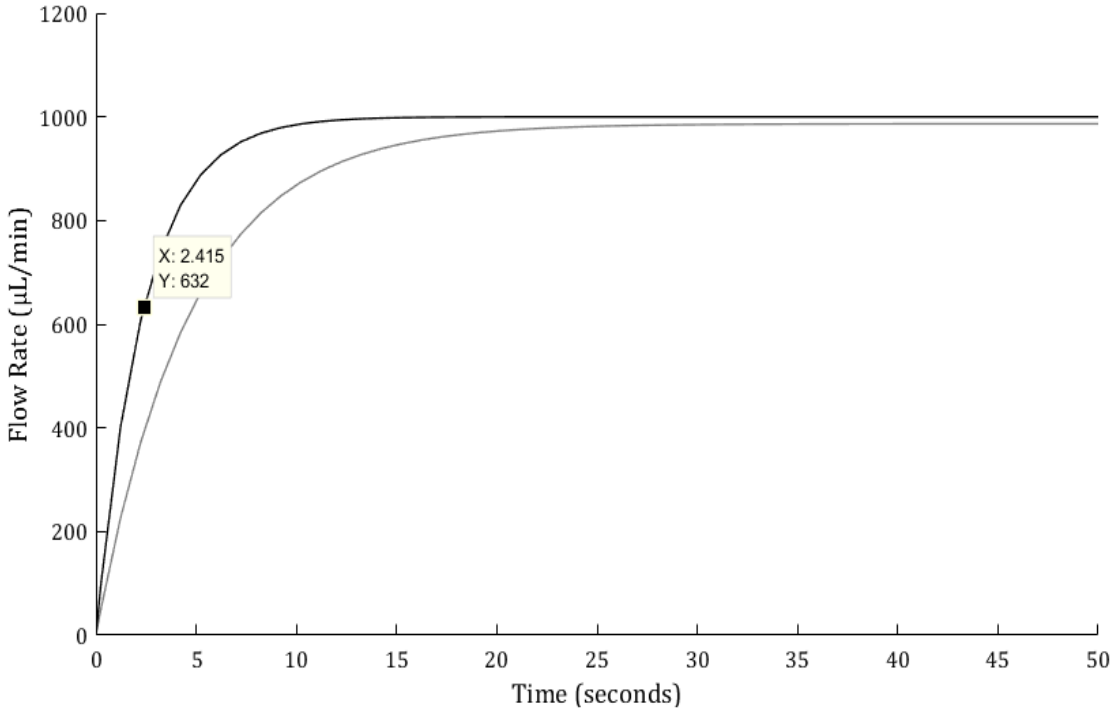

Figure 2.25 - Simulink model output. Data point shows the time constant of the closed-loop response of 2.415 seconds.

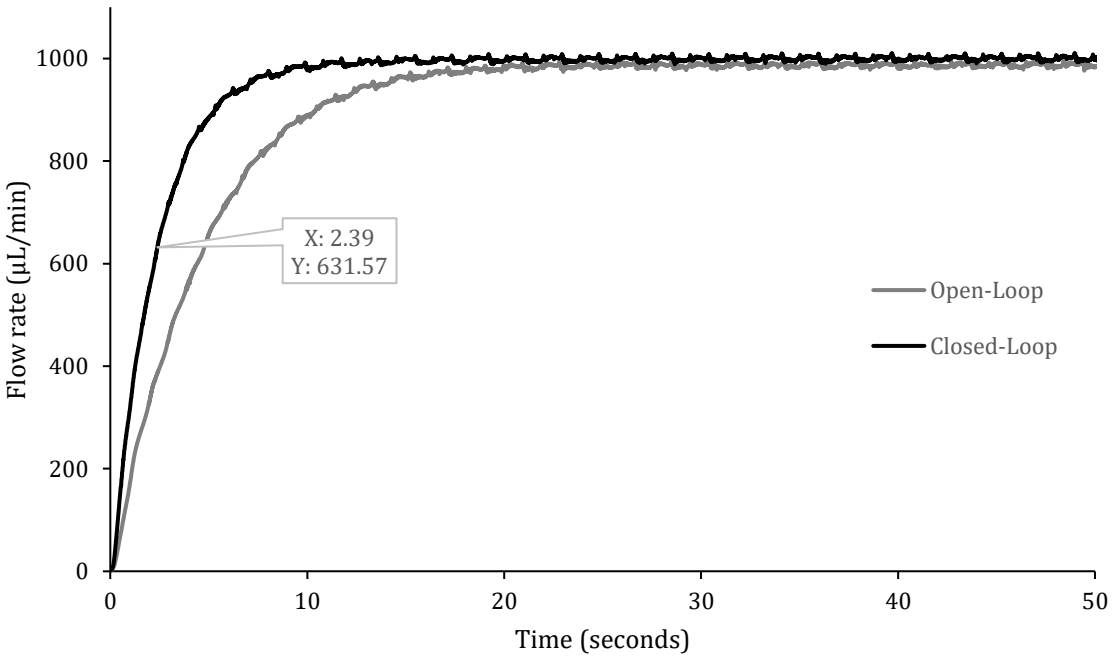

Figure 2.26 – Real world pump response. Data callout highlights the closest datapoint to 63.2% of the final value which gives a time constant of 2.39 seconds.

The correlation between the modelled and real-world systems was good, and the flow rate stability over time was improved. A comparison of the system with and without flow rate control is outlined in chapter 4 and the results presented in chapter 5.

2.4.3 Control commands and interface

Basic control of the pump is achieved through commands sent over a USB serial connection between a computer and the pump's microcontroller. Any serial terminal program can be used to send strings of text to the pump. The firmware interprets the strings and carries out the desired command. For example, a 'ponn' or 'poff' commands turn the pump on and off to the default flow rate of 1000 µl/min. Configuration commands are used to change flow rate, swash plate rotational offset or stepper step time on amongst others. These commands start with a # symbol. To set the flow rate to 1500 µL/min, the user would send #f1500. Features such as closed loop control can be turned on or off using #pf or #pt commands, where p refers to the proportional term in PID control and the 'f' or 't' are the Boolean values of false or true. A full list of serial commands is available in appendix B.

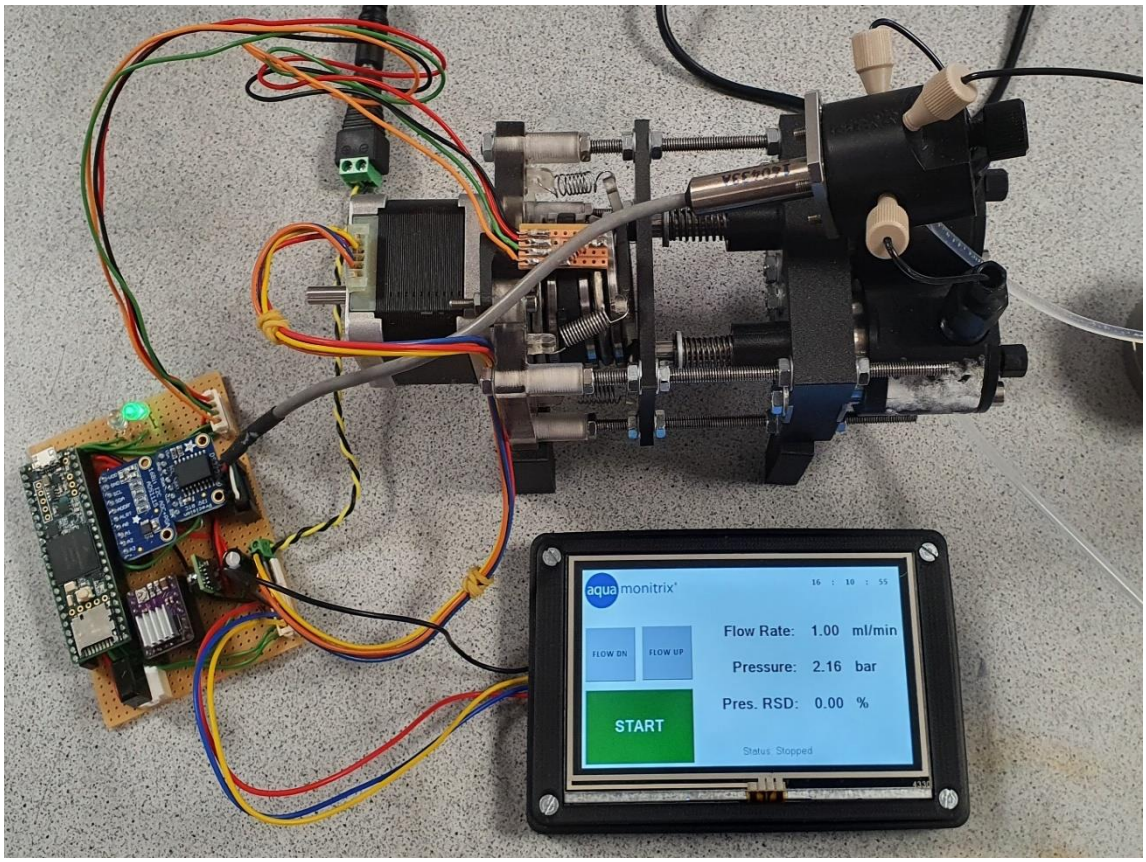

Figure 2.27 - Early prototype pump with HMI attached.

Figure 2.27 shows an early version of the mark 2 pump with the touch screen HMI attached. The HMI itself is a Nextion 4827K043_011 4.3-inch touchscreen. The HMI simply sends the serial commands to the pump microcontroller. While this provided a convenient way to control the pump without a computer, as time progressed a program called SerialPlot was used instead which enabled simultaneous control of the pump and the display and recording of parameters such as pressure, flow, and piston displacement.

2.5 Chapter 2 conclusion

Chapter 2 introduced the novel swashplate high pressure pump and described the advantages of the pump developed in this research over conventional axial piston pumps. The theory of operation was introduced and described how the control of the velocity of the swashplate with a sinusoidal profile, pressure pulsations generated by the movement of the pistons can be greatly reduced. The development path of the pump was presented, highlighting design changes required for more robust operation while a detailed insight of the electronics developed, and control methodologies used was presented.

Chapter 3 Portable system development

Secondary to the development of the pump within this research project was the design and assembly of a system to demonstrate the swash plate pump in a portable unit. This chapter gives a high-level overview of the portable HPLC system and goes on to describe the critical components such as the injection valve and detection cell in more detail.

3.1 Portable system overview

The portable unit was designed to showcase the pump in a robust mobile platform. The portable HPLC system combines four separate subsystems that operate simultaneously. These include the swash plate pump described in chapter 2, the detection system, the injection valve, and the touchscreen HMI. Figure 3.1 illustrates the relationship of these subsystems.

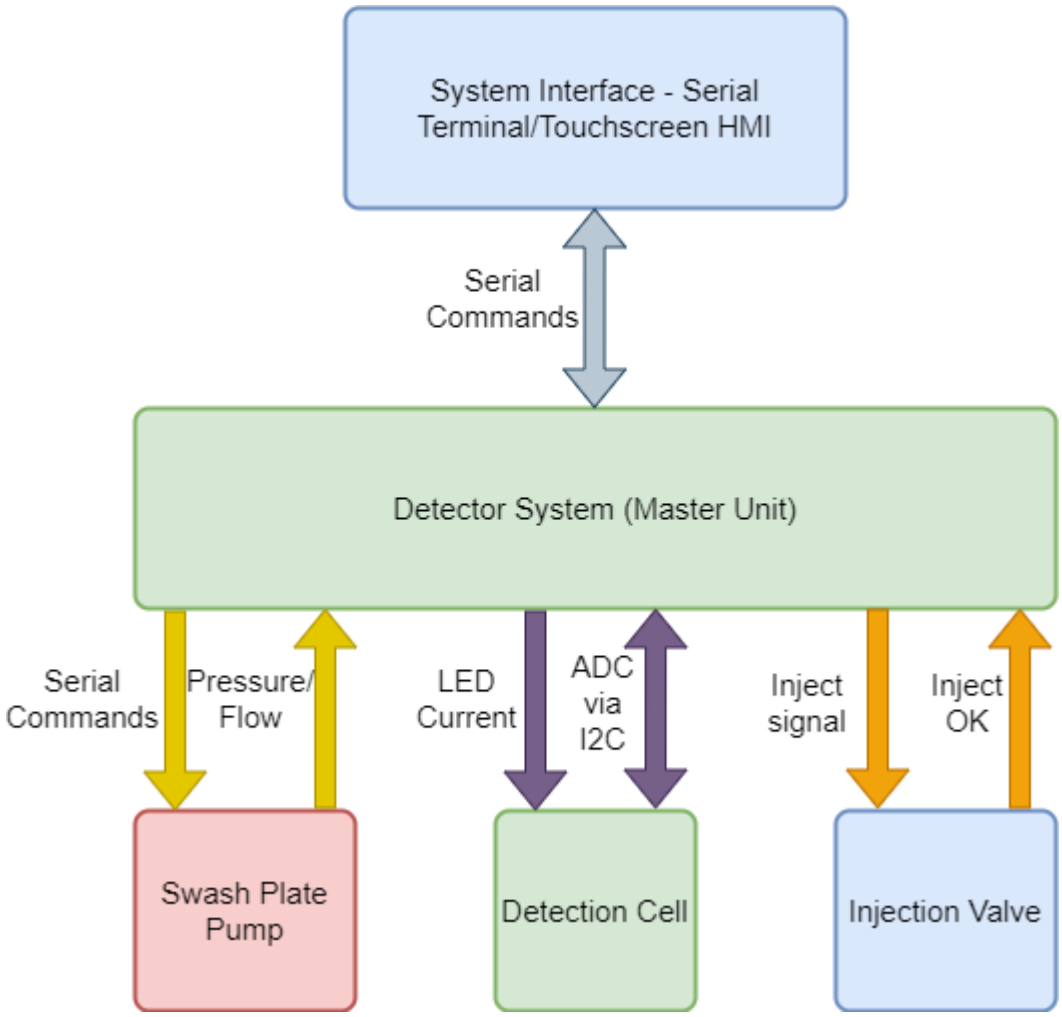

Figure 3.1 - Diagram of the portable HPLC subsystems and their basic inputs and outputs.

Each subsystem can be operated independently using serial commands over a USB connection using a computer. In the case of the portable HPLC system, the detection system acts as the master controller. It asserts control over the swash plate pump and the injection valve, as well as performing data acquisition of signals from the detection cell. The detection system issues commands to the swash plate pump and receives pressure and flow data *via* serial connection. The injection valve is controlled by a simple on/off signal.

A high pulse to the inject pin on the injection valve control board will switch the injection valve to the inject position. After a set period, the valve returns to the load position. The detection system receives a high signal from the injection valve when it reaches the inject position. The detection cell consists of an LED and photodiode. The detection system controls the LED current and reads the signals from the photodiode. Finally the user interfaces with the system through a touchscreen with a simple HMI. The HMI provides basic functionality to start and stop the pump, acquisition, perform manual injections, monitor pressure, and flow values. Figure 3.2 shows the assembled portable system.

Figure 3.2 – Assembled portable HPLC.

The portable system is housed inside a PELI 1510 case onto which a stainless steel backplate is bolted. This combination of case and backplate was used in portable analysers developed in the European funded LIFE Ecosense Aquamonitrix Project – Grant Number: LIFE 17 ENV/IE/000237. Using these parts sped up development time and offered a solid base to build upon. Because the back plate had threaded studs tailored to the system developed in the LIFE project, custom brackets were designed to utilise these studs to mount the pump and other components in a configuration that enabled easy access. Like the swash plate pump development, a digital assembly created using Fusion 360 design software. This allowed the placement of components to be trialled prior to the manufacture. Brackets, clips, mounts, and covers were all rapidly manufactured using the in-house Markforged Mark Two printer. This simplified the design process and realisation of the required pieces. A detailed breakdown of the portable HPLC follows.

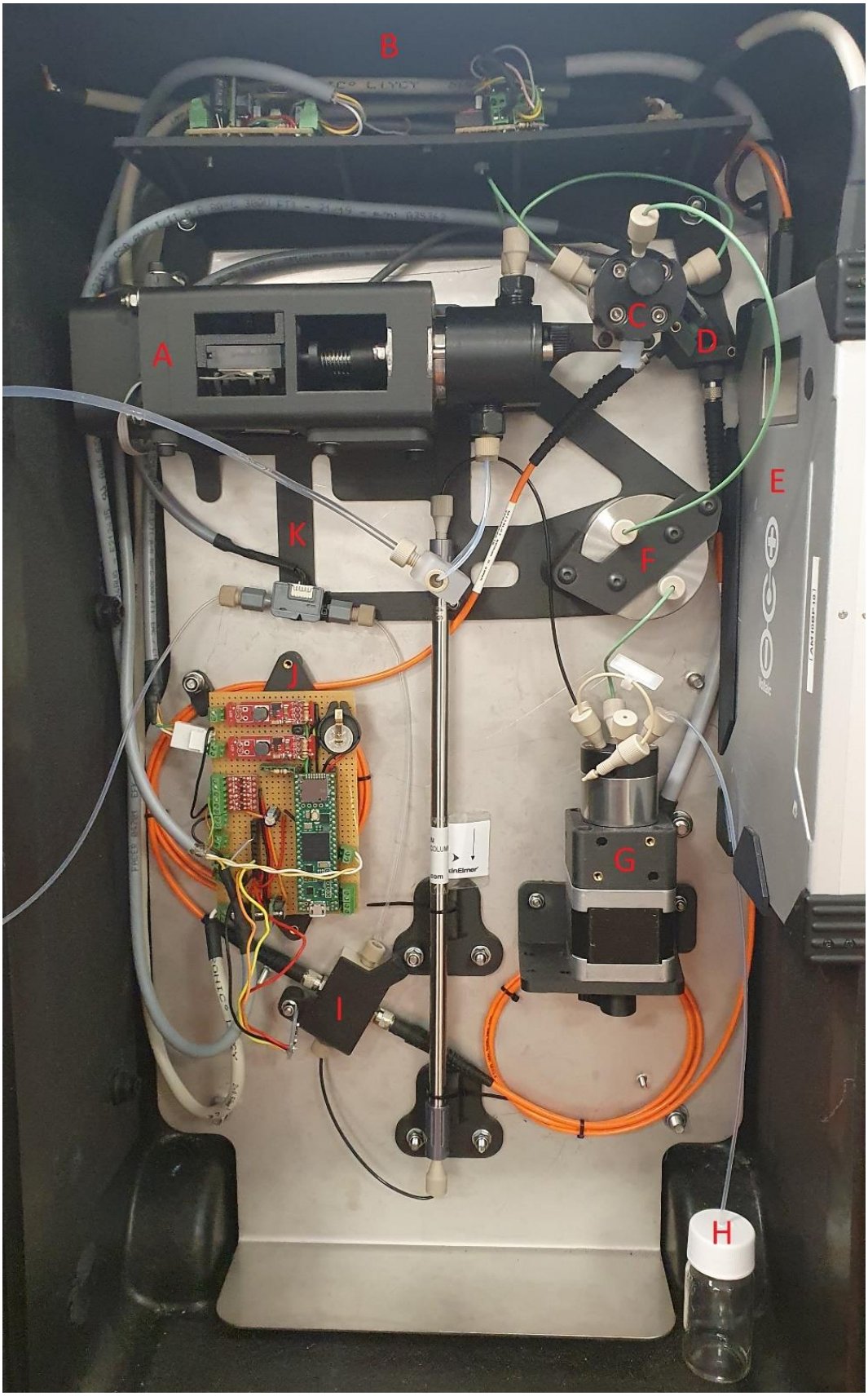

Figure 3.3 - Detailed view of portable HPLC interior. Legend: (A) Swash Plate Pump; (B) Control Electronics Location; (C) Purge Valve; (D) Optical Mount; (E) Battery; (F) Pulse Dampener; (G) Sample Injection Valve; (H) Sample Waste Vial; (I) Detection Cell; (J) Detection System Electronics; (K) Flow Rate Sensor.

Examining figure 3.3 previous, the components are positioned in a way to reduce the chance of leaks onto critical components and air entering the fluidic system after the pump (A). Two of the three electronic modules and the power distribution module are located at the top of the system (B), safe from any potential leaks. The purge valve (C) is the highest fluidic point inside the case to aid the changeover of mobile phase. The LED and Photodiode (D) are mounted in the top-right of the system to eliminate any contact with mobile phase and to minimise the emission of UVC light. Fibre optic cables are used to carry the light into and out of the detection cell. The 24 Volt battery (E) is located on the right-hand side of the case, the same location as used in the LIFE project sensor systems. The pulse dampener (F) as discussed in Chapter 2, and injection valve (G) are mounted below the purge valve. Waste from sample injections is collected in the glass vial (H). The detection cell (I) is orientated in a way that is recommended by the manufacturer, which minimises the chance of an air bubble becoming stuck inside the cell. The main control board (J) is located left-of-centre and is protected by a cover and is offset from the backplate in case of any leaks from the flow sensor (K) above. The separation column is located in the middle of the system for easy access. Two brown glass 1 litre bottles are mounted to the door and are visible in figure 3.2. These are used for the storage of mobile phase and capture of waste. Figure 3.4 below shows a diagram of the fluidic system in the portable HPLC.

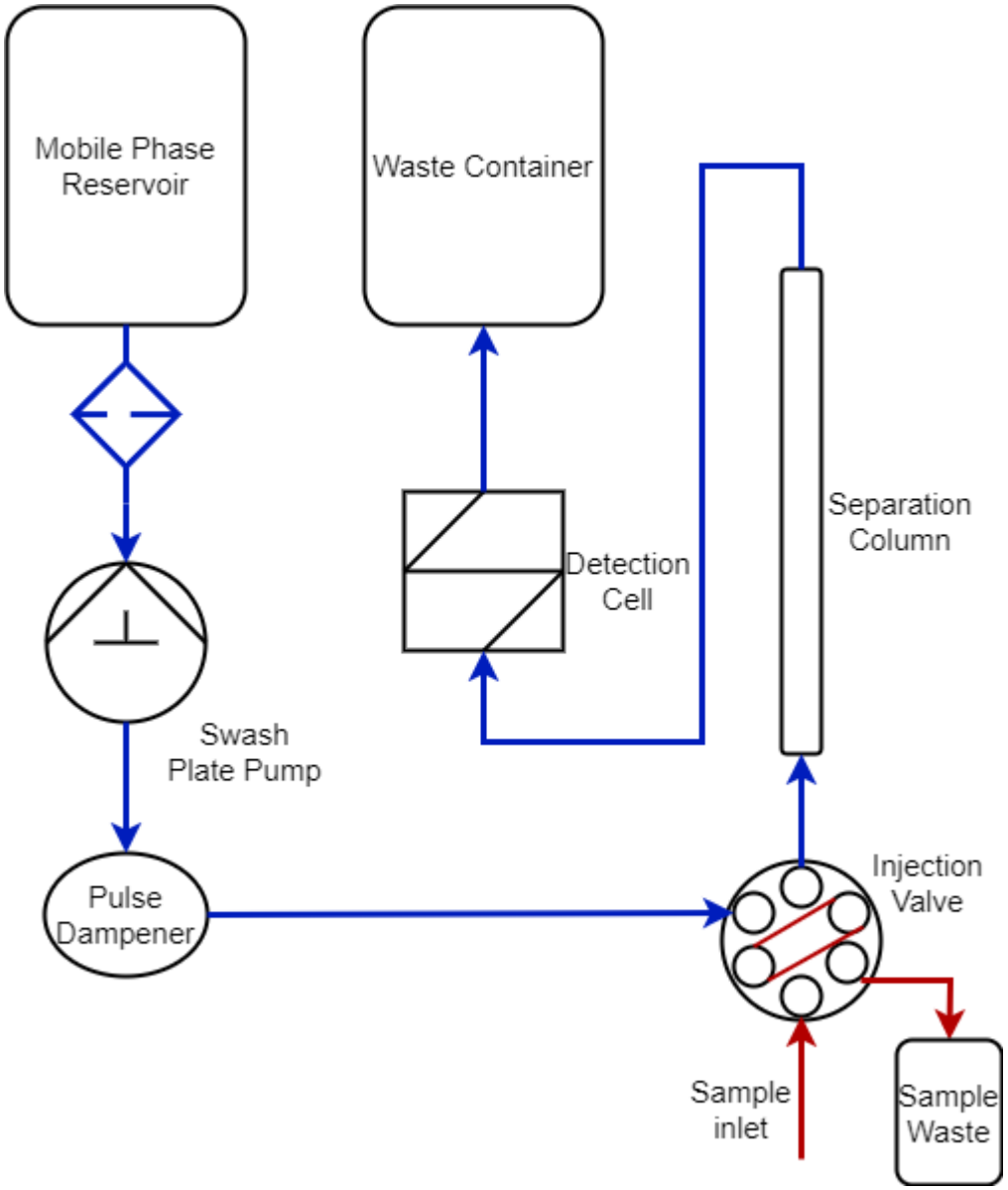

Figure 3.4 - Diagram of the fluidic system used in the portable HPLC.

The configuration shown in figure 3.4 is the path the mobile phase follows through the system during operation. The pump draws from the mobile phase reservoir, in through a filter and out through a pulse dampener. The mobile phase then enters a customised 6-port two position injection valve. This customised valve is discussed in more detail in section 3.2. The sample loop is manually loaded through a needle injection port and is collected in a waste vial. The mobile phase continues out of the injection valve and through the separation column. From there the detection cell and flows into a waste container.

3.2 Automated Injection Valve

3.2.1 Valve Design

To develop the automated injection valve a VICI C2-1346 manual valve was modified by removing the lever and coupling to a stepper motor with control electronics. While off-the-shelf options are available, the option to modify the existing manual valve was simplified by the fact that the specifications for the manual valve were exactly what was required for the portable HPLC system. The final valve design and a view of the internal coupling between the valve and the motor is detailed below in figure 3.5.

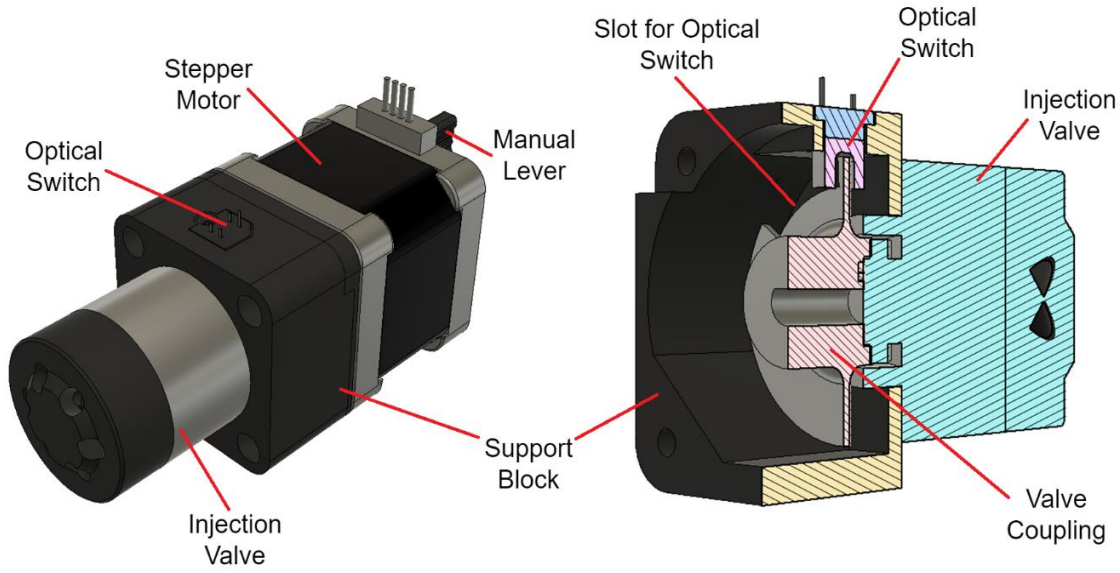

Figure 3.5 - Injection valve design detail.

The VICI valve is coupled to the stepper motor by a custom design support block which aligns the stepper and valve rotor. A coupling with a slot to trigger the RPI-352 optical switch connects the motor shaft to the injection valve rotor. A manual lever is attached to the rear shaft of the stepper motor to enable manual actuation of the valve if required.

3.2.2 Valve Control

The injection valve required a 24 Volt DC supply for the Sanyo Denki 103H5208-5210 double shaft stepper motor which was stepped down to 5 Volts using a Murata OKI-78SR-5/1.5-W36-C DC-DC switching regulator for the embedded system. Stepper motor control used the same stepper motor driver as the swash plate pump, a Texas Instruments DRV8825. The driver is controlled using a DFRobot Beetle which is a miniaturised version of an Arduino Leonardo. A schematic of the injector control board is available in appendix E. Due to the limited number of pins available on the Beetle microcontroller, the step size selection pins were hardwired directly to enable 1/8 step size. The microcontroller controls

the direction and speed of the valve during load and inject operations. The inject operation is triggered by either an externa signal or by using a toggle switch mounted to the control board. Jumper pins are used to select either the switch or external signal and route it to the microcontroller. When a logic high signal is received by the microcontroller, the stepper motor is moved 400 steps clockwise to rotate the valve rotor to the inject position. When the optical switch signal transitions from a logic high value to a low value, the valve is said to be in the inject position and the microcontroller sends a signal out to any external device connected such as the detector board in the portable HPLC. After a set period which is configured in the firmware, the valve returns to the load position and the microcontroller waits for the next signal.

3.3 Detection system development

3.3.1 Detection system design

The detection system in the portable HPLC is designed around an off-the-shelf z-cell manufactured by FIAlab. The z-cell is made of PEEK which was chosen for its chemical compatibility with a wide range of liquids. It has a 10 mm path length and an internal volume of 6 µL. The z-cell was selected to be as close a match to the Dionex VWD 3400-RS flow cell which has a 10 mm pathlength cell with an internal volume of 11 µL. An important feature of the selected cell is the use of SMA-905 connectors to secure the sapphire windows in place. By choosing to run fibre optic cables to the z-cell rather than directly mounting the LED and photodiode to the cell, issues with leaks were mitigated. Fibre patch cables specifically for use with UV wavelengths were sourced from Thorlabs with a 600 µm core selected as recommended by FIAlab. Figure 3.6 gives a high-level overview of the detection system.

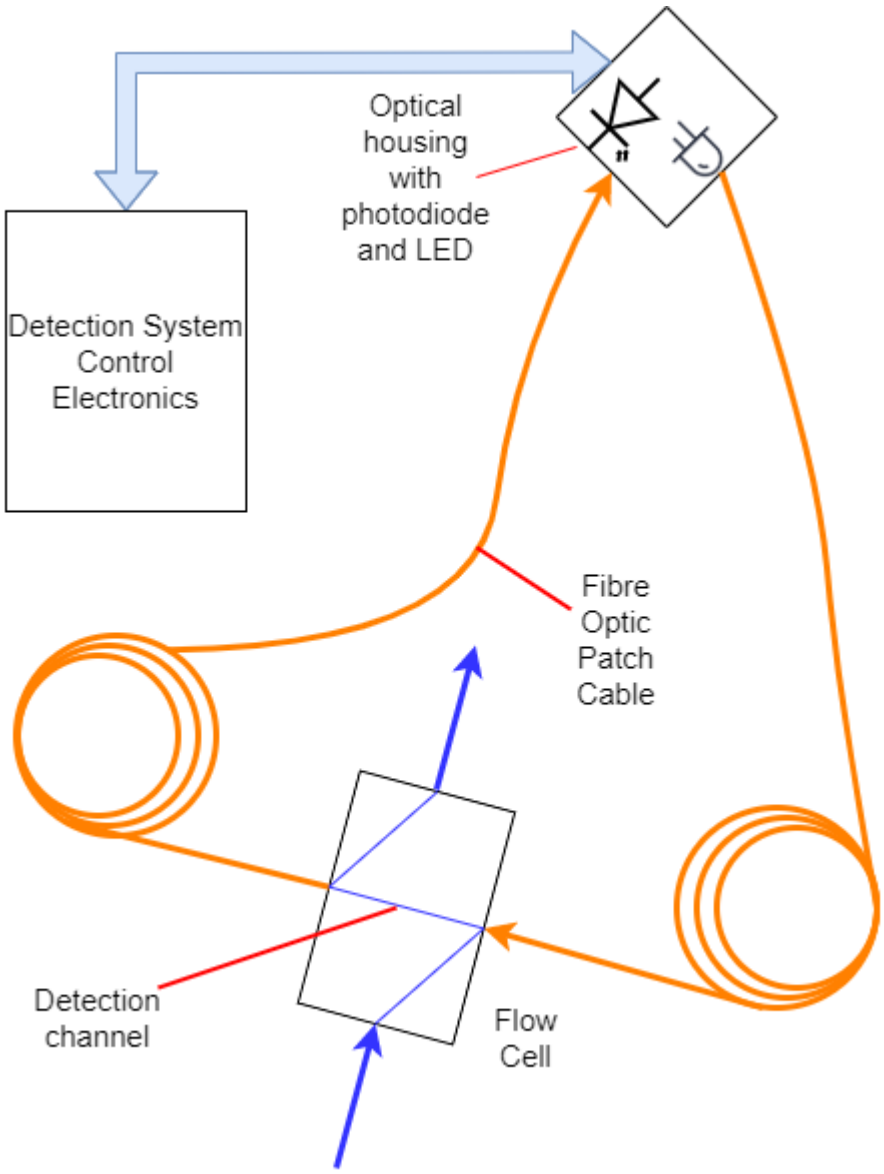

Figure 3.6 - Detector system layout.

The portable system relies on a LED to generate light at a fixed wavelength. The number of LEDs available is limited to the 250 to 280 nm region of the UVC range although there are some offerings at 235 nm also. Early UV detectors utilised low pressure mercury lamps which had peak intensities around 254 nm and became a popular wavelength for use when developing methods. A Seoul Viosys surface mount LED with a peak wavelength of 255 nm was chosen for use in the portable system. The LED is driven with an AL8805 constant current driver and makes use of a PWM input to control the intensity of light emitted. The LED was coupled to the end of one fibre patch cable while a UVC photodiode was coupled to the end of the other to create an enclosed optical path that passes through the flow cell's detection channel. As detailed in Chapter 1, in photometry different compounds absorb light in different regions of the spectrum of light. Within the portable detector system, light transmitted through the detection channel is absorbed by any compounds that have high

absorbance around 255 nm. As the concentration of a compound increases, more light is absorbed and transmission through the cell decreases. On the detection side, the transmission signal is detected by an Sglux TOCON C1 photodiode paired with a Texas Instruments ADS1115 16-bit ADC. The LED and photodiode were mounted away from any fluidic components within the system and shielded cables were routed to the detection system control board. A Teensy 4.1 equipped with an ARM Cortex-M7 microcontroller acquires the data from the ADC, processes it and stores it on a microSD card. A schematic of the detector control board is available in appendix E.

3.3.2 Data acquisition and processing

Choosing the correct sampling rate for a LC detector is important. Too high of a data rate can result in large data files for each separation while too low a data rate may lead poorly defined chromatographic peaks. The first peak in a chromatogram is the narrowest as its molecules spend less time interacting with the stationary phase. Because of this, the molecules stay together in a tight band as they exit the column. This results in a sharp peak being detected. As analytes spend more time interacting with the stationary phase, the band of molecules spread out as they move through the column. Their respective bands are wider as they emerge from the column and flow into the detector. As separations become more efficient, the initial peaks become narrower. While there are many suggested data sampling rates [65], in general a minimum of 8 to 10 data points is required across a peak to enable good reproducibility when repeating separations, while 15 to 20 data points is enough to expose any featured in the chromatogram due to co-elution [66]. Chromatograms generated by a Dionex VWD 3400-RS from separations carried out using a performance check standard (Phenomenex AL0-3045) and a HPLC isocratic systems diagnostics mix (Merck 48270-U), were examined. The system operated at a sampling rate of 20 Hz and peak width at half height for the narrowest peaks was measured for each standard. From these measurements, a minimum data sampling rate was calculated for 15 points across the width of a peak. This was done by dividing the peak width in seconds by the number of points required. The inverse of the resulting period between each point represented the frequency of sampling.

Table 3.1 - Data sampling rate for 15 points across peak width.

Component	*Peak Width - Half Height (minutes)*	*Sampling Rate (Hz)*		
		8 points	*15 points*	*20 points*
Uracil	2.8	2.86	5.36	7.14
Methylparaben	4.65	1.72	3.23	4.30

The sampling rate figures presented in table 3.1 show the frequency required to represent a chromatographic peak with the number of data points outlined. When looking to implement a sampling rate in the portable detector system, 20 data points was selected based on the results from the Uracil peak analysis. Rounding up the calculated sample rate value for Uracil, a minimum sampling frequency of 8 Hz would be required. However as the Dionex VWD 3400-RS detector had been used at 20 Hz for all experimentation and testing, the portable detector system was set to 16 Hz as it was as close to the Dionex detector as possible using the software library for the analogue to digital converter.

The ADS1115 is a delta-sigma type ADC, which samples the input signal at 250 kHz. The signal is filtered and averaged based on the configured output sampling rate. The lower the output sampling rate, the more samples are averaged, the lower the noise on the output signal. The ADS1115 has configurable sampling rates from 8 Hz to 860 Hz. Within the detector system firmware, a software library for the ADS1115 ADC was configured to sample the TOCON C1 photodiode signal at a rate of 32 Hz. The ADC was configured to sample continuously and send a signal to the microcontroller when a sample was ready to read from the register. When the microcontroller receives the signal, it executes an interrupt function which reads the value from the ADC and stores it in an array. This array is part of a running average filter which was configured to average 24 samples. The running average value was sampled at 16 Hz for the final output which was written to a CSV file and stored to the microSD card.

As discussed in section 3.3.1, the portable detector system measures the transmission of light through the optical cell. The transmittance signal T from the flow cell can be defined as the ratio of the transmitted intensity I to the incident intensity I_0 [67].

$$T = \frac{I}{I_O} \tag{3.1}$$

To generate comparable chromatograms, the transmission value must be converted to absorbance. Absorbance can also be calculated by the relationship between the incident intensity I_0 and the transmitted light I based on Beer's Law as follows:

$$Absorbance = log_{10}\frac{I_0}{I} \tag{3.2}$$

Transmission and absorbance have an inverse relationship. That is, when transmittance is 100%, absorbance is zero. Therefore equation 3.2 above becomes:

$$Absorbance = log_{10}\frac{1}{T} \tag{3.3}$$

When processing the transmittance values stored on the microSD card, Microsoft Excel was used to convert the values to absorbance. A portion of the transmittance signal before the initial peak was used as the incident intensity, where no absorbance is occurring, and transmission is therefore at 100%. The converted data was then imported into Unichrom software where peak areas and retention times were calculated.

3.4 Portable system control

3.4.1 Control commands

In a similar way to the swash plate pump, control and communication with the system is carried out through a serial terminal program. The Teensy 4.1 development board enables direct serial commands to be issued to the system *via* USB connection. While any serial terminal program can be used, a program called SerialPlot was the preferred serial terminal software as it could graphically display real-time data from the system and can store multiple commands that can be sent with the press of a button. Figure 3.7 shows an early prototype connected to a laptop running SerialPlot software with a transmission plot visible on-screen.

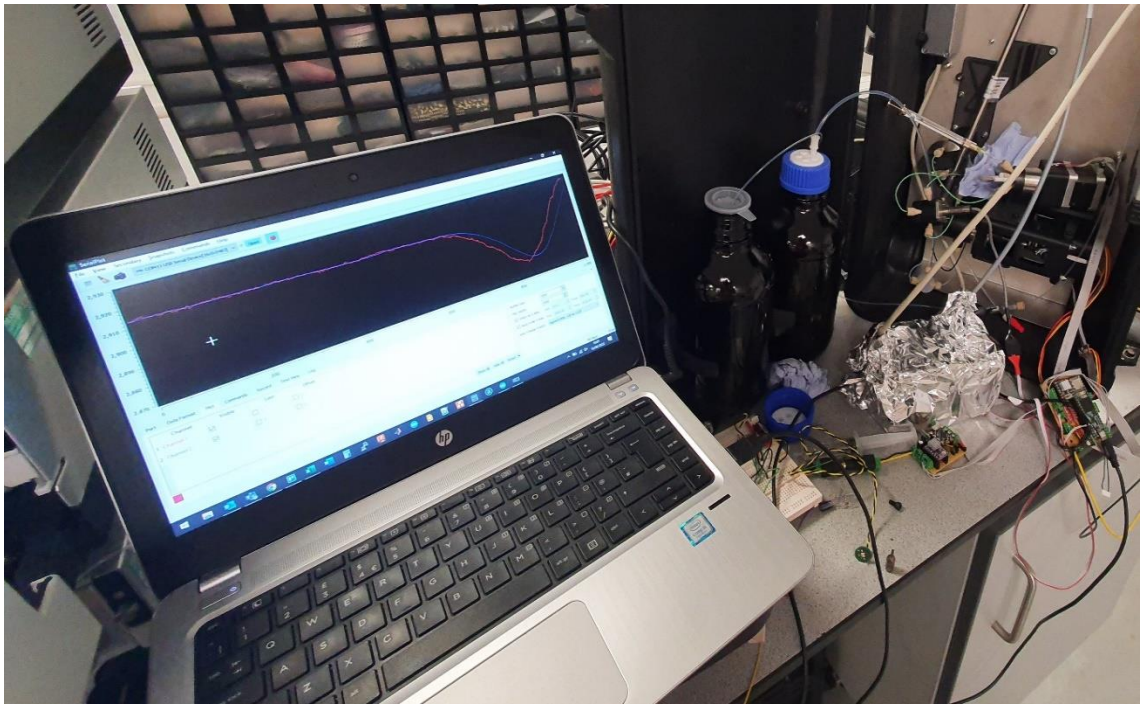

Figure 3.7 - Early portable HPLC prototype with real-time transmission plot using SerialPlot software.

When communicating with the detector system, simultaneous control of the detector, injector and pump was enabled. For example sending an 'init' command would initialise the system by turning on the LED and pump. A 'run' command would check that the 'init' command had been issued, switch the injector valve to the inject position and begin data acquisition. A full list of serial commands for the system is available in appendix B.

3.5 Chapter 3 conclusion

Chapter 3 gave a high-level overview of the development of the portable liquid chromatograph in which the pump described in chapter 2 was used. Customisation of an off-the-shelf manual injection valve was presented along with the development of the detection system for UV analysis of samples injected onto the column. Finally, the integration of control methods of the valve, detector and pump was described.

Chapter 4 Pump experimental methods, procedures, and results

This chapter is split into two sections. Section 4.1 deals with the experimental setup and procedures carried out to determine the performance of the swash plate pump while section 4.2 presents and discusses the results from the experiments described in section 4.1. For chapters 4 and 5, "benchtop pump" shall be used to represent the Dionex LPG-3400M HPLC pump, while the term "benchtop detector" will represent the Dionex VWD-3400RS UV-Vis detector. The combination of the Dionex pump and detector shall be referred to as the "benchtop HPLC." This will help distinguish between the benchtop and portable components being compared.

4.1 Pump characterisation and performance

While there are resources relating to the installation and operational qualification of HPLC systems, little information is available for the performance verification relating to LC pumps themselves. Therefore a combination of sources was assessed to compile a list of parameters important to the performance of an LC pump. According to Snyder [23] the most important specifications include short-term precision, pump noise, drift, and accuracy. The pump performance attributes detailed by Herman Lam [68] include flow rate accuracy and a pressure test. Datasheets from a selection of modern HPLC modular and standalone pumps were examined for common performance specifications [69][70][71][72]. Along with parameters assessed such as power consumption, table 4.1 below summarises the specifications selected for characterisation.

Table 4.1 - Outline of pump performance parameters measured and their analytical impact.

Section	*Parameter*	*Requirement*	*Potential Impact*
4.1.1	Power Consumption	Not specified	Limit the number of samples carried out in the field.
4.1.2	Piston Displacement Profile	Linear delivery stroke	Less than ideal stroke will cause pulsations.
4.1.3	Flow Rate Accuracy	±2% [68]	Important for transfer of methods between systems, repeatability of retention times.
4.14	Flow Rate Drift	Not Specified	
4.1.5	Pressure Ripple	±2%[74]	Peak area variability.
4.1.6	Pressure Leak Test	Pressure decay: < 5.17 bar/min [68]	Flow issues, pump noise in chromatogram baseline.
4.1.7	Repeatability Assessment	±3% for precision. [74]	Important for transfer of methods between systems, repeatability of retention times.

4.1.1 Power consumption

Power consumption is an important factor when it comes to selecting components for portable battery powered systems. With the approach taken in this research, analysis times are similar to those seen on laboratory systems; up to 15 minutes per sample. Therefore an efficient pumping solution is required to maximise run-time in the field.

Experimental setup

To determine the power consumption of the pump, the current in milliamps was measured with the pump under load. To generate the load on the pump, a 50 cm length of PEEK tubing

with an inner diameter of 75 µm was connected to the outlet port of the pulsation dampener and was fed back into the water reservoir. This was to generate a back pressure that the pump would be subjected to under normal operating conditions. PTFE tubing of 3.175 mm inner diameter was connected to the inlet tee of the pump and a filter attached on the intake end. The filter was placed into a reservoir containing deionised water. A Keithley 2110 digital multimeter was combined with KI-Tool software running on a computer to capture the power demand. The multimeter was connected in series between a 24 Volt power supply and the pump control board as seen in figure 4.1. To measure the current draw, the positive terminal of the power supply was connected to the input terminal of the multimeter. The output from the multimeter (ground terminal) was then connected to the positive terminal of the pump control board. The negative terminal of the power supply was connected directly to the negative terminal of the pump control board. The multimeter was also connected to a computer *via* USB cable, where data was recorded and exported to an excel file.

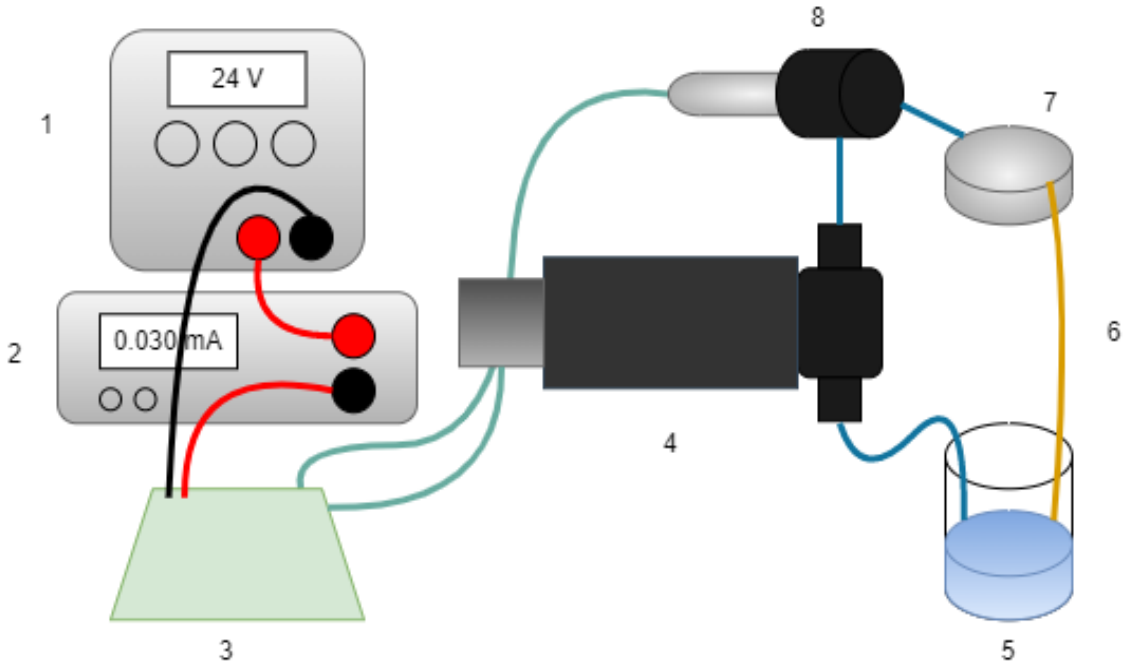

Figure 4.1 - Diagram of power consumption test setup. 1: 24 Volt power supply. 2: Benchtop multimeter. 3: Swash Pump circuit board. 4: Swash Pump. 5: Deionised water reservoir. 6: Pressure tubing. 7: Pulse dampener. 8: Pressure sensor manifold.

Experimental procedure

With the fluidic circuit primed and electronic circuit connected, the power supply and multimeter were switched on. The multimeter was set to the DCI setting on the front panel to view real time current draw. With the pump at rest prior to the experiment starting, the

current draw was noted. The swash pump was set to a flow rate of 1 ml/min and turned on. At this flow rate, it was expected that 107 bar of backpressure would be generated by the deionised water flowing through the 50 cm length of yellow tubing. Next the current limiting potentiometer was adjusted to reduce the current the motor could draw from the stepper driver. Once the stepper began to stall, the potentiometer was adjusted to increase the current until the motor ran smoothly. This set the minimum current required for the swash plate. These steps were completed prior to data acquisition to allow the flow rate to settle.

After approximately 5 minutes, once the flow rate had stabilised the KI-Tool software was started, and communication established with the multimeter. Once connected, the maximum data collection rate was selected and test duration of 15 minutes set, the log data command was executed. When the data logging was complete, the pump was disconnected from the fluidic and electric circuits and the 2 mm swash plate replaced with the next swash plate. The test was repeated for the 3.175 mm and 4 mm swash plates.

4.1.2 Swash plate comparison & piston displacement profile

In a positive displacement piston pump, ensuring the pistons are reciprocating correctly is key to maximum pump efficiency. Deviations in displacement due to mechanical wear, pump malfunction or operation outside of the maximum parameters can lead to unwanted fluctuations in flow rate. To ensure the swashplate pump correctly operates the piston displacement was measured. The piston displacement profile was recorded along with flow and pressure data for the 2 mm, 3.175 mm, and 4 mm swash plates.

Experimental Setup

The objective of this test was to ensure the piston was reciprocating as expected while the pump was operating. The initial examination carried out involved installing each swash plate into the pump to measure the actual linear displacement of both pistons as shown in figure 4.2. The pump heads were removed to facilitate the recording of these measurements. Next, the pump was run with each swash plate in turn where the raw values from the linear transducer were recorded as the swash plate turned. This was carried out with both constant and sinusoidal swash plate velocities to compare them to the ideal displacement profile.

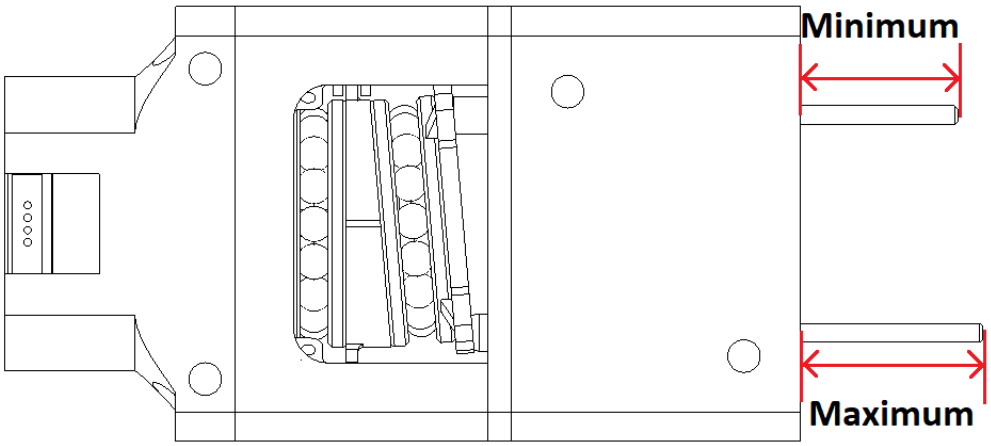

Figure 4.2 - Top-view diagram of swash pump illustrating the maximum and minimum piston position measured for each piston.

Experimental Procedure

The piston measurements were taken using a digital vernier calliper which was zeroed before each measurement. The 2 mm swash plate was installed into the pump. For piston displacement measurements, the swashplate was set so piston A was at the lowest point which ensured piston B was at its highest point. Measurements were taken from the tip of the sapphire plunger to the face of the pump chassis for each piston. The swash plate was manually advanced 180 degrees after which measurements were taken again.

The next step involved recording the values from the linear displacement sensor mounted on the pump. The raw values were recorded for at least 70 seconds. This included the initial 10 seconds with the pump at rest, the next 30 seconds with the swash plate rotating with a sinusoidal velocity and the final 30 seconds with the swash plate rotating at a constant velocity. Data was plotted in excel and compared to the ideal displacement profile.

4.1.3 Flow rate accuracy

Flow rate accuracy is important when transferring methods between LC systems. Differences in flow rate between systems, will result in varying retention times. The accuracy of the flow rate should ideally be independent of operating pressure and ambient temperature.

Experimental Setup

To determine the flow accuracy and precision, the pump was configured as shown in figure 4.3 below. Similar to the power consumption test described previously, the pump was set up to pump through a length of small diameter tubing to simulate normal operating conditions. The outlet was placed into a small glass vial to weigh the contents after every flow rate tested.

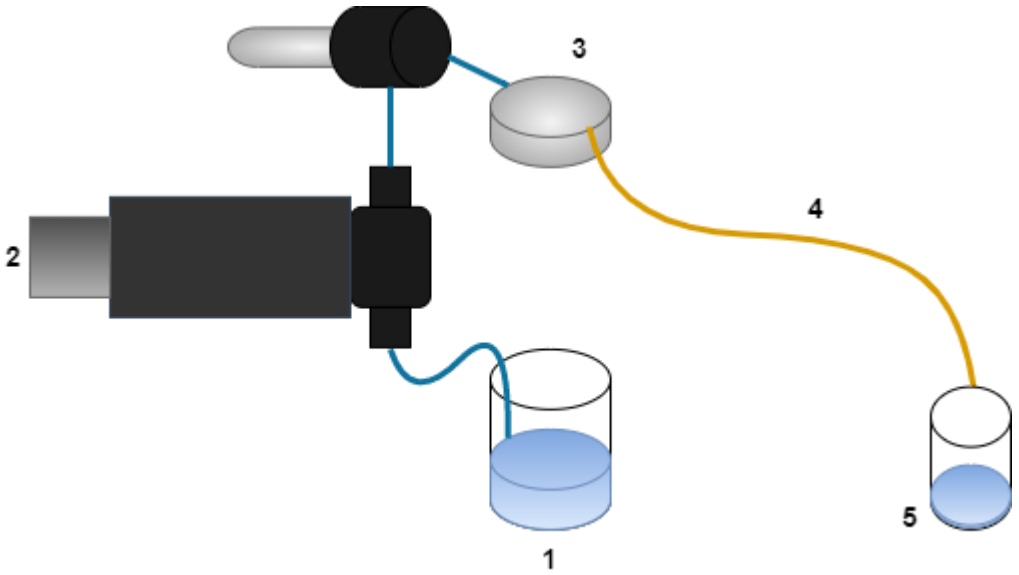

Figure 4.3 - Diagram of flow accuracy and precision test setup. 1: Deionised water reservoir. 2: Swash Pump. 3: Pulse dampener. 4: Pressure tubing. 5: Collection vial to be weighed.

Experimental Procedure

To facilitate collection of water from the outlet tubing 5 dry glass vials were weighed using analytical scales. The dry weight and flow rate was written on the side of each vial for identification. The pump flow rate was set to the initial value of 250 µL/min and the command to start pumping was sent. After a brief period of time, the first glass vial was placed under the outlet and water was collected for 10 minutes. A countdown timer was used to keep track of time. Once the 10-minute period was up, the outlet tubing was removed, and the vial was immediately weighed. This weight was written on the vial and noted in a lab notebook also. This procedure of timed weighing was repeated for each of the remaining flow rates as set out in table 4.2. The accuracy of the pump was calculated using the weight of water collected divided by the length of time it was collected for. The pump flow rate was set to the next flow rate and the procedure repeated.

Table 4.2 - Outline of pump flow rates tested, duration of collection of pump output and expected back pressure.

Flow Rate (µL/min)	***Duration of collection (mins)***	***Back pressure (bar) @ 20°C***
100	10	10.7
250	10	26.8
500	10	53.7
1000	5	107.3
1500	5	161 .0
2000	5	214.7

4.1.4 Flow rate drift

Pump flow rate drift is an important parameter to characterise [23]. Maintaining a stable flow rate over an extended period is important to ensure repeatability of results. While no specific specification is set out for flow rate drift, an approach like that undertaken in ASTM 685 for detector drift was carried out. This involved the recording of flow rate data over the course of at least 1 hour.

Experimental Setup

To measure flow rate drift, the swash plate pump used a similar experiment configuration as the flow rate accuracy was used with the addition of a flow rate sensor. This was used to track the flow rate for the duration of the experiment. Pressure and temperature values were also tracked. All sensor data was collected through a serial monitor on a computer for analysis.

Experimental Procedure

Power to the pump was turned on and data collection through the serial monitor was initialised. The pump flow rate was set to a value of 1 mL/min and the command to start pumping was sent. The test was left to run for a minimum of 1 hour, after which the pump was stopped, and the data collected was saved. This procedure was carried out with the pump in open loop and closed loop control modes to highlight the effectiveness of the control system using the flow sensor.

4.1.5 Pressure ripple

Pressure ripple or pump noise is expected in a reciprocating pump due to the movement of the pistons and the operation of the check valves. Depending on the sample component, pump noise can affect the detection limit of a detector.

Experimental Setup

The analysis of pressure ripple was carried out in two separate experiments. The first experiment involved testing at multiple flow rates on both benchtop pump and the swash plate pump. The experimental setup of this test was like those seen previous, where a 50 cm length of 75 µm inner diameter tubing was used to generate backpressure. Each pump was set to run at increasing flow rates and pressure data was recorded using the pressure sensor from the benchtop pump. For the swash plate pump. the output tubing from the pulsation dampener was connected to the outlet unit of the benchtop pump. The outlet unit houses the pressure sensor and was done to facilitate the long-term reliable collection of pressure data.

The second method for measuring pressure ripple follows the suggested O.I.M.L R112-E94 standard [74] where back pressure of at least 140 bar is monitored, at a flow rate of 1 ml/min over a 10-minute period. A 65 cm length of 0.075 mm inner diameter tubing was used to generate up to 140 bar of back pressure and was connected to the outlet from the benchtop pump pressure manifold. Again, this was repeated for the swash plate pump.

Experimental Procedure

For the initial test, each pump was run with increasing flow rates from 250 µL/min to 2250 µL/min in 500 µL/min increments with data being recorded through Chromeleon software. For the R112-E94 method, the flow rate was set to 1 ml/min and the flow was started. Once the flow rate had settled, the pressure sensor value was recorded using Chromeleon software. Pressure readings for each pump was collected for at least 10 minutes.

4.1.6 Pressure leak test

A pressure leak test is a good indication of check valve and piston seal condition. By pressurising the pump heads and monitoring the pressure drop after flow has stopped any issues with the internal components of the pump heads is exposed. A pressure decay of less than 5.17 bar/min (75 psi/min) is acceptable [68]. Figure 4.4 illustrates the expected response and possible unwanted deviations.

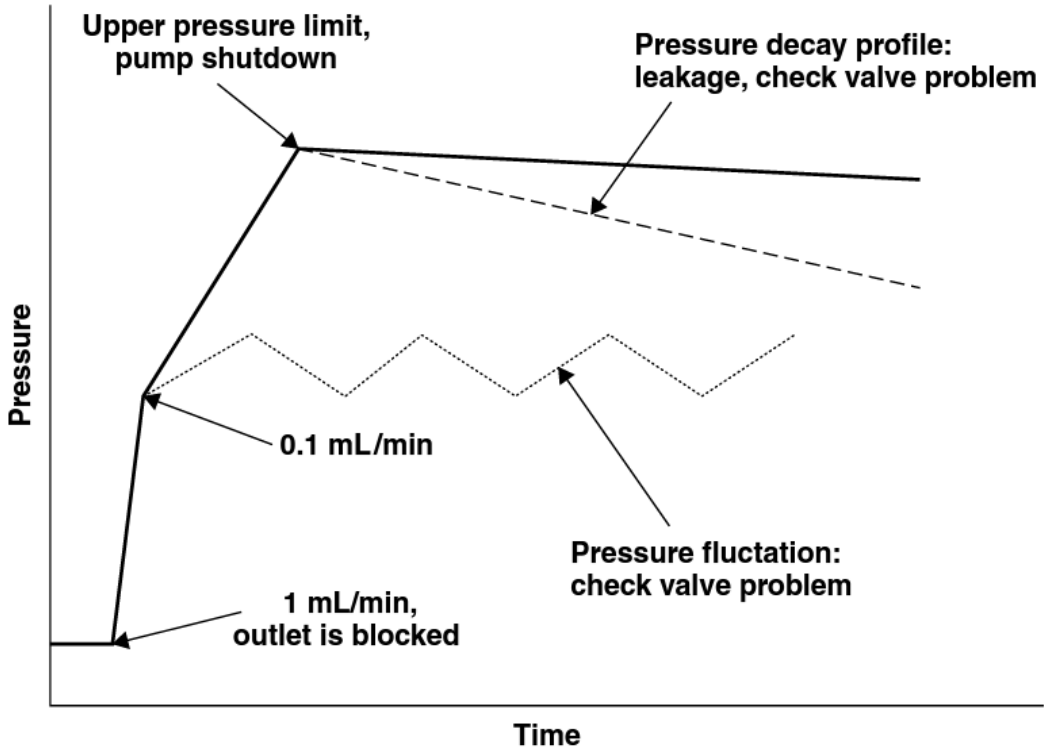

Figure 4.4 - Ideal and undesirable pressure response during a pressure leak test [68].

Experimental Setup

The setup and the procedure outlined below is described in section 11.2.1 of HPLC verification practices by Herman Lam [68]. A glass reservoir was filled with 50 ml of methanol and the pump was primed. The outlet port at the pump pressure manifold was left open with no tubing connected.

Experimental Procedure

The pump flow rate was set to 1 ml/min and the start command was issued. After a few seconds of pumping, a cap was threaded into the outlet port of the pressure manifold. The pressure value was monitored. Once it reached a value of 206 bar (3000 psi) the flow rate was reduced to 0.1 ml/min. Once the pressure reached 275 bar (4000 psi) the pump was stopped, and the pressure drop recorded for a duration of 15 minutes.

4.1.7 Pump repeatability and flow rate precision

As detailed in chapter 1, a poor performing pump can lead to issues with retention times, peak areas, and baseline noise. To validate the work done to develop the pump, a repeatability study was carried out to observe the operational performance of the pump. A column performance check standard was obtained (Phenomenex AL0-3045) and 120 injections were carried out over three days within a 5-day period.

Experimental Setup

Fluidic setup

This assessment was carried out using the benchtop HPLC. To assess the swash plate pump, it was integrated into the LPG-3400M pump. This would allow the software controlling the benchtop HPLC to operate as normal during analysis, while the swash pump was delivering solvent in place of the benchtop pump. 1.375 mm inner diameter PTFE tubing was connected to the swash pump inlet tee with a filter placed on the intake end. This was then placed into the solvent reservoir. As illustrated in figure 4.5 below, the outlet tubing from the equilibration head (1) was disconnected from the outlet unit (2). The outlet tubing from the swash pump was connected to the input port (3). This would allow pressure values to be collected during each sample analysis. The automated injection valve outlined in chapter 3 was used to perform the injections of sample onto the column. The outlet port (4) of the outlet unit was connected to this injection valve through which the solvent flowed on to the column and detector. The samples were analysed using the benchtop detector and captured using Chromeleon software.

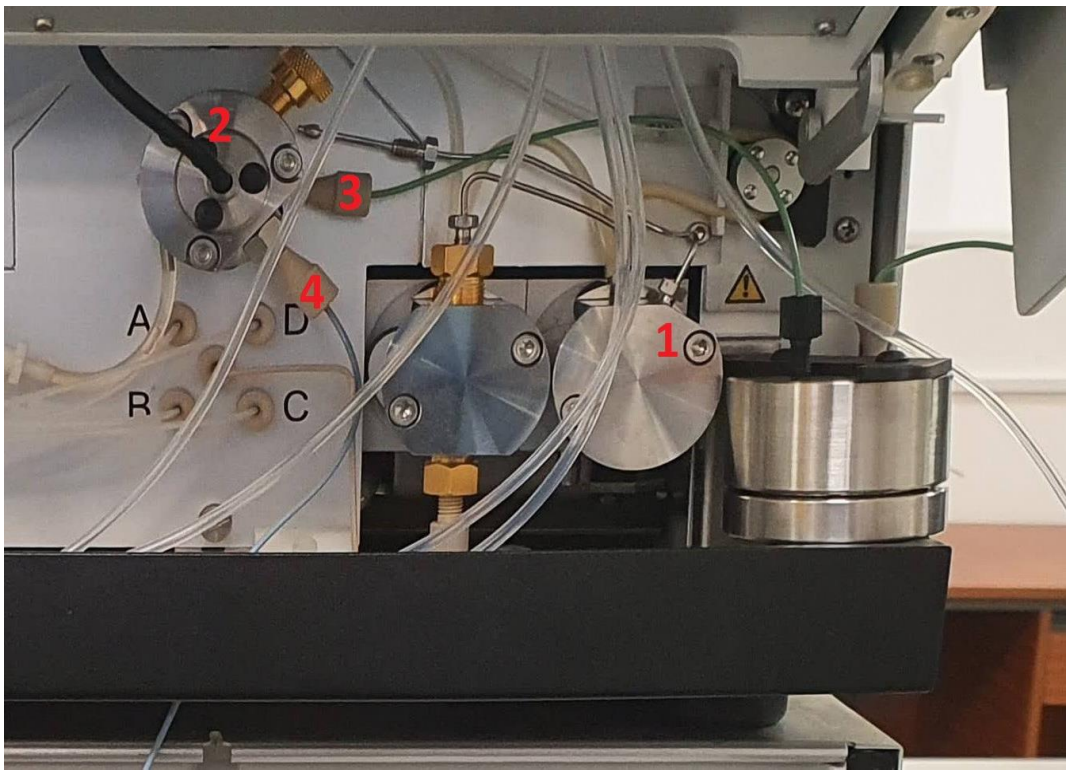

Figure 4.5 - Integration of swash plate pump with Dionex LPG-3400M HPLC pump.

Electronic/Software setup

This software would enable a simplified way of comparing the chromatograms, looking at aspects of each chromatogram such as retention factor, peak area, and baseline noise. Chromeleon has the ability to create a control program which executes control commands in a sequential manner. This enabled precise and repeatable data acquisition for each sample injected. The program written and used for this experiment was as follows:

Pressure.LowerLimit = 0 [bar]

Pressure.UpperLimit = 358 [bar]

MicroPump_Pressure.Average = On

0.000 Autozero

Wait Ready

Inject

MicroPump_Pressure.AcqOn

UV_VIS_1.AcqOn

10.00 MicroPump_Pressure.AcqOff

UV_VIS_1.AcqOff

End

A sequence of 120 samples was created to which the program above was applied to. By utilising the digital input ports on the benchtop pump, the software was configured to start data acquisition when a positive 5 Volt signal was applied to the digital port. This 5 Volt signal was generated when the automated injection valve was commanded to inject. After 10 minutes of data acquisition, the system would wait for the next injection to occur. This was repeated for the 120 samples.

The Phenomenex AL0-3045 column performance check standard contained the sample components Uracil, Acetophenone, Toluene and Naphthalene. Uracil is of importance as it is the unretained component in the mixture. This means that in theory, Uracil will not be retained by the stationary phase inside the column and can be used to calculate the dead time and void volume at a known constant flow rate. It would also be used to calculate the

flow rate precision. The importance of the dead time is related to the calculation of the retention factors of sample components. The retention factor normalises the retention time, which allows comparison between columns of different lengths or the same length column at a different flow rate [73]. Based on the datasheet for the column performance check standard, the following test conditions were used for the repeatability experiment:

Test conditions

- Column: PerkinElmer Universal H-C18, 250 x 4.6 mm, 5 µm particle size
- Mobile Phase A: Acetonitrile
- Mobile Phase B: Water
- Isocratic, A:B 60:40
- Flow Rate: 1 ml/min
- Injection Volume: 1 µL
- Detection: UV at 254 nm

As the standard was supplied in a 2 ml vial, the decision was made to dilute the solution to 2.5% of its original volume to maximise the number of injections that could be performed for this assessment and other experiments.

Experimental Procedure

Prior to injecting the first sample, the benchtop pump and detector were turned on and left idle for at least 1 hour. This was done to ensure components within the system warmed up correctly and had stabilised. At the same time, the swash plate pump was turned on, the flow rate set to the desired 1 ml/min and started to pump the 60:40 acetonitrile/water mobile phase. This ensured the column was fully equilibrated and the pump flow rate was stable. After 1 hour the 1 µL sample loop was manually loaded with a needle tipped 100 µL syringe through a needle port on the injection valve. 20 µL of standard was loaded to ensure the loop was thoroughly flushed with fresh sample. Once the sample loop had been filled, the inject switch was actuated and the sample was injected onto the column. Data acquisition automatically began as detailed in the previous section. After 10 minutes, the system would wait for the next injection. The sample loop was loaded again and the inject switch actuated. This was repeated for each sample until the end of the day. The initial warm up was performed at the start of each day of the repeatability assessment.

4.2 Pump experimental results and discussion

4.2.1 Power consumption

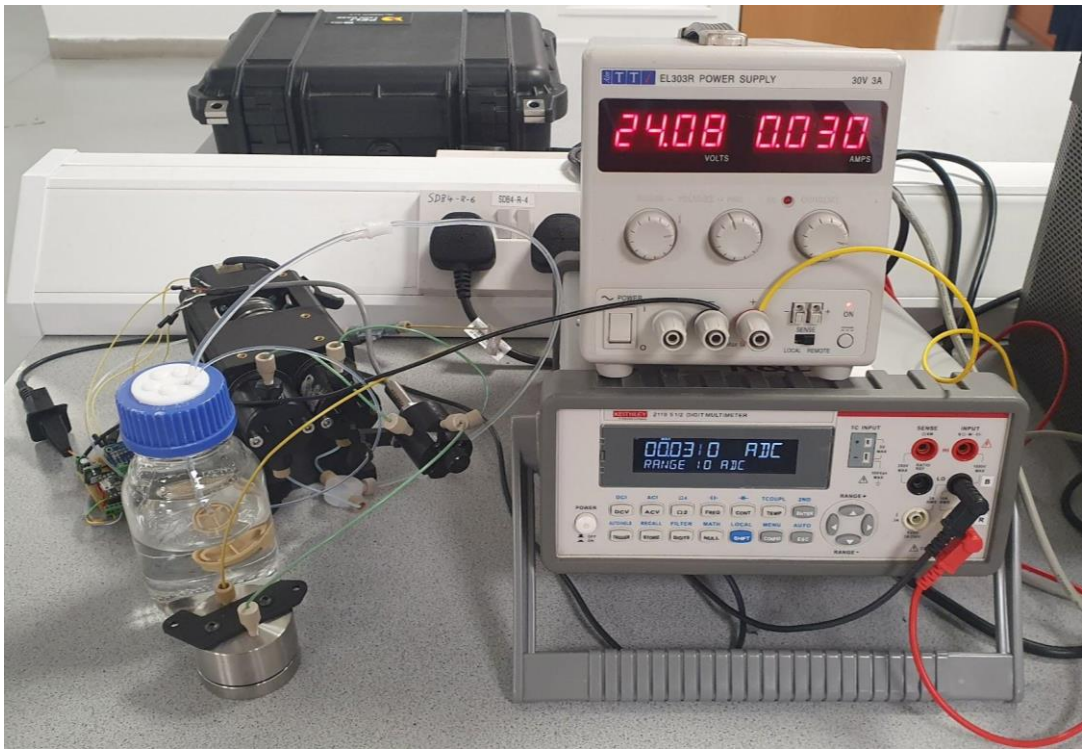

Figure 4.6 - Power consumption test setup.

Figure 4.6 shows the experimental setup used for the power consumption test. Baseline current consumption for the control electronics was noted to be 30 mA. Data was recorded for the 2 mm, 3.175 mm, and 4 mm swash plates. 15 minutes of data was recorded for each swash plate at a rate of 46 Hz. This was the maximum rate the Keithley benchtop multimeter could achieve through the KI Tool software. Table 4.3 below reports the current values measured for each swash plate while figure 4.7 illustrates the processed results, showing the difference in power consumption for each swash plate.

Table 4.3 - Average and peak current values in milliamps measured during the 15-minute test.

Swash Plate Displacement (mm)	***Average Current (15 minutes)***	***Peak Current***
2	107.62	229.81
3	125.41	265.37
4	171.16	296.92

Power consumption is measured in Watts, which is a way of describing the rate of power flow. The system is powered by a 24 Volt supply. By using equation 5.1 below, we can convert the current values measured into Watts.

$$Power\ (Watt) = Voltage\ (Volts) \times Current\ (Amps) \tag{5.1}$$

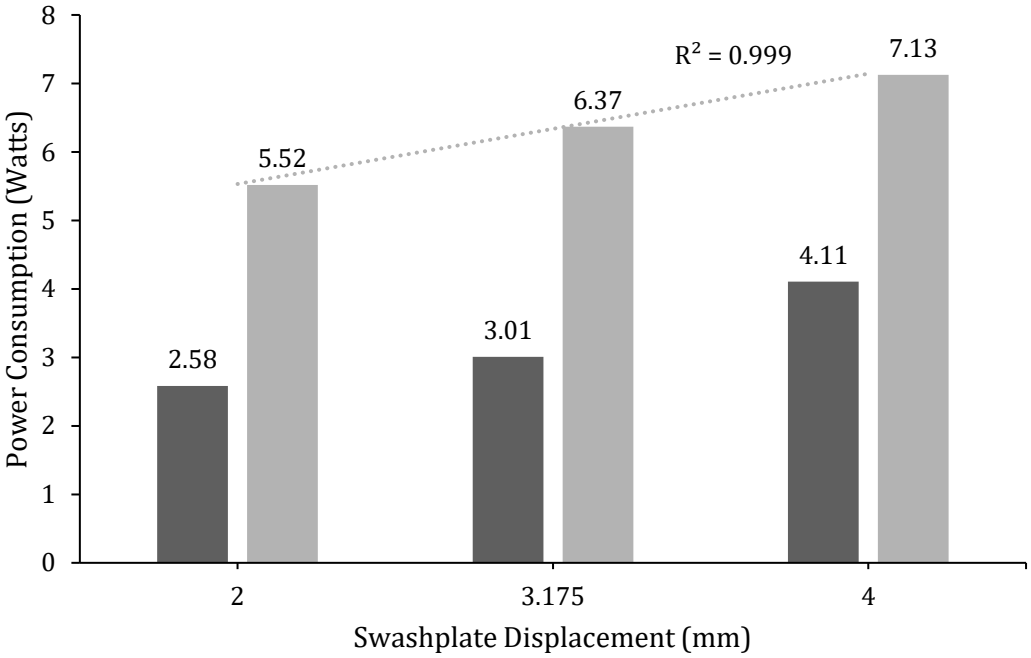

Figure 4.7 – Average power consumption (dark grey) and maximum consumption (light grey) in Watts, over 15 minutes at a flow rate of 1 ml/min with an approximate backpressure of 100 bar.

Examining figure 4.7, the combined power consumption of the pump and the control electronics, gave the generally expected response; increasing the swash plate angle increases the power consumption of the pump. However, the relationship between swash plate displacement and power consumption was expected to be linear.

Regarding the average power consumption, the 3.175 mm plate uses 16.67% more power while the 4 mm plate uses 59.30% more when operating at a flow rate of 1 ml/min. A possible explanation lays with the manual adjustment of the current limiting potentiometer. When observing the peak current value from each set of swash plate test data, a linear relationship exists as seen with the trend line in figure 4.7. When looking at a small section of the recorded data as seen in figure 4.8, an interesting observation is made.

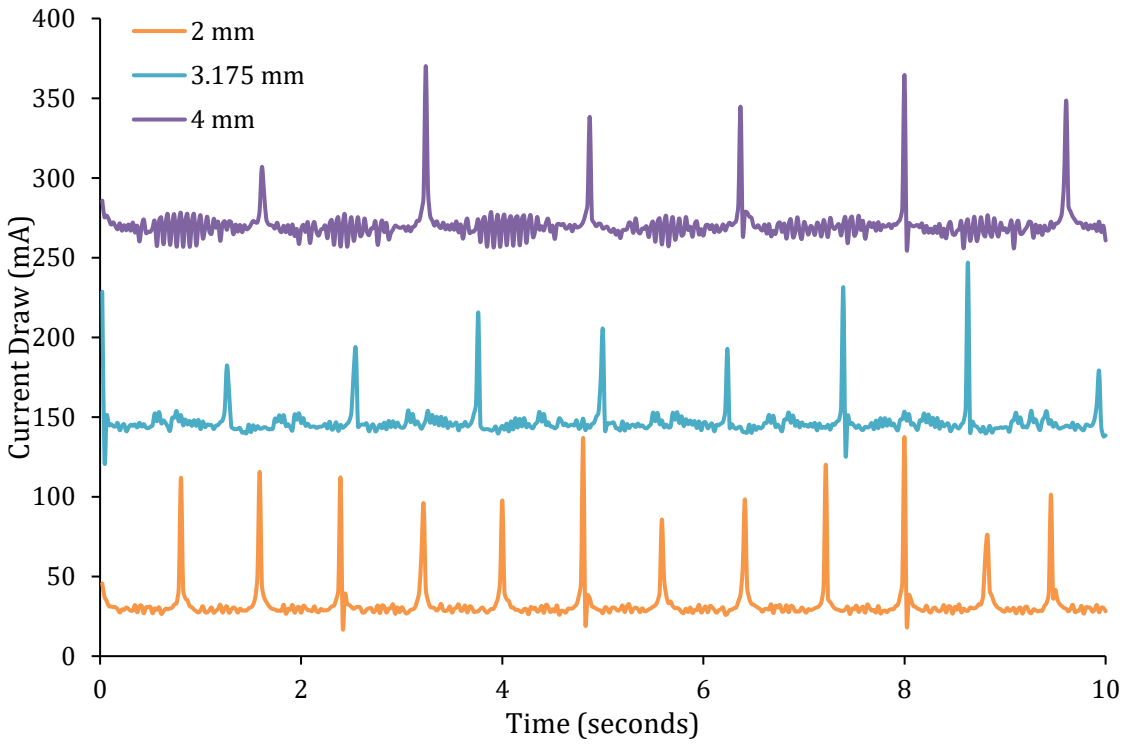

Figure 4.8 – A 10 second window of recorded milliamp values for each swash plate. Each peak represents the changeover of fluid delivery from one piston to the other at a flow rate of 1 ml/min with an approximate backpressure of 100 bar.

Examining the baseline between the peaks, the 4 mm swash plate generates more noise. A plausible theory is that the current limiting potentiometer was not adjusted correctly, and the motor could draw more current than required. This resulted in a noisy signal as the stepper motor advanced forward step by step but did not affect the peak current draw.

As shown in figure 4.7 the peak power consumption values gave a linear response. For the 2 mm and 3 mm swash plates, the average value was 47% of the peak value. Using this percentage and applying it to the peak value for the 4 mm plate, the average power consumption for the 4 mm plate should have been 3.35 Watts rather than 4.11 Watts recorded. This calculated value would have given the expected linear relationship for the average values.

Estimating system run time using the 2 mm swash plate, a 10 % safety factor, and an observed 50 mA current draw for the portable system, using the 24 Amp-hour battery the system would have a theoretical 136 hours of run time on a single charge. A comparison with some of the reported portable systems and the commercially available Axcend Focus LC is presented in table 4.4.

Table 4.4 - Comparison of battery run time of portable systems.

Portable System	***Pumping System***	***Battery Run Time***
Tulchinsky *et al*. [36]	Dual Piston Reciprocating	~ 8 hours
Ishida *et al*. [37]	Electroosmotic	~ 24 hours
Sharma *et al*. [31]	VICI nanoflow	~ 8 hours
Chatzimichail *et al*. [41]	Pressurised Gas	> 24 hours
Axcend Focus LC [46]	High-pressure syringe	> 10 hours
Portable system with swash pump	*Swash plate - Dual Piston Reciprocating*	*> 100 hours*

While not a comprehensive power audit of the full system, the results show that the portable system using the swash plate pump can run for at least 100 hours using the Voltaic V88 battery.

4.2.2 Swash plate comparison and piston displacement profile

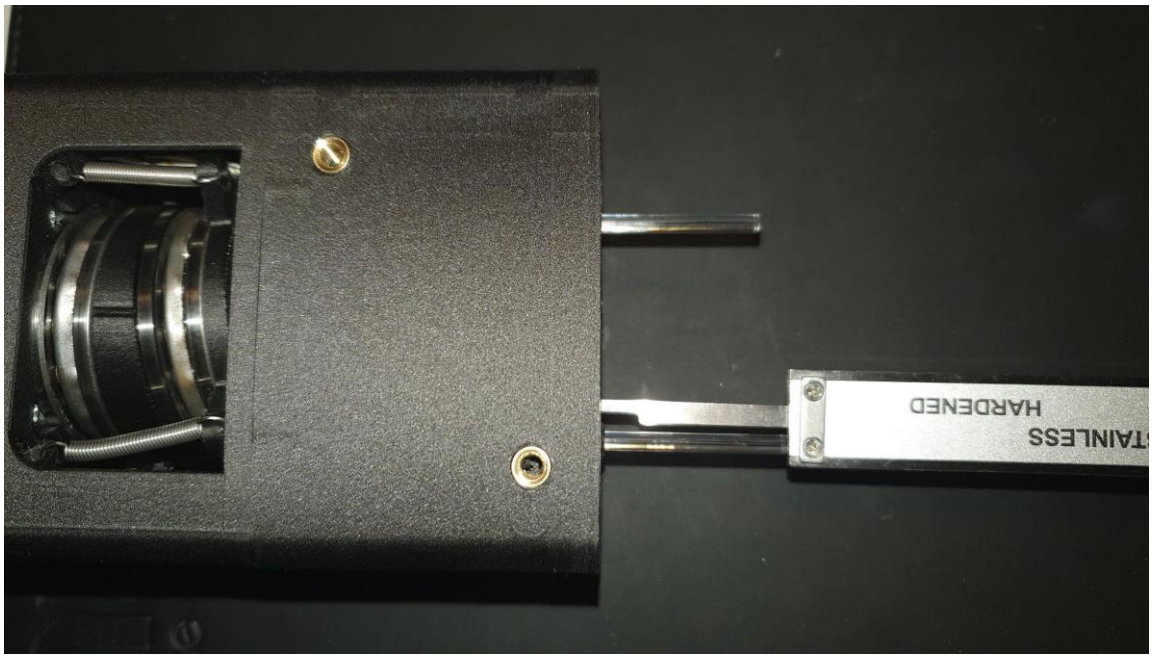

Figure 4.9 - Measurement of piston displacement using a digital calliper.

The swash plates were printed using a Markforged Mark Two FDM 3D printer with a layer height of 100 µm. Examining the swash plate files within the slicing software for the 3D printer gave an insight to the expected displacement values. These were compared to the actual printed parts with only a 0.5% error in displacement measured. However the more important measurement is that of the piston displacement as shown in figure 4.9, measurements of which are presented in table 4.5.

Table 4.5 - Displacement error for each swashplate

Expected Displacement (mm)	*Piston A Measured (mm)*	*Piston B Measured (mm)*	*Average Measured (mm)*	*% Error*
2.02	1.94	1.92	1.93	-4.45
3.17	3.15	3.11	3.13	-1.26
3.9	3.92	3.90	3.91	+0.2

While the figures in table 4.5 above do not exactly match the designed values, the calculation of flow rate is based on the actual displacement values programmed into the pump firmware. The percentage errors are compensated for by the swash plate rotating faster. Taking the 4.45 % error of the 2 mm swash plate for example, only results in a 0.047 mm/s increase in piston velocity.

Next, the piston displacement profile for all three swash plates was assessed for linearity during sinusoidal swash plate velocity. The constant swash plate velocity was also used for visual comparison.

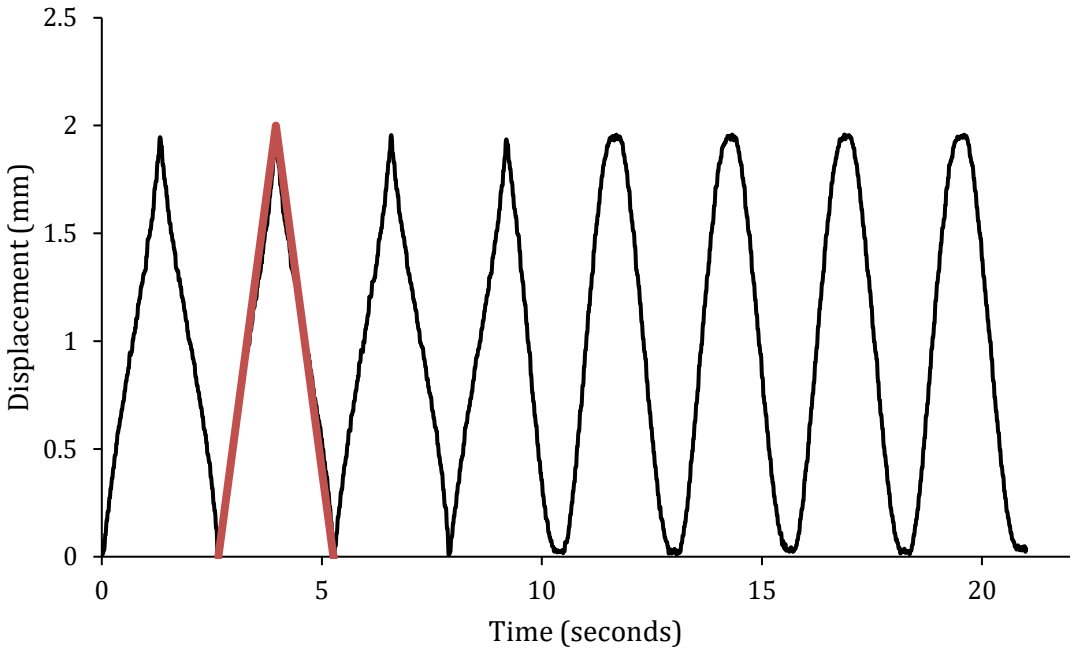

Figure 4.10 – Piston displacement profile for the 2 mm swash plate with both sinusoidal and constant swash plate velocity. The ideal piston displacement profile is highlighted in red.

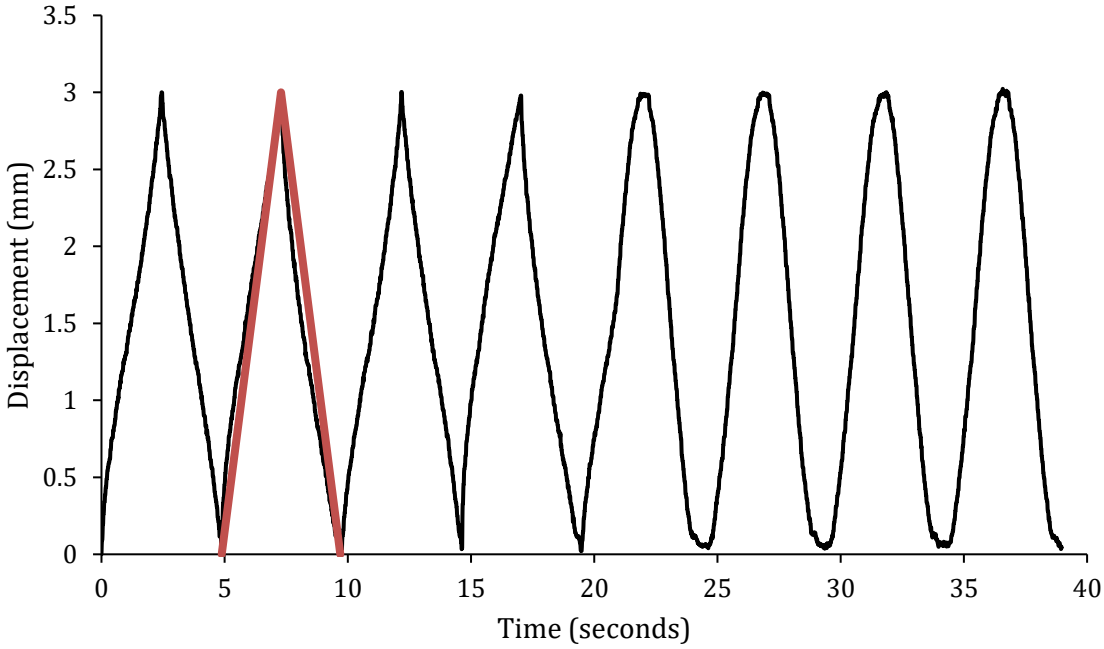

Figure 4.11 - Piston displacement profile for the 3.175 mm swash plate with both sinusoidal and constant swash plate velocity. The ideal piston displacement profile is highlighted in red.

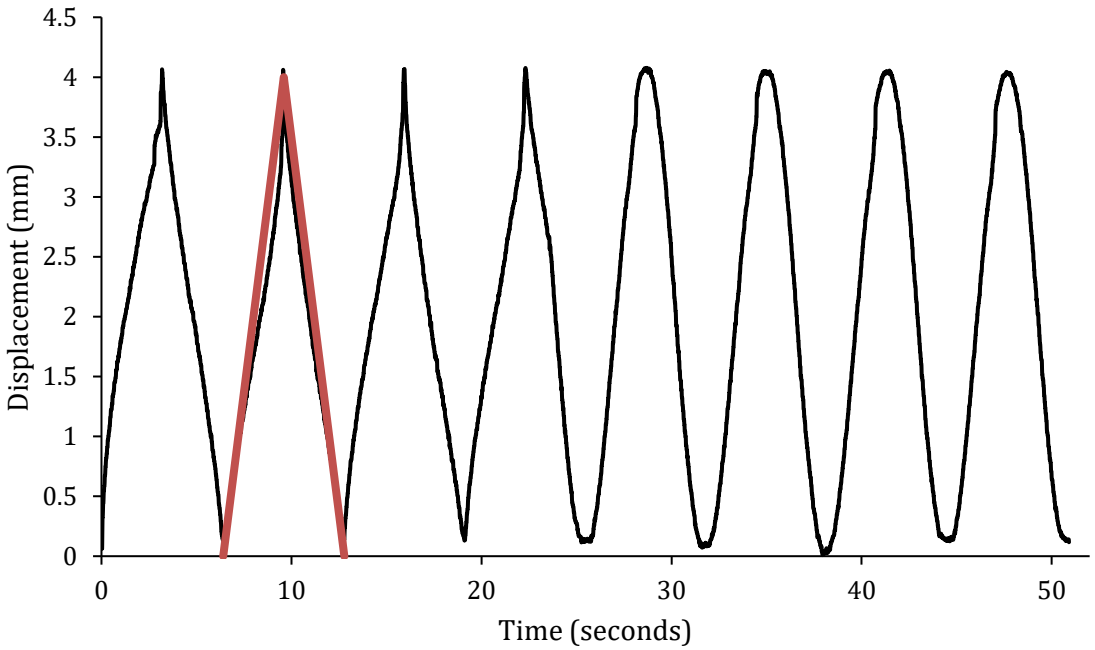

Figure 4.12 - Piston displacement profile for the 4 mm swash plate with both sinusoidal and constant swash plate velocity. The ideal piston displacement profile is highlighted in red.

Figures 4.10 to 4.12 represent the piston displacement profiles of the 2-, 3.175-, and 5-mm swash plates taken during a benchtop assessment with no pump heads attached. The ideal piston displacement profile is highlighted by the red lines in each.

Table 4.6 highlights the linearity of the delivery stroke of the piston during the assessment as well as piston displacement data taken from the power audits of each swash plate. The power audit data is more representative as the pump was fully operational and pumping at 1 ml/min with approximately 100 bar back pressure.

Table 4.6 - Comparison of sinusoidal swash plate velocity delivery stroke linearity from initial assessment to operational test.

Swash Plate Displacement (mm)	***Assessed Linearity (r^2)***	***Operational Linearity (r^2)***
2	0.997	0.995
3.175	0.994	0.994
4	0.990	0.997

The result of using a sinusoidal piston velocity from early testing can be seen in figure 4.13. In this case, water was pumped through a pressure coil at 1 ml/min. The black pressure trace represents the pressure pulsations during sinusoidal swash plate velocity while the grey trace represents the pressure pulsations seen with a constant swash plate velocity. The visible reduction in pressure pulsation confirms the benefit of running the swashplate with a sinusoidal velocity.

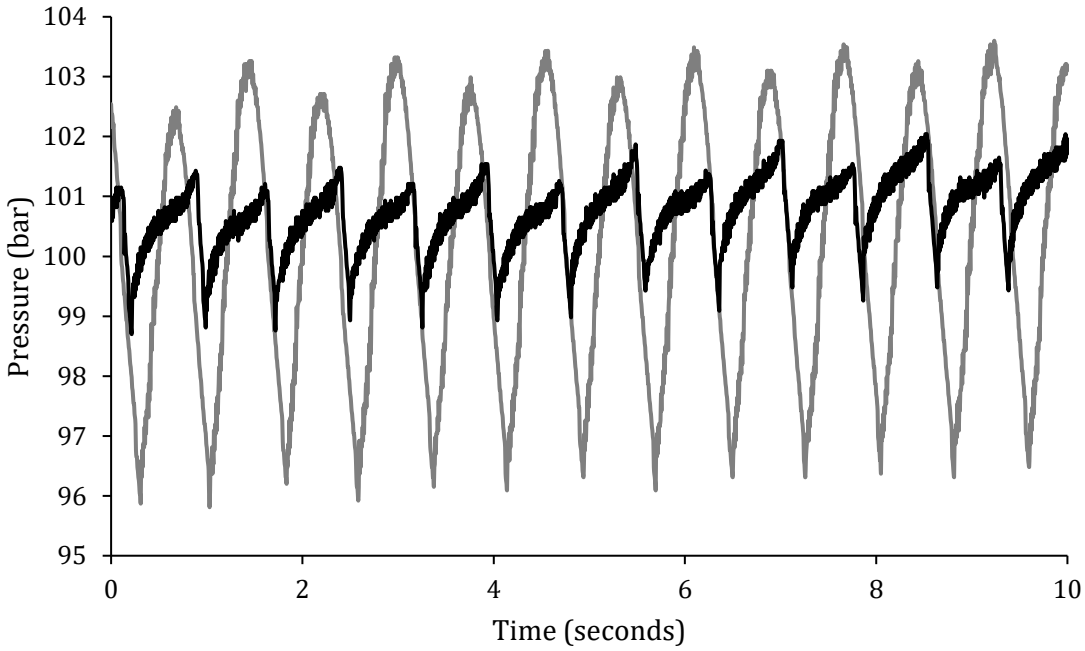

Figure 4.13 – Comparison of pressure profiles from a sinusoidal (black) and a constant (grey) piston velocity at a flow rate of 1 ml/min and an average backpressure of 100 bar. Pulsation RSD for constant velocity id 2.15% while sinusoidal velocity is only 0.6 %.

4.2.3 Flow rate accuracy

As previously mentioned, flow rate accuracy is important for the transfer of separation methods between systems. The following results are taken from the swash plate pump at various flow rates. Timed collection of water was weighed in vials and compared to the setpoint. Figure 4.14 shows an example of vials filled during the swash pump assessment, while table 4.7 shows the results.

Figure 4.14 – Vials used in determination of the swash plate pump flow rate accuracy.

Table 4.7 - Swash Plate Pump flow rate accuracy.

Flow Rate (ml/min)	*Actual Measured (ml/min)*	*% Accuracy*
0.1	0.100	100.00
0.25	0.250	100.00
0.5	0.497	99.48
1	0.991	99.10
1.5	1.480	98.68
2	1.966	98.29

As expected, the swash plate pump performs well with the percentage error ranging from 0 to 1.71%. The 1ml/min value is important as it is comparable to most of the flow accuracy figures presented in table 4.8.

However at pressures approximately above 150 bar, the 3D printed chassis struggles with the forces generated, causing the chassis to flex with the rotation of the swash plate. This results in the flow rate accuracy figure dropping as the flow rate increases.

Table 4.8 – Swash plate pump compared to reported flow rate accuracy of benchtop HPLC pumps.

Manufacturer	***Pump Model***	***Conditions***	***Reported Flow Accuracy %***
Agilent	1260 Infinity II (G7110B)	Water at 100 bar	± 1
Dionex	GP-50	% Of setting	± 0.5
Dionex	LPG 3400-M	At 250 µL/min	± 0.5
Knauer	AZURA P 6.1L	Ethanol at 5 – 80% flow range	± 0.25
Knauer	AZURA P 4.1S	Ethanol:Water/10:90 at 5 – 50% of flow range	± 2
Shimadzu	LC-40D	Not specified	± 1
Waters	515	Methanol at 1ml/min 70 – 140 bar approx.	± 1
Waters	1515	Methanol at 1ml/min 70 – 140 bar approx.	± 1
-	*Mark 2 Swashplate*	*D.I. Water. Full flow range, 10 – 200 bar approx..*	*0 to 1.71% 0.9 % at 1 ml/min*

Though the wide range of conditions complicates comparison overall, the swash plate pump performs well compared to the more expensive benchtop equivalents.

4.2.4 Flow rate drift

The swash plate pump flow rate was monitored over a 60-minute period for both open loop and closed loop control. Figures 5.10 and 5.11 show the response from the open loop test.

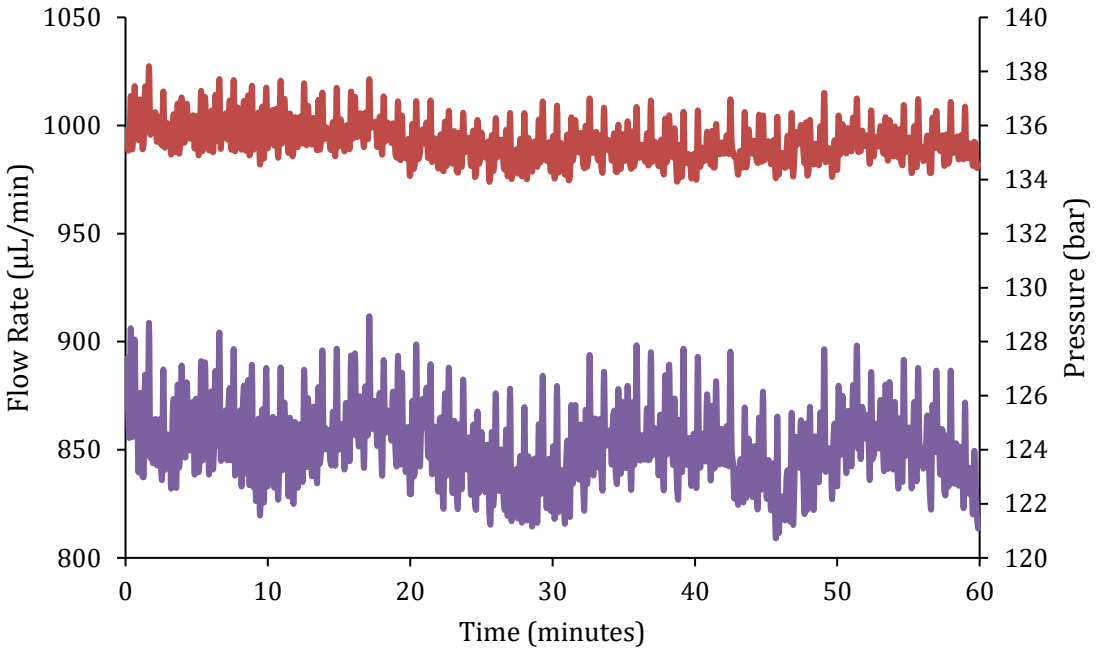

Figure 4.15 - Pressure (purple) and flow rate (red) variation while pumping D.I. water through a back pressure coil at a flow rate of 1 ml/min over a 60 minute period

A slight decrease in flow rate is observed in figure 4.15, where the approximate flow rates of 998 µL/min and 989 µL/min represent the starting and final flow rate of the assessment. This represents a 0.15 µL/min decrease in flow rate over 60 minutes. A decrease in backpressure is seen, which is measured at 0.04 bar/min. This represents a drop from 125.65 bar to 122.98 bar over the 60-minute period. The drop in back pressure is more likely a consequence of the increase in temperature rather than a decrease in flow rate. Figure 4.16 represents the relationship between temperature and pressure.

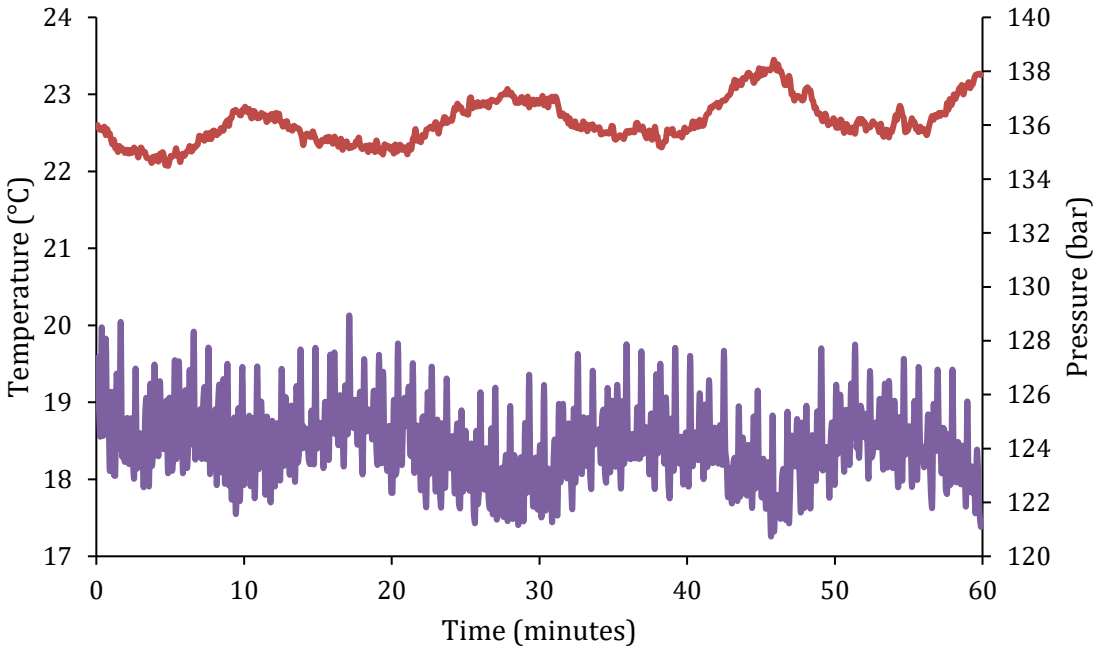

Figure 4.16 – Pressure (purple) and temperature (red) variation while pumping D.I. water through a back pressure coil at a flow rate of 1 ml/min over a 60 minute period..

It can be seen in the figure above that pressure and temperature are inversely related. As temperature rises, pressure drops. A 1 °C increase in temperature can reduce viscosity by 1% which in turn decreases the back pressure. Over the course of the hour, the temperature rises from 22.5 °C to 23.3 °C. Theoretically this would see a decrease in back pressure of 2.39 bar with an observed value of 2.66 bar. Calculating pressure drop due to flow rate drift would result in a 3.27 bar drop in pressure. Therefore temperature accounts for the pressure drop and the drift in flow rate observed is independent. The next assessment saw the use of the closed loop control system using the flow sensor.

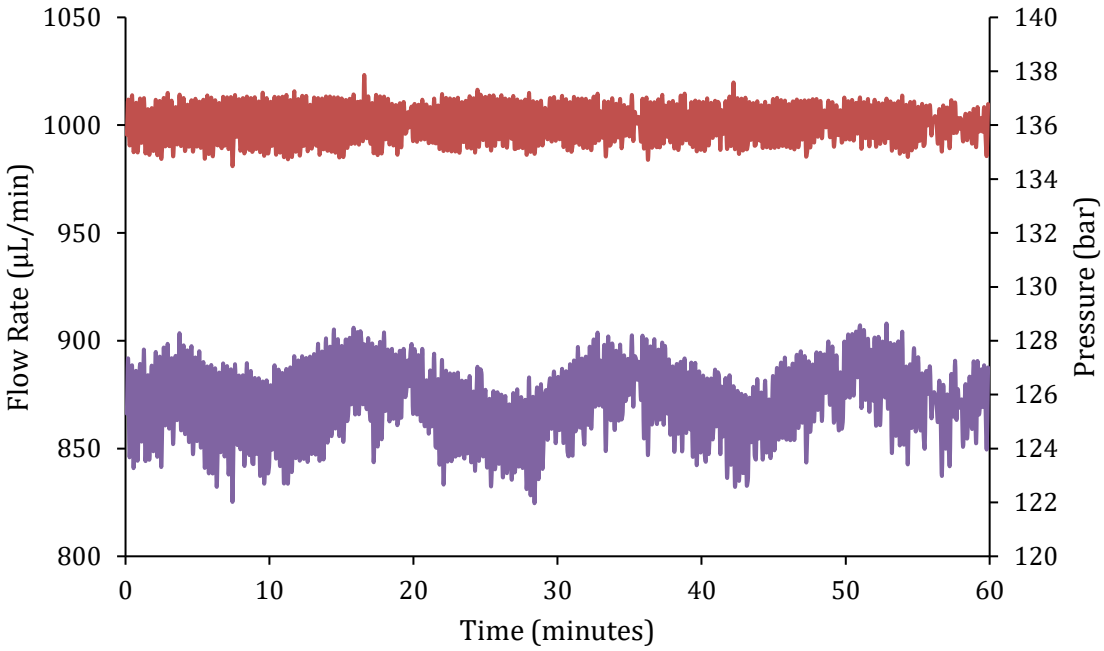

Figure 4.17 – Pressure (purple) and flow rate (red) variation while pumping D.I. water through a back pressure coil at a flow rate of 1 ml/min over a 60 minute period..

With the closed loop control system turned on, the flow stability has been dramatically improved. The rate of flow drift seen in figure 4.17 measures 0.0066 µL/min. It is also clearly visible that the flow rate is not affected by changes in the back pressure due to temperature swings. Figure 4.18 details temperature *versus* pressure below.

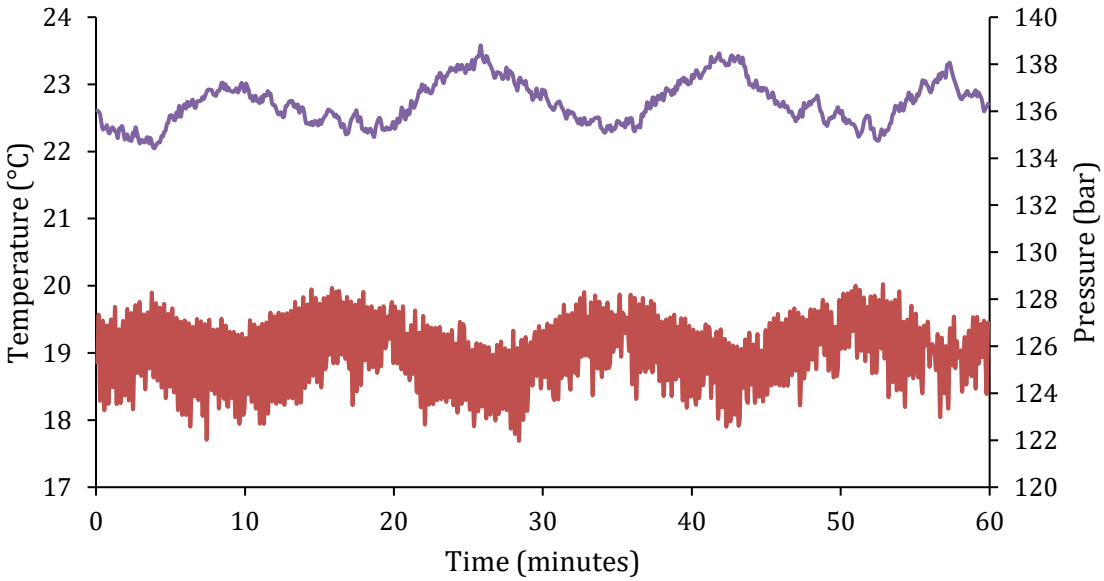

Figure 4.18 – Pressure (red) and temperature (purple) variation while pumping D.I. water through a back pressure coil at a flow rate of 1 ml/min over a 60 minute period.

Although the drift seen in the open loop test is broadly acceptable, the closed loop performance represents what should be expected of high performance pumping solutions for liquid chromatography systems. At a drift rate of 0.00666 µL/min, it would take over 25 hours for the flow rate to increase by 10µL. At a drift rate of 0.15µL/min, it would take just over 1.1 hours for the flow rate to increase by 10µL. Table 4.9 summarises the flow rate drift assessment.

Table 4.9 – Swash plate pump flow rate drift, open loop *versus* closed loop control.

Op. Mode	***Flow Rate Change (µL/min)***	***Pressure Change (bar/min)***	***Temperature Change (°C/min)***	***Time for flowrate to change by 10 µL (hours)***
Open Loop	0.15	0.044	0.013	1.1
Closed Loop	0.0066	0.011	0.005	25

4.2.5 Pressure ripple

Minimising pressure ripple is important as it can cause issues with baseline noise in detectors which may cause issues with peak areas for low concentration analytes. The results presented were collected during two separate tests. The first was an assessment over a range of flow rates through a 50 cm pressure coil of 75 µm inner diameter. Table 4.10 summarises the results.

Table 4.10 – Pressure ripple, benchtop vs swash plate pump.

Flow Rate	***Benchtop %RSD***	***Swash %RSD***	***Benchtop Backpressure (bar)***	***Swash Backpressure (bar)***
250	1.369	1.148	25.44	32.73
750	0.707	0.880	80.06	81.03
1250	0.715	0.774	131.25	132.59
1750	0.898	0.742	181.68	184.84
2250	1.05	0.772	231.83	232.08

The swash plate pump gave comparable RSD and pressure values to the benchtop pump, over the flow rate range as visualised in figures 4.19 and 4.20.

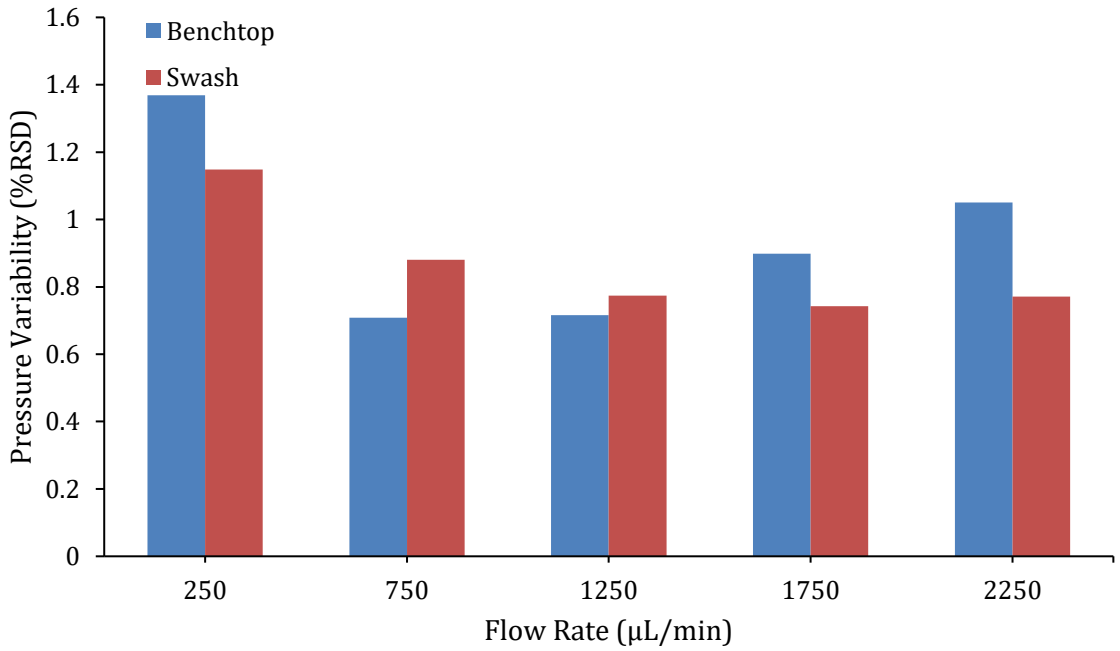

Figure 4.19 – Pressure variability of the benchtop (blue) and swash plate pump (red) at a flow rate of 250, 750, 1250, 1750 and 2250 µL/min, pumping D.I. water through 50 cm of 75 µm I.D. tubing.

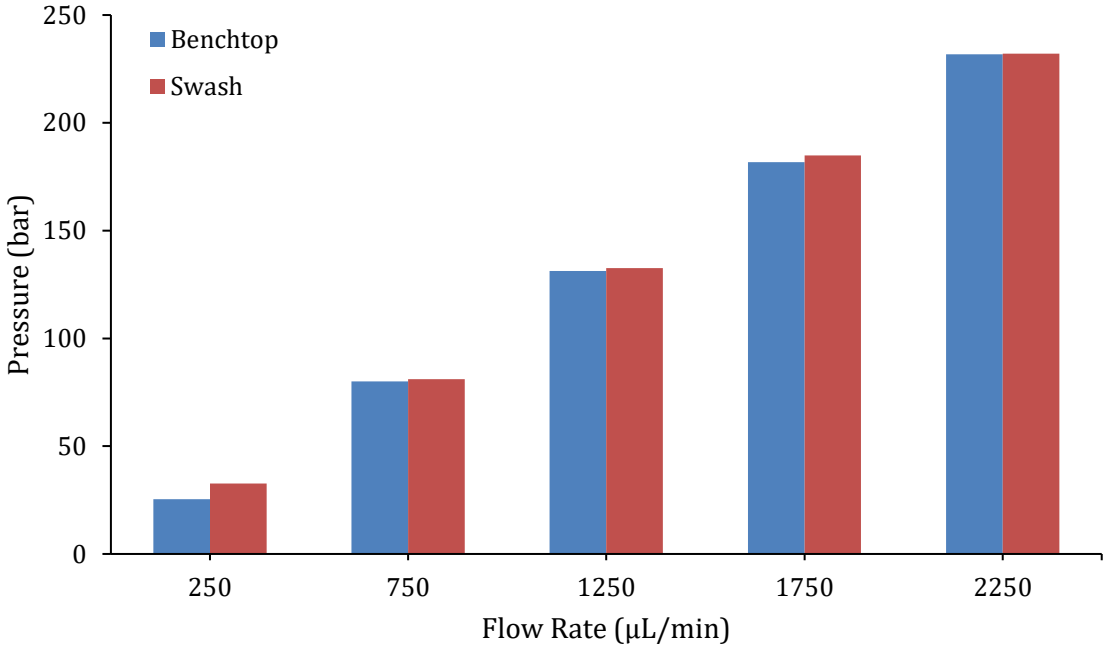

Figure 4.20 – Pressure values recorded for the benchtop and swash plate pump at a flow rate of 250, 750, 1250, 1750 and 2250 µL/min, pumping D.I. water through 50 cm of 75 µm I.D. tubing.

The second assessment involved running the benchtop and swash plate pumps at 1ml/min with at least 140 bar of back pressure. Cooler laboratory temperatures with the use of a

back pressure coil (65 cm of 75 µm I.D. tubing) resulted in a higher-than-expected backpressure of 150 bar. However this was still acceptable for the assessment.

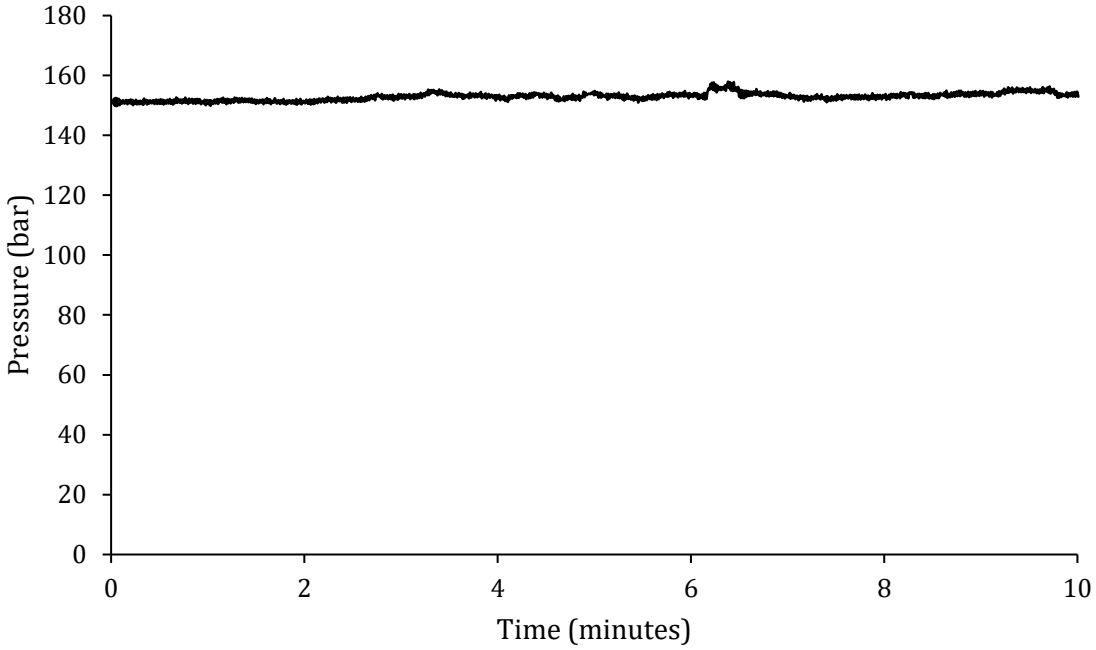

Figure 4.21 – Pressure trace recorded for the benchtop pump at a flow rate of 1 ml/min pumping D.I. water through 65 cm of 75 µm I.D. tubing.

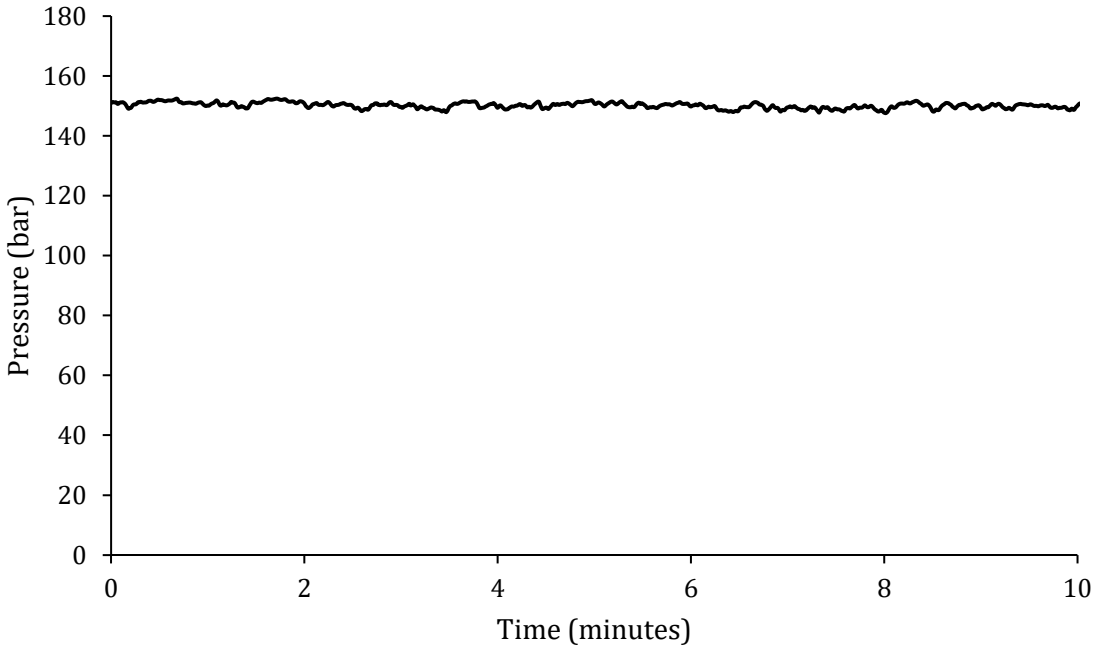

Figure 4.22 – Pressure trace recorded for the swash plate pump at a flow rate of 1 ml/min pumping D.I. water through 65 cm of 75 µm I.D. tubing.

The cause of the instability in the pressure signal around 6 minutes in figure 4.21 is unknown, however it does not affect the assessment. Datasheets for various pumps report

the pressure ripple as the percentage amplitude of the pressure value. The pressure values highlighted in table 4.11 represent the values calculated from figures 4.21 and 4.22.

Table 4.11 – Comparison of reported benchtop pump pressure ripple to the swash plate pressure ripple.

Manufacturer	***Pump Model***	***Reported Pressure Ripple %***
Agilent	1260 Infinity II (G7110B)	< 2
Dionex	LPG 3400-M	< 1 *1.51 % at 150 bar*
Knauer	AZURA P 6.1L	< 2
Waters	515	< 2
Waters	1515	< 2
-	*Mark 2 Swash plate*	*1.45 % at 150 bar*

Again, the swash plate pump offers comparable pressure deviation and ripple values to a benchtop HPLC pump.

4.2.6 Pressure leak test

The pressure leak test was carried out using the method described by Lam [68]. However when attempting to slowly bring the pressure value up as described in his method, the pressure value as seen in figure 4.23 rose dramatically, even under low flow rates. This was potentially due to the close proximity of the pressure sensor to the pump heads. The maximum recorded pressure observed was 295.9 bar, with Lam's method calling for flow to be stopped at 275 bar.

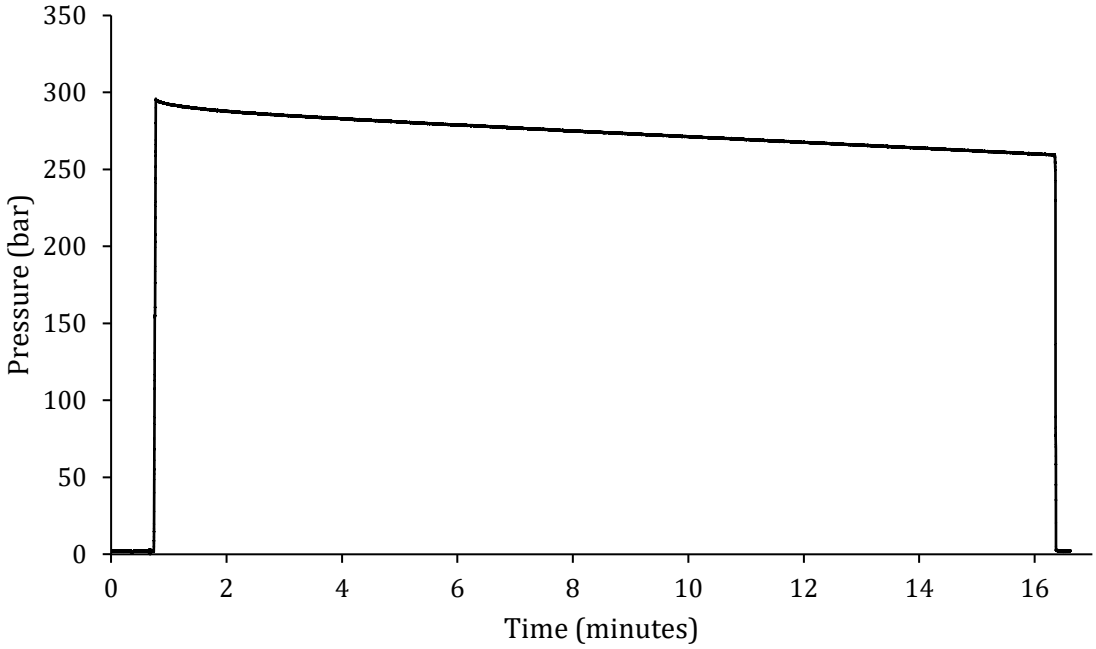

Figure 4.23 – Pressure leak test results representing the pressure drop over a 15 minute period.

Due to the manual operation of the pump, the 20 bar overshoot in pressure resulted in a leak rate greater than the permitted 5.17 bar/min for the first minute of data collection. However, once the pressure fell below the 275 bar limit, the leak rate was well below the specification with the maximum recorded as 2.79 bar/min as seen in figure 4.24.

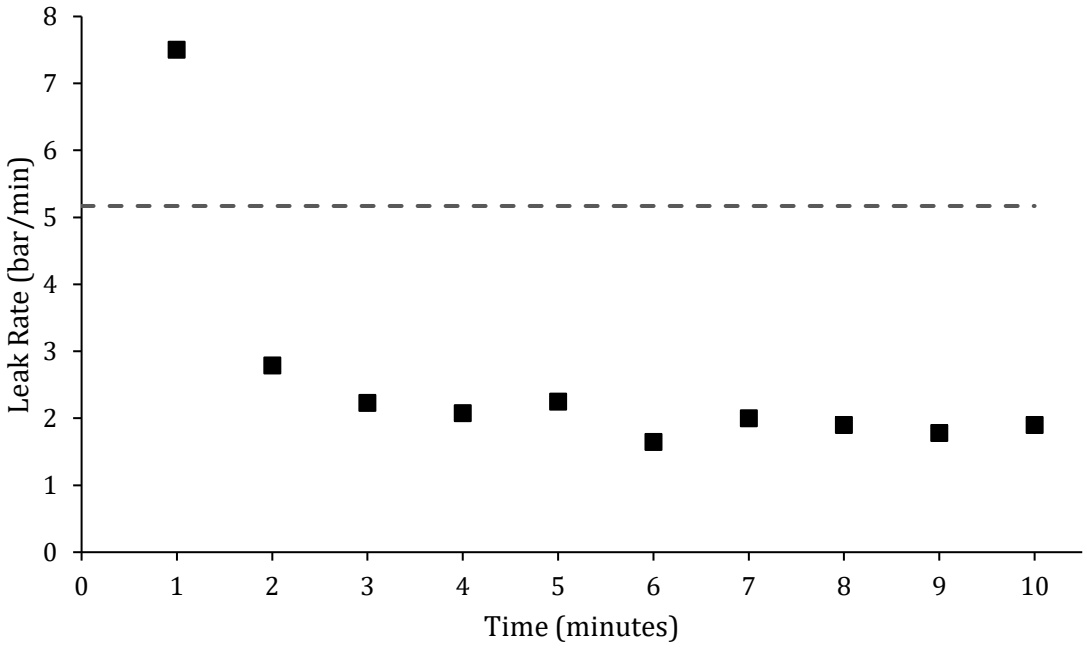

Figure 4.24 – Pressure leak test results with the leak rate in bar/min represented by the squares and the maximum leak rate represented with the dashed line.

4.2.7 Pump repeatability and flow rate precision

Two repeatability studies were carried out to observe the operational performance of the pump. The first and more comprehensive assessment was conducted before the flow rate sensor was introduced into the pumping system. A column performance check standard was obtained (Phenomenex AL0-3045) and 120 injections were carried out over three days within a 5-day period. The second, shorter assessment was carried out as a comparison to show the performance improvement by implementing closed loop control with 20 injections being performed. The experiments were performed with the swash plate pump connected to a custom injection valve, all of which was hooked up to the benchtop HPLC to perform the data acquisition.

Assessment 1

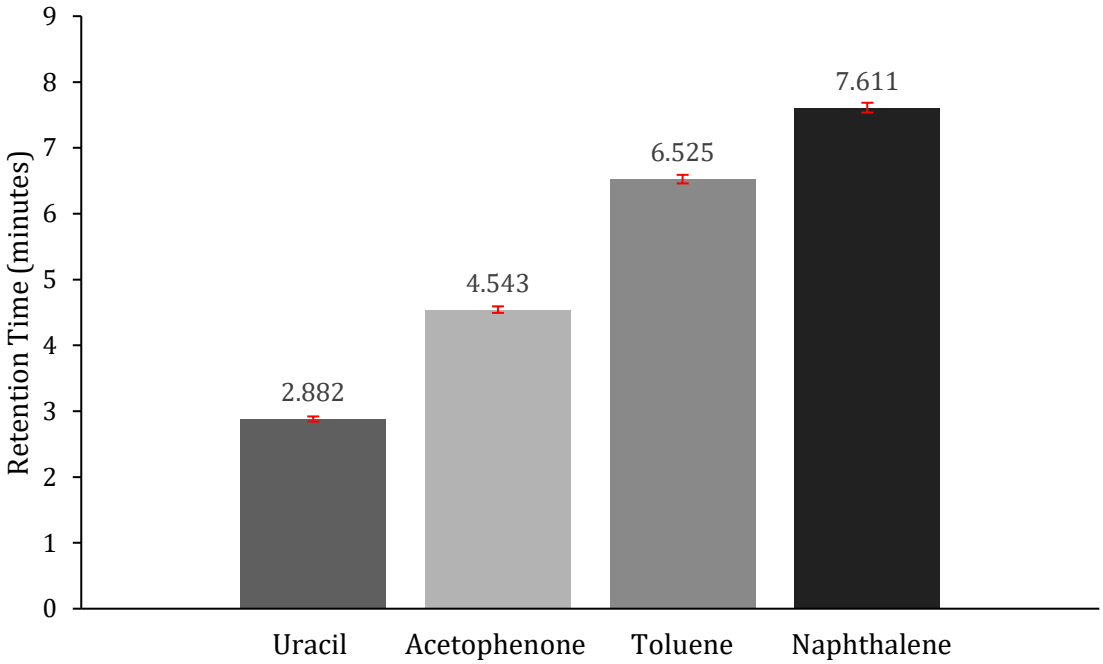

Figure 4.25 - Average peak retention times over 120 injections. Error bars represent retention time percentage RSD as follows: Uracil 1.34%, Acetophenone 1.09%, Toluene 1.00%, and Naphthalene 0.98% Separation conditions: Column C18 250 x 4.6 5µm particle size, Isocratic 60:40 Acetonitrile:DI Water, Flow rate 1 ml/min, Injection volume 1µL, Detection UV at 254nm.

Figure 4.25 illustrates the retention times of each analyte from the 120 injections carried out. Good repeatability was observed over the three days of testing which can be seen through the small relative standard deviation values represented in table 4.12. Figure 4.26 illustrates a selection of chromatograms from the study.

Table 4.12 - Peak retention time variance.

Analyte	***Uracil***	***Acetophenone***	***Toluene***	***Naphthalene***
Retention Time RSD %	1.34	1.09	1.00	0.98

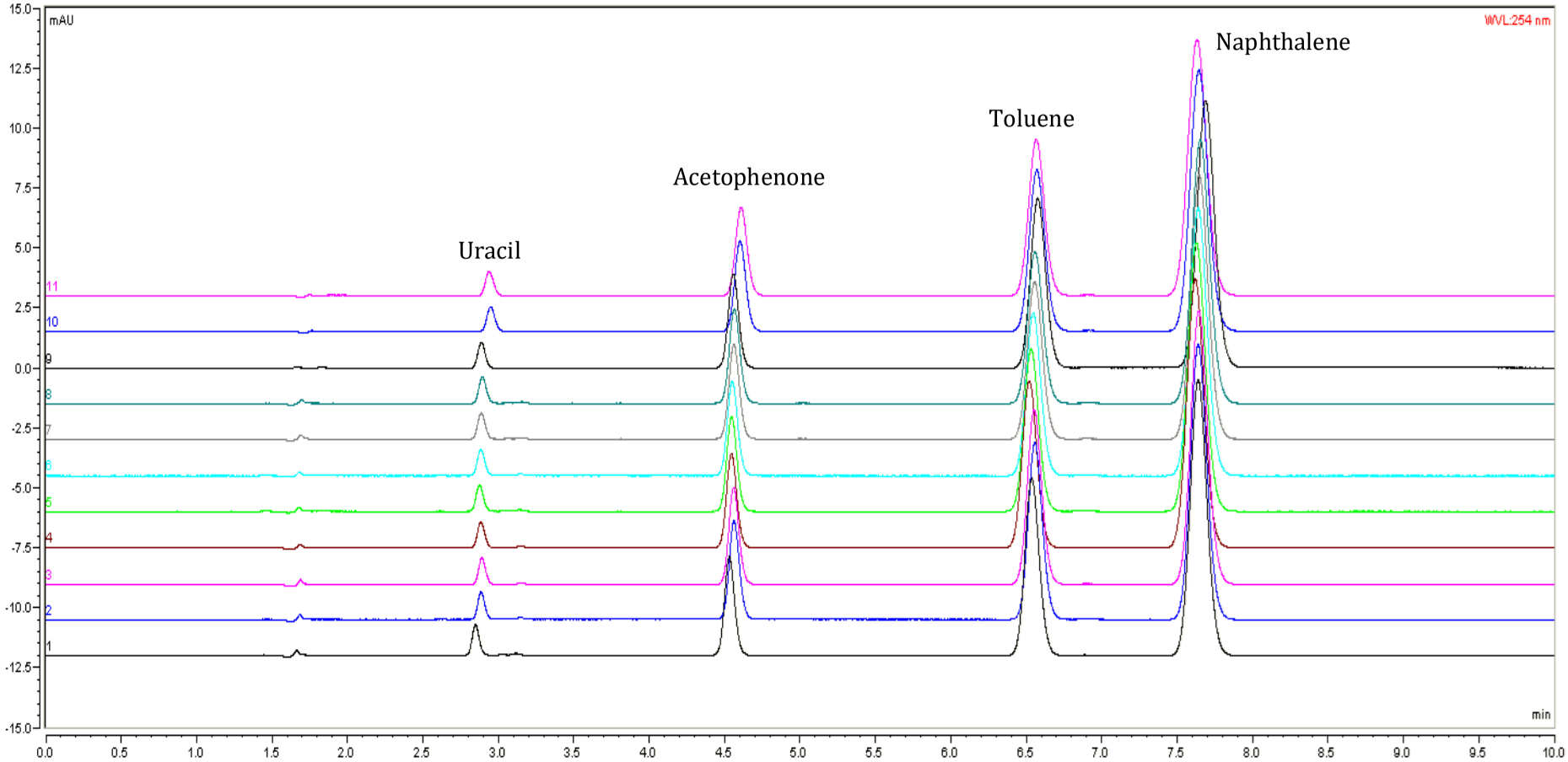

Figure 4.26 - A selection of chromatograms illustrating the first to final injection of the study. Separation conditions: Column C18 250 x 4.6 5µm particle size, Isocratic 60:40 Acetonitrile:DI Water, Flow rate 1 ml/min, Injection volume 1µL, Detection UV at 254nm.

Assessment 2

A smaller batch of 20 injections was carried out using the same column performance check standard as before to demonstrate the improved flow stability of the pump. Figure 4.27 illustrates the retention times for each analyte over the 20 injections. The addition of the flow sensor significantly improved the peak retention times compared to those seen in table 4.12. Table 4.13 below shows the relative standard deviation for each analyte, while figure 4.28 shows the chromatograms from this experiment.

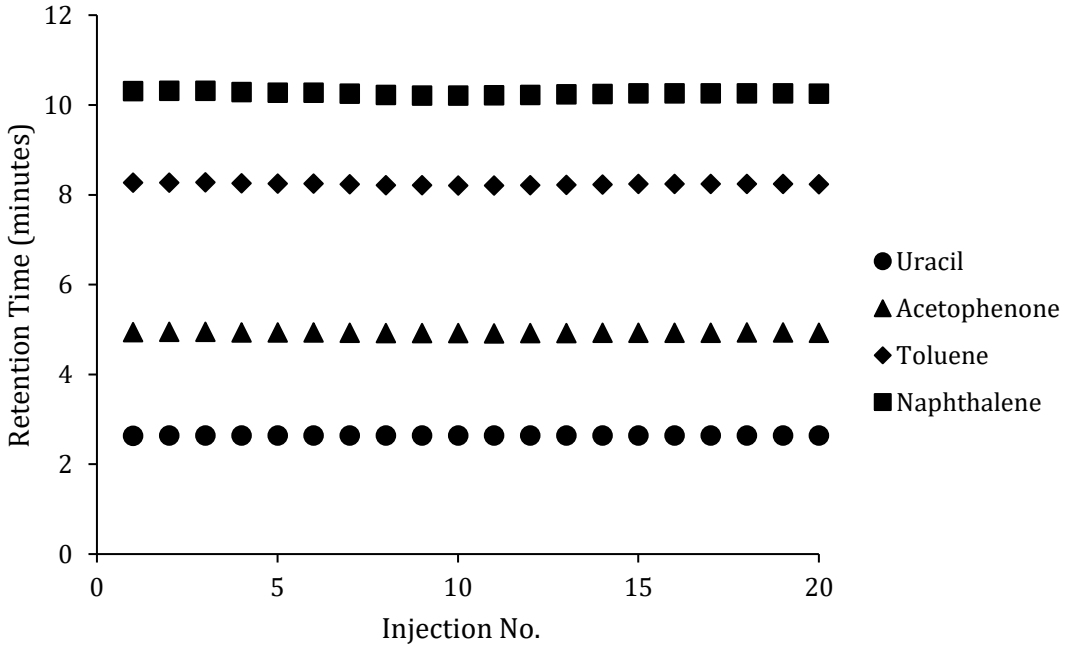

Figure 4.27 - Peak retention times over 20 injections with the flow sensor on the pump. Separation conditions: Column C18 250 x 4.6 5µm particle size, Isocratic 60:40 Acetonitrile:DI Water, Flow rate 1 ml/min, Injection volume 1µL, Detection UV at 254nm.

Table 4.13 - Peak area and retention time variance with flow sensor

Analyte	***Uracil***	***Acetophenone***	***Toluene***	***Naphthalene***
Retention Time RSD %	0.08	0.20	0.25	0.31

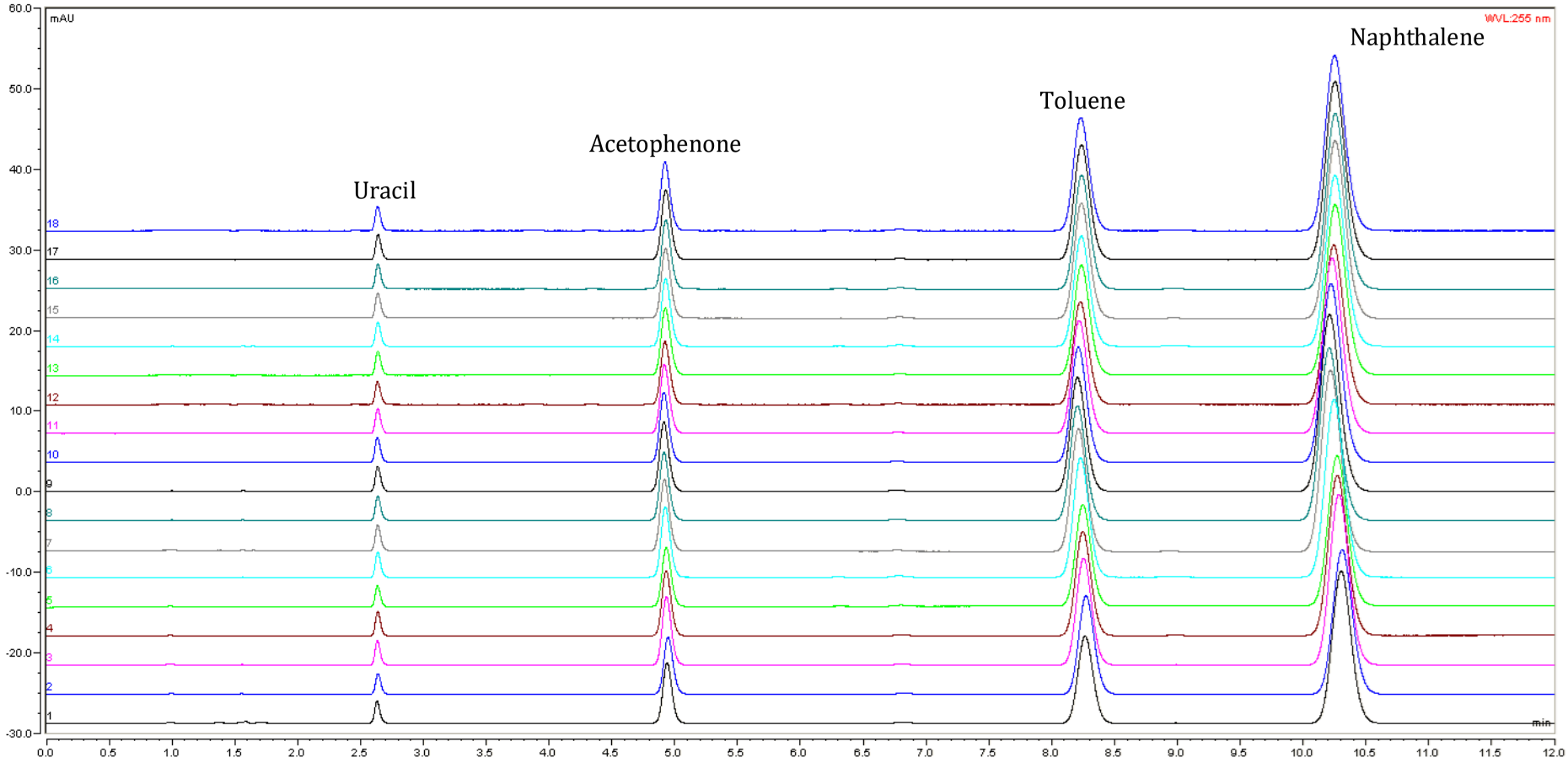

Figure 4.28 - A selection of chromatograms illustrating the first to final injection of the study. Separation conditions: Column C18 250 x 4.6 5µm particle size, Isocratic 60:40 Acetonitrile:DI Water, Flow rate 1 ml/min, Injection volume 1µL, Detection UV at 254nm.

Table 4.14 – Comparison of flow precision values based on peak retention times reported for benchtop instruments.

Manufacturer	***Pump Model***	***Reported Flow Precision % RSD***
Agilent	1260 Infinity II (G7110B)	0.07
Dionex	GP-50	0.1
Dionex	LPG 3400-M	0.05
Knauer	AZURA P 6.1L	0.04
Knauer	AZURA P 4.1S	0.5
Shimadzu	LC-40D	0.06
Waters	515	0.1
Waters	1515	0.1
-	*Mark 2 Swash plate*	*0.08*

Table 4.14 presents the reported flow rate precision values from a selection of benchtop HPLC pumps. The majority of the commercial pump flow precision values are based on retention times. For example, operation manuals for the Knauer 4.1 report that flow precision is measured using an ethanol & water mix at 1 ml/min. Datasheets for the Knauer P6.1L, Agilent 1260 and Waters 515 refer to measurement of flow precision based on retention times. As described in section 4.1.7 the retention time of the unretained component Uracil is used to report flow precision. Based in this, the swash plate pump flow rate precision is comparable to the more complex and higher-cost benchtop equivalents.

4.3 Chapter 4 conclusion

This chapter reported the low power consumption of the pump and how, with a 2 mm swash plate, could provide over 100 hours of runtime when coupled with the portable system described in chapter 3. Flow rate accuracy has been shown to be as low as 1.71% at 2 ml/min, while flow rate drift is less than 0.0066 µL/min over 60 minutes when the pump is operating with closed-loop control. Pressure ripple test provided comparable results to commercially available pumps while the leak test proved successful with a leak rate of 2.79 bar/min reported, well below the 5.17 bar maximum specified. Finally, two assessments of pump repeatability and flow rate precision were carried out. Pump repeatability was assessed initially over 120 injections followed by a second assessment with the worst reported repeatability value of 1.34% for Uracil. Flow rate precision based on the retention time of Uracil was calculated to be 0.8% RSD.

Chapter 5 Portable system experimental methods, procedures, and results

In this chapter the experimental setup and the assessment of detector noise, drift, and linearity for the portable HPLC is described. The term detector in this case refers to all of the electronics, optics, software, and the flow cell. These assessments were conducted using the methods outlined in ASTM 685-93. The purpose of which was to compare the detector of the portable HPLC to a benchtop detector. This chapter is concluded with a comparison of the separation of four parabens carried out on the portable HPLC and the benchtop HPLC. Table 5.1 summarises the parameters assessed in this section.

Table 5.1 - Outline of detector performance parameters measured and their analytical impact.

Section	***Parameter***	***Requirement***	***Analytical Impact***
4.2.1	Detector Noise Detector Drift	$< 10^{-5}$ AU [68] $< 10^{-4}$ AU/h [68]	Negative effect on LOD & LOQ
4.2.2	Detector Linearity	$r > 0.999$ [68]	Concentrations reported outside of the linear range may not be accurate.
4.2.3	Portable and Benchtop detector comparison	Comparable noise and sensitivity.	Negative effect on LOD & LOQ
4.2.4	Portable and benchtop HPLC comparison	Comparable chromatograms.	Can portable system produce benchtop HPLC results.

5.1 Portable system characterisation and performance

Section 5.1 discusses the experiments conducted and their setup in order to assess the portable detector and portable HPLC system.

5.1.1 Detector noise and drift

Experimental Setup

This assessment was carried out to determine both the short-term and long-term noise as well as the drift of the portable system detector outlined in Chapter 3. The detector was turned on and left to stabilise for a period of at least 24 hours prior to the noise and drift assessment as per ASTM 685-93. The main deviation from the ASTM protocol was that the assessment of the detector was carried out while the flow cell was in a dry state. This was done as the data sheet for the Dionex VWD-3400RS gave specifications for noise and drift with dry analytical flow cells. It also satisfied the static conditions required under the protocol. Table 5.2 compares the main attributes for each detector.

Table 5.2 - Comparison of portable detector and Dionex VWD-3400RS specifications.

Attribute	***Portable Detector***	***Benchtop Detector***
Light Source	LED	Deuterium/Tungsten Lamp
Wavelength (nm)	255 nm Fixed	190 - 900 nm Variable
Bandwidth (nm)	11 nm	6 nm @ 245 nm
Flow Cell Pathlength (mm)	10	10
Flow Cell Internal Volume (µL)	6	11

Experimental Procedure

Once the 24-hour period of stabilisation was complete, data acquisition began. The portable detector LED current was adjusted until the transmittance was at 50% of maximum or 1.5 Volts. Data was recorded for 1 hour along with temperature. According to the ASTM 685-93 protocol, the ambient temperature could not change more than 2°C.

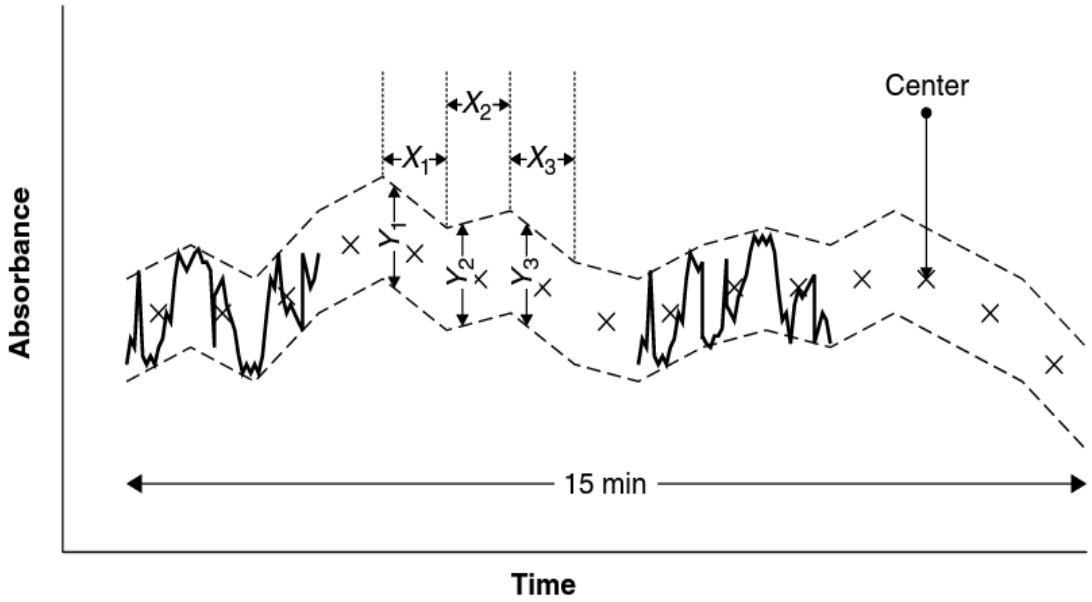

Figure 5.1 - Method for determination of short-term noise [68].

Figure 5.1 illustrates the method for the determination of short-term noise. A 15-minute window from the 1 hour of acquired data was selected. The data was divided into fifteen segments, where for each segment parallel lines were drawn to enclose the variation in the signal. The distance between each of these parallel lines was summed, divided by fifteen and the divided by the cell length in centimetres. The calculated value represents the short-term noise in absorbance units (AU).

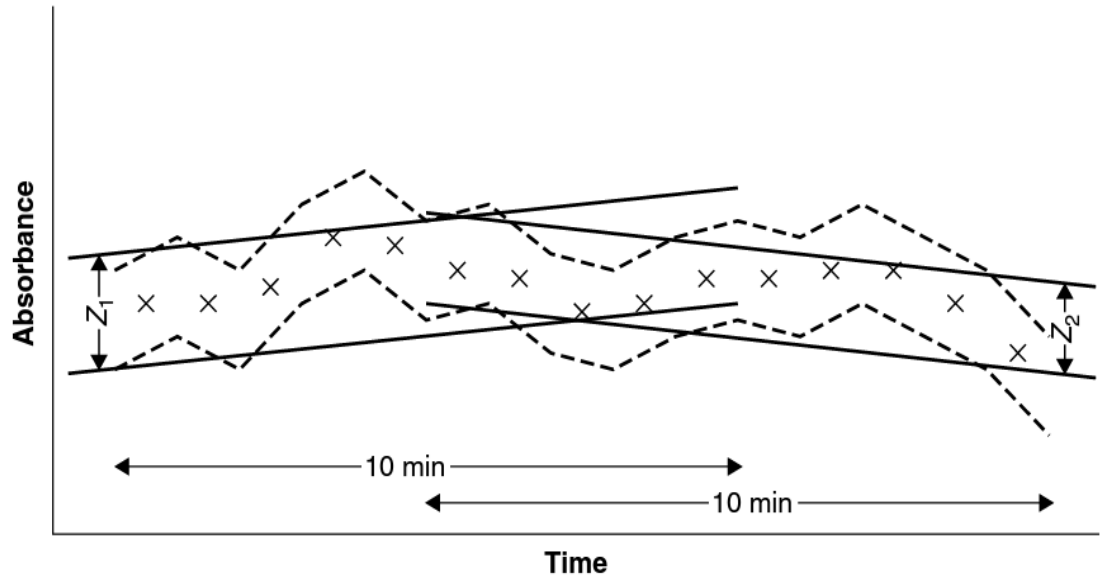

Figure 5.2 - Method for the determination of long-term noise [68].

Figure 5.2 depicts the determination of the long-term noise. The same 15-minute window of data was used with the centre point of each of the 1-minute segments plotted. Two 10-

minute segments were created, with parallel lines drawn at the minimum distance from each other, enclosing the centre points from the short-term noise test. The calculated long-term noise in absorbance units is the larger of the two values of the distance between the parallel lines.

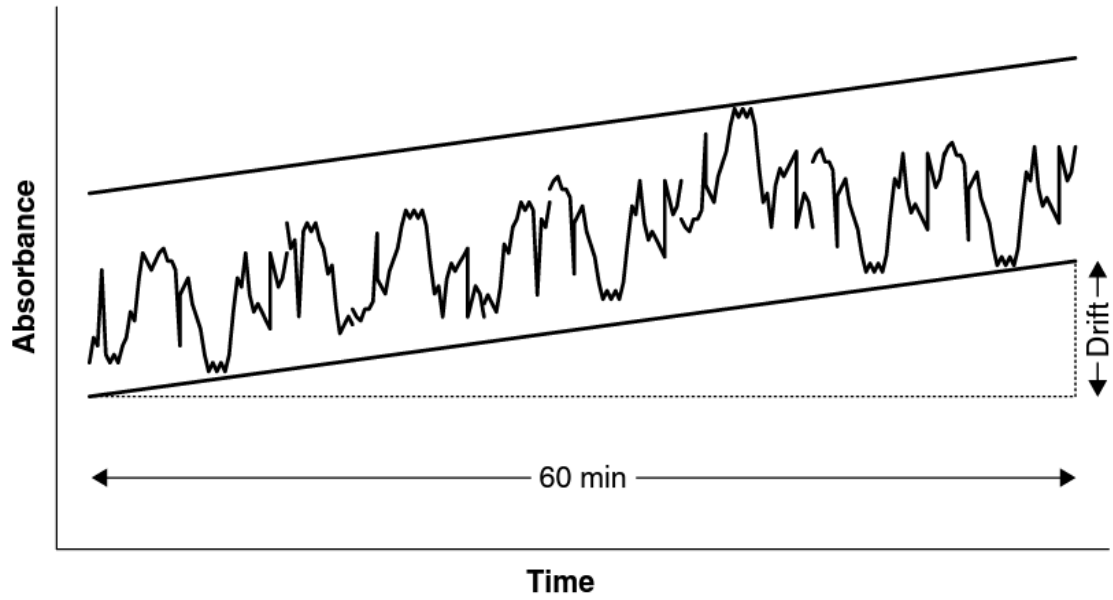

Figure 5.3 - Method for the determination of detector drift [68].

Figure 5.3 shows the procedure for the determination of detector drift. 1 hour of data acquired was assessed. Two parallel lines enclosing the data are drawn. The difference in height between the start of the hour and the end of the hour is expressed as drift in absorbance units per hour (AU/h).

5.1.2 Detector linearity comparison

Experimental Setup

Like the setup procedure in the previous section, the two detectors were turned on and left to sit idle for a period of 24 hours prior to assessment. The benchtop detector was set to 255 nm to match the wavelength of the LED in the portable detector. As per the ASTM E-685 standard, the concentration of the analyte used in the linear range assessment should generate a response above 2 AU. A 5000 ppm toluene in methanol stock solution was made. Dilutions covering a range from 0.1 to 1000 ppm were made to assess the linear range of each flow cell. The aim was to capture the detector responses in the 0 to 2 AU range.

The fluidic setup involved connecting PTFE tubing to the inlet of each flow cell using the appropriate finger tight nut. The samples were loaded directly into the flow cell through a luer slip connector on the end of the tubing. PTFE tubing was connected to the flow cell outlet from which the waste was collected.

Experimental Procedure

For the benchtop detector, the blank sample was loaded into the flow cell using a 1ml disposable syringe. The detector was zeroed through the Chromeleon software and manual data acquisition began. Each standard was left in the flow cell for a minimum of one minute. As the standards were loaded into the flow cell in increasing concentration, a new syringe was used. These syringes were kept for the portable detector assessment. Once all the standards had been assessed, the data acquisition was stopped and saved. Data was exported to an excel spreadsheet for further processing.

The procedure for the portable detector was carried out in the same manner, however the detector readout is a transmittance value. As transmittance and absorbance are inversely related, the LED current was adjusted to give a value just below the saturation of the photodiode. For the TOCON C1 photodiode used in the portable detector, this value was 5% below the supply voltage or 3135 mV. The transmittance signal was recorded through a serial terminal and saved as a CSV file for post processing where the transmittance would be converted to absorbance.

5.1.3 Portable and benchtop detector comparison

A direct comparison between the portable detector and benchtop detector was conducted to compare baseline noise, peak height, and area. The benchtop detector was placed in-line between the portable detector and the separation column. This experiment was carried out prior to the assembly of the portable HPLC system which enabled easy integration to the benchtop unit.

Experimental Setup

The setup consisted of the major components of the portable HPLC being integrated with the benchtop HPLC. Like that seen in section 4.1.7, the swash plate pump was connected into the benchtop pump's outlet unit as well as the automated injection valve connected to the input ports on the back of the benchtop pump to automate data acquisition. The separation column outlet was connected to the benchtop detector while the outlet of the detector was connected to the portable HPLC detector. Figure 5.4 summarises the setup.

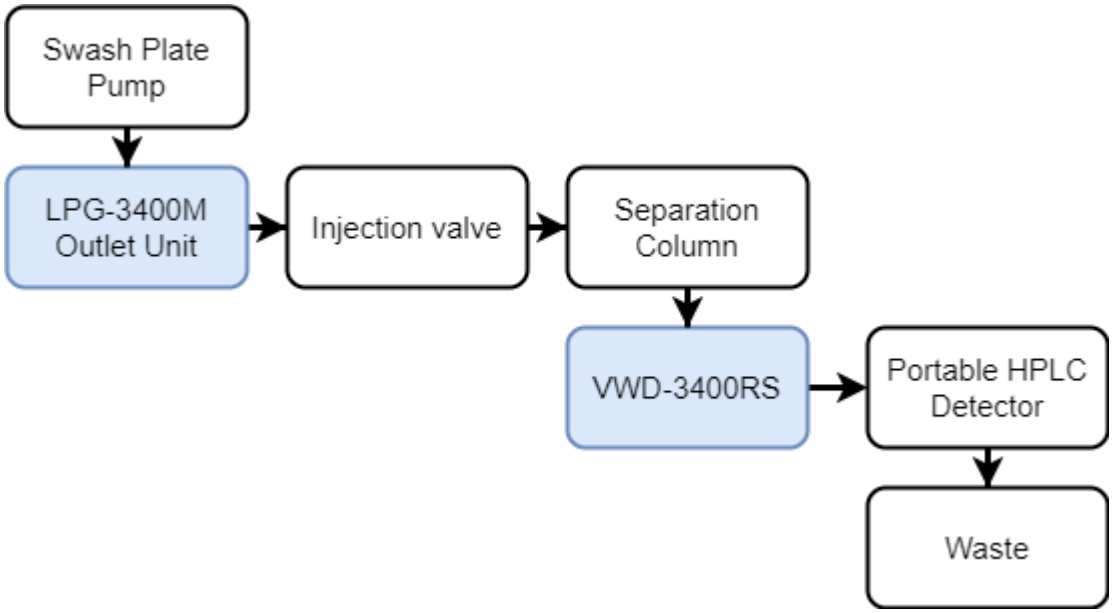

Figure 5.4 – Integration of portable HPLC components (white) with the benchtop pump and detector (blue).

Test conditions

- Column: PerkinElmer Universal H-C18, 250 x 4.6 mm, 5 µm particle size
- Mobile Phase A: Acetonitrile
- Mobile Phase B: Water
- Isocratic, A:B 60:40
- Flow Rate: 1 ml/min
- Injection Volume: 1 µL
- Detection: Benchtop - UV at 255 nm

Experimental Procedure

The swash plate pump was set to the flow rate of 1 ml/min and turned on. The 1 µL sample loop was loaded with the Phenomenex AL0-3045 dilution used in the pump repeatability assessment. Five injections were made with data acquisition on both the benchtop and portable systems synchronised.

5.1.4 Portable and benchtop HPLC system comparison

While the assessment detailed in the previous section compared both detectors in an integrated experimental setup, the following comparison compares both systems separately, with the fully assembled portable HPLC system being compared to the benchtop HPLC. Separation parameters between the two systems would be compared.

Experimental Setup

For this experiment, an isocratic separation of four paraben compounds was carried out on the benchtop HPLC and the portable HPLC system using the same column and mobile phase. The purpose was to compare the chromatograms of each system to see if the portable HPLC developed is comparable to a high-spec laboratory system. The following test conditions were used for the comparison:

Test conditions

- Column: Waters NovaPak C18, 150 x 3.9 mm, 4 µm particle size
- Mobile Phase A: Methanol
- Mobile Phase B: Water
- Isocratic, A:B 60:40
- Flow Rate: 1 ml/min
- Injection Volume: 5 µL
- Detection: UV at 255 nm

Both systems were turned on and allowed to settle for at least an hour prior to analysis. The wavelength of the benchtop detector was set to 255 nm to match that of the portable detector. Similar to the repeatability study described in section 4.1.7, a program was written to control the benchtop HPLC data acquisition based on the output signal from the automated injection valve. A 500 ml batch of the mobile phase was made and loaded into a solvent reservoir on the benchtop system. Once the fluidics were purged with the mobile phase, the column was connected. The column was then flushed with ten column volumes of mobile phase at a flow rate of 1 ml/min to equilibrate the column.

Experimental Procedure

The 5 µL sample loop was manually loaded with the paraben mixture and acquisition automatically began once the injection switch was toggled. Once five injections of the paraben mixture were analysed by the benchtop HPLC, the column and solvent reservoir were disconnected and transferred over to the portable system. The portable system fluidics were purged with the mobile phase and the column was connected. The column was given a short duration flush while the 5 µL sample loop was transferred on to the injection valve in the portable HPLC. Five injections were performed with data being recorded to a microSD card in the portable HPLC detector electronics module. The data was captured in CSV format where it was imported into UniChrom software for post processing.

5.2 Portable system experimental results and discussion

Section 5.2 presents and discusses the results of the experiments described in section 5.1.

5.2.1 Detector noise and drift

Detector noise and drift assessments were carried out using the ASTM 685-93 protocol. Figure 5.5 represents the output from the short-term noise test divided into the fifteen segments.

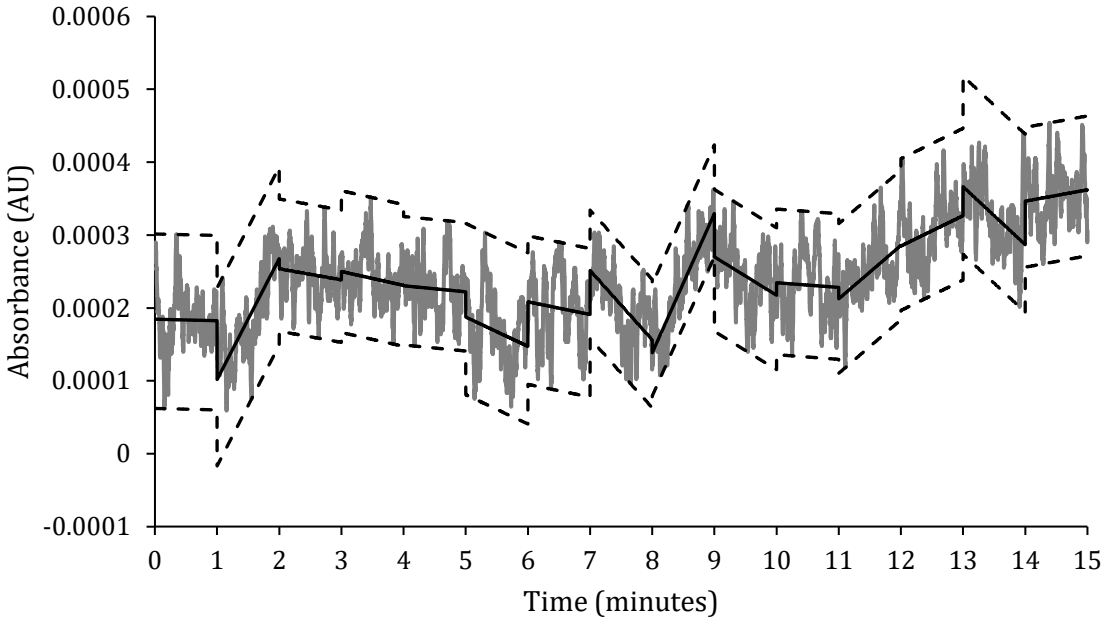

Figure 5.5 - Portable detector short term noise. Dry flow cell, static conditions.

The black line represents the trend for each segment from which the parallel dotted lines were drawn. The average distance in absorbance units (AU) between the maximum and minimum dotted lines for the fifteen segments is 2.03×10^{-4} AU which represents the short-term noise of the detector.

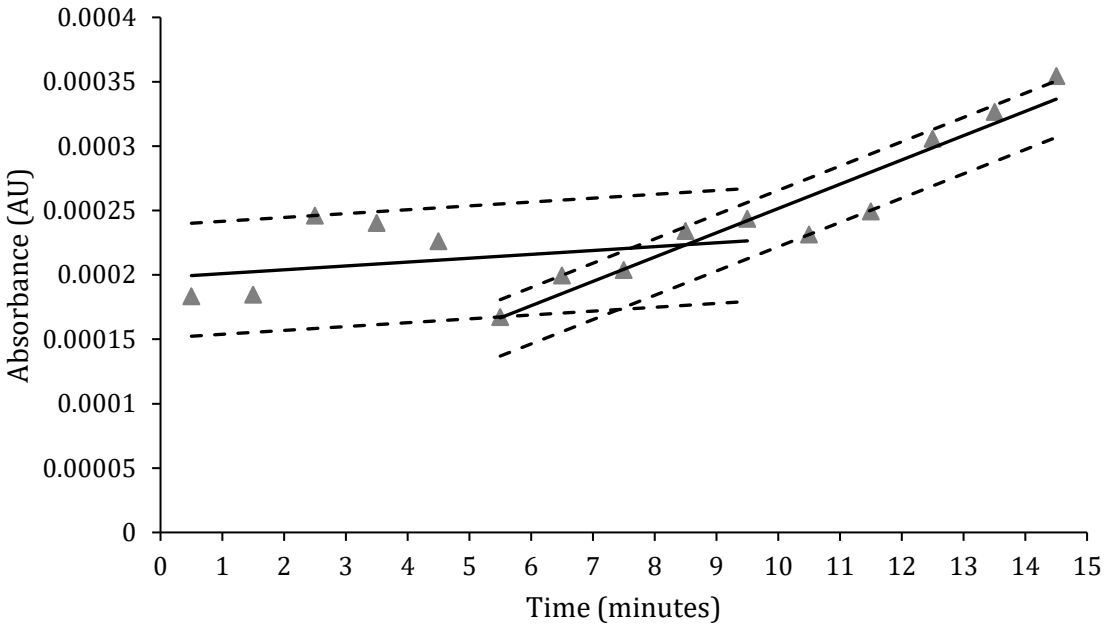

Figure 5.6 - Portable detector long term noise. Dry flow cell, static conditions.

Figure 5.6 represents the long-term noise test. Again the distance between the dashed parallel lines is measured. The larger value of the two values is considered the long-term noise. In this case, a measurement of 4.38×10^{-5} AU was observed for the first 10 minutes of the 15-minute assessment.

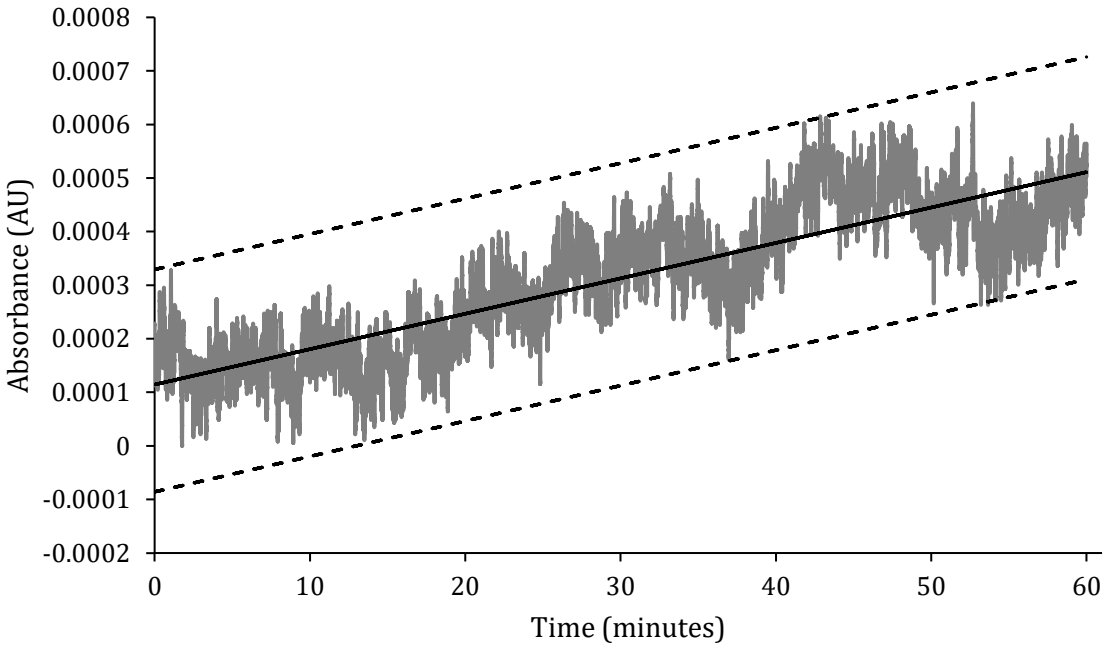

Figure 5.7 - Portable detector drift. Dry flow cell, static conditions.

Finally the detector drift was assessed over a 60-minute period. The drift is measure by the absolute value of the difference in the initial and final value of the lower dashed line seen in figure 5.7. From the above assessment a value of 3.97×10^{-4} AU per hour was recorded. Table 5.3 summarises the results of the noise and drift assessments as well as compares the values to several benchtop UV-VIS detectors. Noise specifications have been normalised to micro values (10^{-6}) while drift specifications have been normalised to 10^{-4} values for easier comparison.

Table 5.3 – Comparison of noise and drift values based on ASTM 685-93

Manufacturer	***Model***	***Noise (AU)***	***Drift (AU/h)***
Agilent	G7114A	$< \pm 2.5 \times 10^{-6}$	$< 1 \times 10^{-4}$
Dionex	VWD-3400RS	$< \pm 3.5 \times 10^{-6}$	$< 1 \times 10^{-4}$
Knauer	AZURA UVD 2.1	$\pm 15 \times 10^{-6}$	3×10^{-4}
Shimadzu	SPD-40	$\leq 4 \times 10^{-6}$	$\leq 1 \times 10^{-4}$
Waters	2489	$\leq 5 \times 10^{-6}$	$\leq 1 \times 10^{-4}$
Portable Detector	-	$\leq 203 \times 10^{-6}$ *(ST)* $\leq 43.8 \times 10^{-6}$ *(LT)*	$\leq 3.97 \times 10^{-4}$

As expected, the noise and drift values are higher than those reported for benchtop UV-VIS detectors, although the portable detector drift is close to that of the Knauer AZURA UVD 2.1. The simple arrangement used in the portable HPLC while rugged, does not have the performance for low level detection.

5.2.2 Detector linearity comparison

A range of toluene standards was made for this assessment ranging from 0.1 to 1000 ppm. For both detectors, each standard was introduced into the detection channel using a 1 ml syringe. was difficult on both detectors. As figure 5.8 shows, there was difficulty in achieving a stable response below 5 ppm on both the portable detector and the benchtop detector.

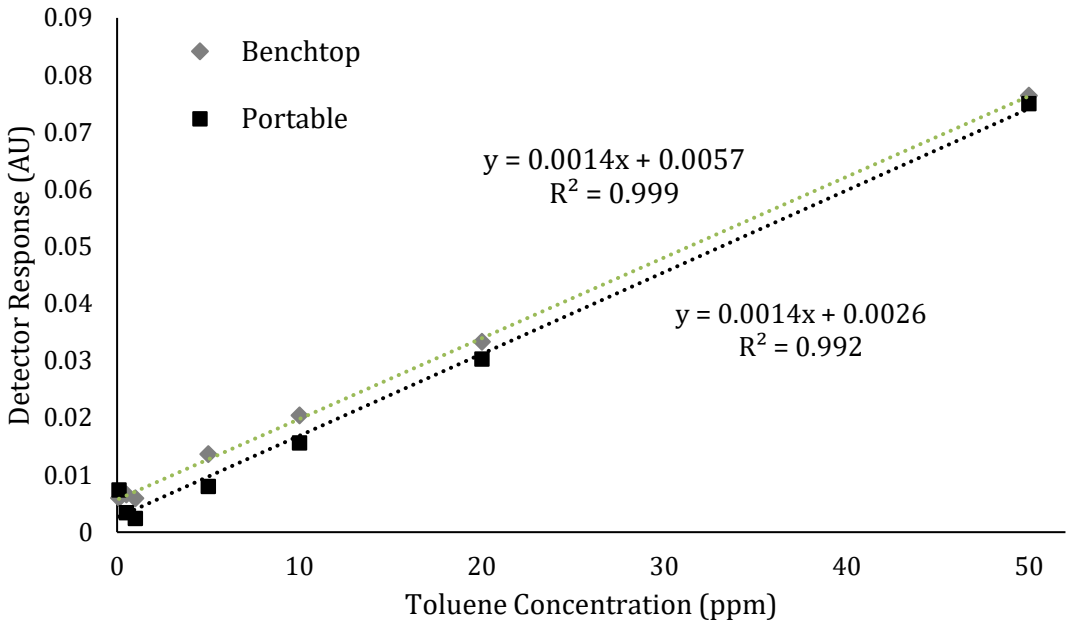

Figure 5.8 - Response of the benchtop and portable detectors to (n = 7) toluene dilutions ranging from 0.1 to 50 ppm. The slope of the linear regression shows a similar sensitivity between the benchtop and portable detectors.

The linear regression figures are based on the 0.1 to 50 ppm values for each detector. The linear regression for each detector is calculated over the seven increasing concentrations of Toluene. Taking the outliers into account, the benchtop detector reports an R^2 value of 0.999 at 255 nm while the portable system reports an R^2 value of 0.992 at 255 nm. The poor performance at the low end of the standard for both detectors is due in part to the sensitivity in flow, where small syringe plunger movements would alter the signal. Both detectors upper linearity is reported at 900 ppm toluene. The response for each detector for 1000 ppm drifted out of the linear range as seen in figure 5.9. This represents an upper limit of linearity of 1.22 AU for toluene on the benchtop detector and 1.30 AU for the portable detector. The linear regression values reported for the high concentration range and low concentration range are shown in table 5.4 below.

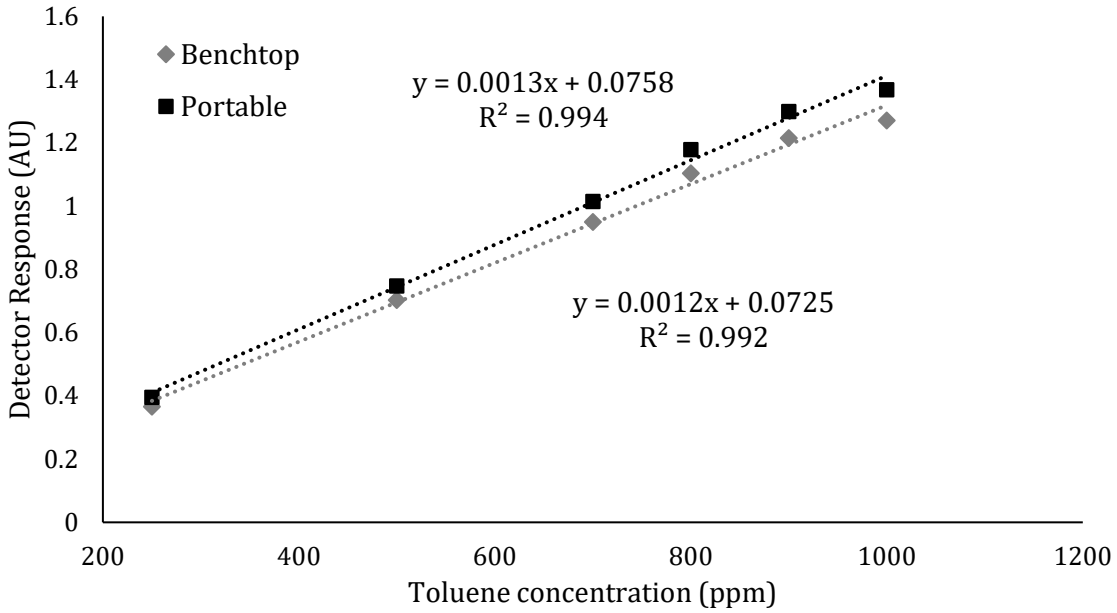

Figure 5.9 – Response of the benchtop and portable detectors to (n = 6) toluene dilutions ranging from 250 to 1000 ppm.

Table 5.4 - Linear regression comparison.

Detector	***Linear Regression***	***Range (ppm)***
Benchtop	0.999	0.1 - 50
Portable HPLC	0.992	0.1 - 50
Benchtop	0.992	250 - 1000
Portable HPLC	0.994	250 -1000

The portable detector performance is closely matched to the benchtop detector with exception at the lower concentrations of toluene. Due to the detector sensitivity to flow, difficulties in acquiring acceptable responses limits the usability of the setup in the portable system. Both systems report an R^2 value of 0.999 when calculating the linear regression using the 900 ppm standard as the upper limit.

5.2.3 Portable and benchtop detector comparison

The initial comparison took place before the assembly of the portable HPLC. The swash plate pump, injection valve and detector were integrated with the benchtop HPLC with the aim of a direct comparison between the benchtop and portable detectors. Of the five injections carried out, three represented acceptable chromatograms shown in figure 5.10.

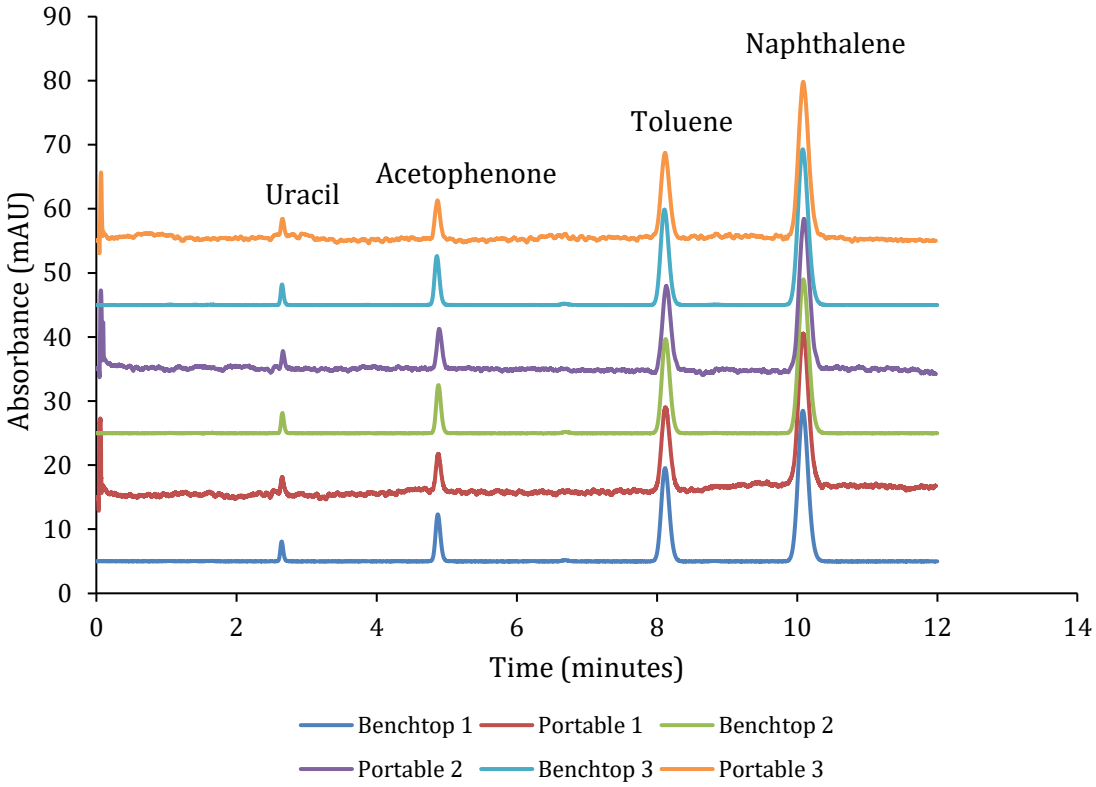

Figure 5.10 - Comparison of three chromatograms from the benchtop and portable detectors representing uracil, acetophenone, toluene and naphthalene. Separation conditions: Column C18 250 x 4.6 5µm particle size, Isocratic 60:40 Acetonitrile:DI Water, Flow rate 1 ml/min, Injection volume 1µL, Detection UV at 255 nm.

The overlaid chromatograms in figure 5.210 above illustrate the performance of the portable unit. Concentrations for the analytes were as follows; uracil 0.25 ppm, acetophenone 5.5 ppm, toluene 235.5 ppm and naphthalene 235.5 ppm. Table 5.5 gives a comparison of the peak height and area of each analyte from the portable system runs as a percentage of the equivalent data from the benchtop detector.

Table 5.5 - Portable detector peak areas expressed as a percentage of Benchtop detector peak areas.

Analyte	***% Benchtop Peak Height***	***% Benchtop Peak Area***
Uracil	83.83	85.42
Acetophenone	80.60	84.87
Toluene	89.72	94.64
Naphthalene	98.98	100.99

The portable detector shows reduced peak height and area for three of the four compounds in the mixture. Values for naphthalene are comparable to the benchtop detector. Starting with uracil, as presented in the preceding two sections the portable detector noise and linearity are relatively poor for low level detection. As uracil is at low levels in the sample, the sensitivity for the compound is poor. It should be noted that the peak absorbance wavelength for uracil is around 255 nm which may explain higher sensitivity than acetophenone which has a peak absorbance value around 190 nm and is over twenty times higher in concentration than uracil. Toluene and naphthalene are both at high levels in the sample. Although their peak absorbance values are over of 260 nm, naphthalene has a higher absorbance at 255 nm than toluene. This explains why naphthalene is almost identical to the benchtop detector values. The slightly higher peak area percentages are potentially due to band broadening as the analyte exited the benchtop detector and made its way to the portable detector.

Table 5.6 - Portable and benchtop detector baseline noise comparison.

Detector	***Noise (AU)***
Portable	6.93×10^{-4}
Benchtop with swash pump	1.42×10^{-5}
Benchtop detector with benchtop pump*	2.04×10^{-5}

* Chromatograms included in appendix C.

Table 5.6 outlines the baseline noise prior to uracil from the separations shown in figure 5.10. A ten second window of data was analysed for the highest and lowest value. The portable detector as expected, showed the highest noise levels, 48 times higher than the benchtop detector during the same separation. For comparative purposes and to rule out noise caused by the swash plate pump, previous separations conducted using the benchtop pump and detector were analysed in the same way. Baseline noise using the swash plate pump was 1.43 times lower than the separations carried out with the benchtop pump.

Limit of detection (LOD) and limit of quantification (LOQ) were calculated using baseline noise. LOD is calculated as the signal-to-noise ratio (S/N) = 3 while LOQ is calculated as S/N = 10. As no calibration curves were generated, the LOD and LOQ for the benchtop detector and portable detector are reported in AU. Based on the noise values in table 5.6, table 5.7 outlines the LOD and LOQ for the portable and benchtop detectors.

Table 5.7 - Portable and benchtop detector limit of detection and limit of quantification comparison.

Detector	***LOD (AU)***	***LOQ (AU)***
Portable	20.79×10^{-4}	6.93×10^{-3}
Benchtop with swash pump	4.26×10^{-5}	1.42×10^{-4}
Benchtop detector with benchtop pump*	6.12×10^{-5}	2.04×10^{-4}

5.2.4 Portable and benchtop HPLC system comparison

A HPLC isocratic systems diagnostic mix containing methyl paraben, ethyl paraben, propyl paraben and butyl paraben was sourced from Sigma Aldrich (Wicklow, Ireland). Using the certificate of analysis as a guideline, a methanol-water mobile phase was used on a Waters NovaPak C18 150 x 3.9 mm column. An isocratic separation of the four parabens occurred in under 10 minutes. Concentrations for the paraben mixture is shown in table 5.7.

Table 5.8 – Paraben mixture component concentrations.

Analyte	***Concentration (ppm)***
Methyl paraben	10
Ethyl paraben	14
Propyl paraben	15
Butyl paraben	25

Using the full benchtop system with the mobile phase set to flow at 1 ml/min, five back-to-back injections were made onto the column and the resulting chromatograms can be seen in figure 5.11 below. The column was held at room temperature due to lack of a column oven. The sample loop, column and mobile phase were then transferred over to the portable system. Once the system was primed and equilibrated, five back-to-back injections of the same sample were carried out as shown in figure 5.12. Following the two sets of chromatograms is a comparison of peak retention times and areas. Along with a system void volume comparison, the separation parameters of retention factor, efficiency, selectivity factor, peak height and area, and resolution, will be discussed.

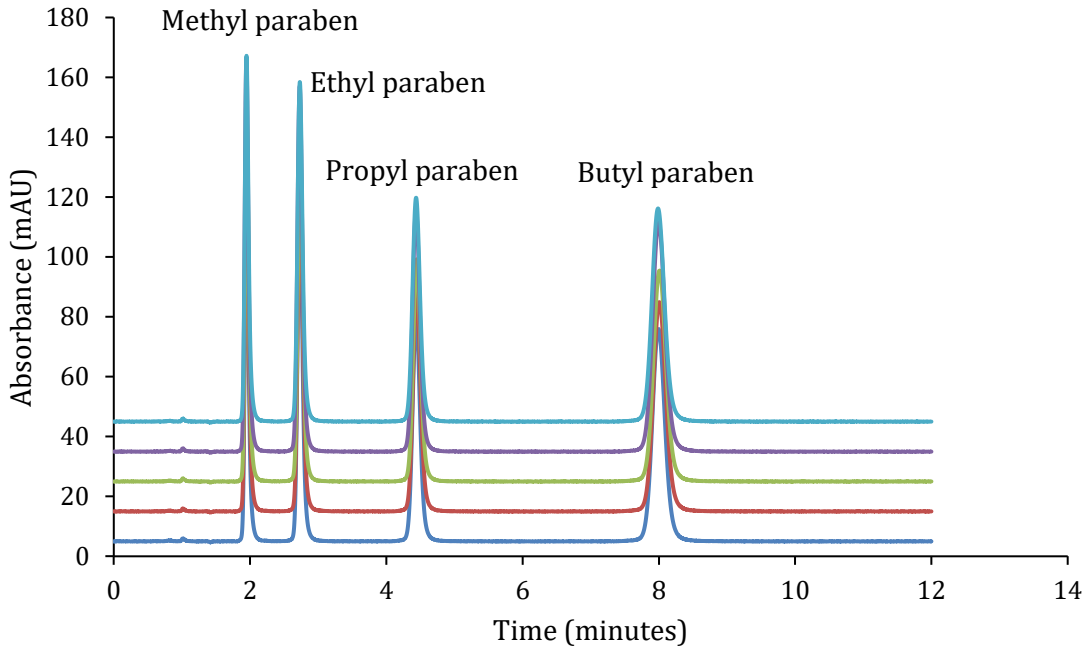

Figure 5.11 - Chromatograms of five paraben mixture separations performed on the benchtop HPLC. Column C18 150 x 3.9 4µm particle size, Isocratic 60:40 Methanol:DI Water, Flow rate 1 ml/min, Injection volume 5µL, Detection UV at 255nm.

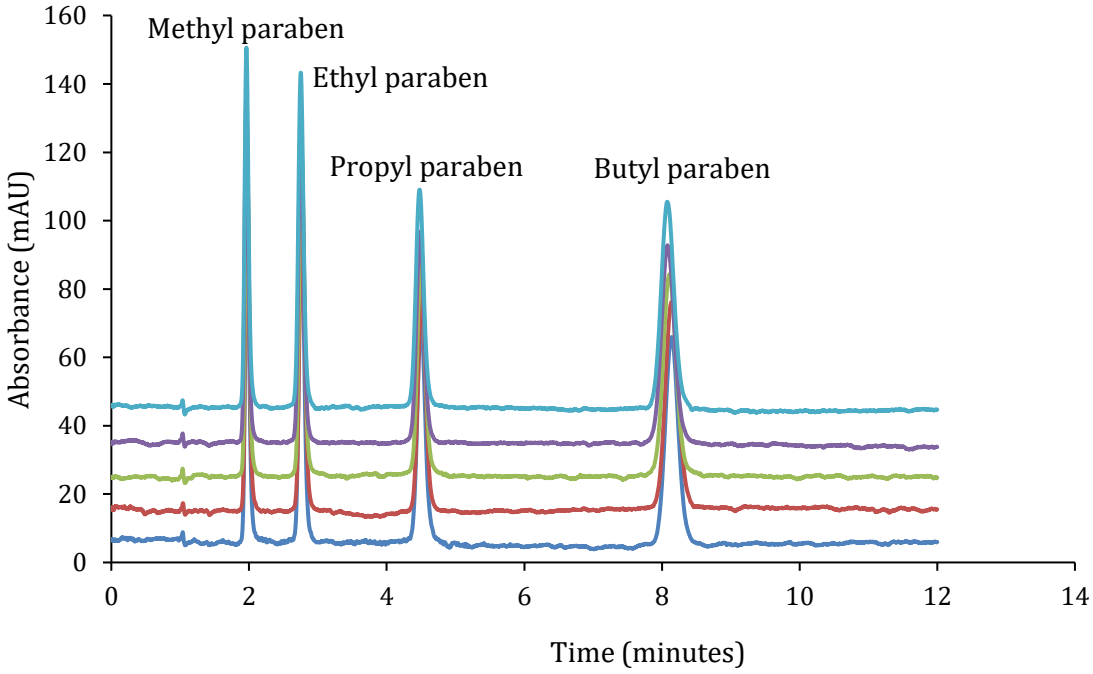

Figure 5.12 - Five overlaid chromatograms of paraben mixture separation performed on the portable HPLC system. Column C18 150 x 3.9 4µm particle size, Isocratic 60:40 Methanol:DI Water, Flow rate 1 ml/min, Injection volume 5µL, Detection UV at 255nm.

The following sections discuss the features and separation parameters of the two sets of chromatograms seen in figures 5.11 and 5.12.

Peak areas and retention times

Table 5.9 – Separation retention times of the benchtop and portable systems.

Analyte	***Benchtop Retention Time***	***Portable Retention Time***
Methyl paraben	1.949	1.966
Ethyl paraben	2.732	2.759
Propyl paraben	4.440	4.494
Butyl paraben	7.998	8.109

Table 5.10 – Separation peak areas of the benchtop and portable systems.

Analyte	***Benchtop Peak Area***	***Portable Peak Area***
Methyl paraben	8.763	7.348
Ethyl paraben	10.666	8.917
Propyl paraben	10.488	8.651
Butyl paraben	16.321	13.519

Comparable retention times seen in table 5.8 show that the fluidic system including the pump and injector are working as desired. The reduced peak areas presented in table 5.9 from the portable system however point to a less than ideal performance of the detector. The peak widths from both systems are similar but the peak heights reported by the portable system are on average 16.76% less than those reported by the benchtop detector. This is in line with the findings in the previous section for lower analyte concentrations and explains the lower peak areas seen here.

A ten second window of baseline noise was taken around the 6-minute point of the fifth injection reveals results broadly in line with those seen previously in table 5.6. Baseline noise on the benchtop system of 2.15×10^{-5} AU is observed while the portable system noise is 4.32×10^{-4} AU.

System void volume

Chromatograms from both the benchtop and portable system show an injection peak which can be used to calculate the void volume of each system and represent the dead time of the separation. Figure 5.13 shows a close-up of the injection peaks overlaid. Because the flow rate is 1 ml/min, the void volume is approximately 1 ml for each system. Using these dead times the retention factors for the analytes can be calculated.

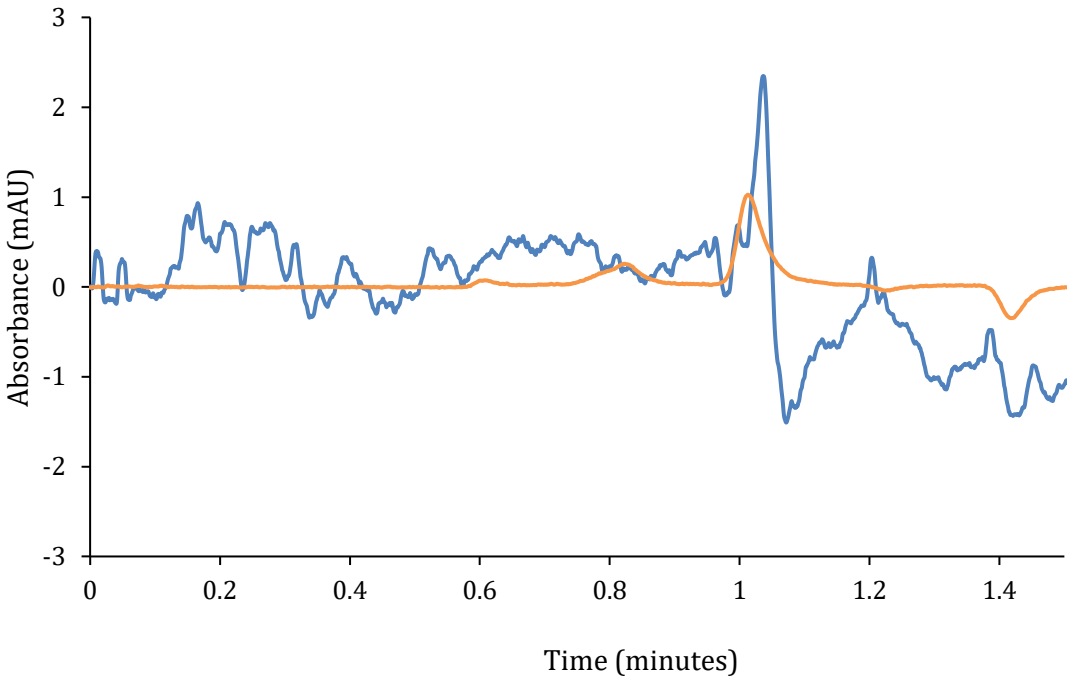

Figure 5.13 – Overlaid chromatograms from the benchtop and portable systems giving dead times of 1.01 and 1.04 minutes, respectively.

Retention factors

The retention factor k, is a method of measuring the retention of an analyte on the separation column. It is represented by equation 1.2, previously seen in chapter 1:

$$k = \frac{t_R - t_0}{t_0}$$

Where t_0 is the dead time and t_R is the retention time of the peak of interest. Table 5.10 compares the average retention factors of the analytes from the separations carried out on both systems.

Table 5.11 – Separation retention factors of the benchtop and portable systems.

Analyte	***Benchtop Retention Factor***	***Portable Retention Factor***
Methyl paraben	0.925	0.896
Ethyl paraben	1.698	1.661
Propyl paraben	3.385	3.333
Butyl paraben	6.899	6.818

With the ideal retention factor value existing between 1 and 5 for simple matrices or 2 to 10 for more complex matrices, the retention factor for methyl paraben is less than ideal. In the case of this separation it is not a problem as the sample contains known analytes. With a sample of unknown composition however, there is a chance of interfering peaks with a retention factor less than 1. In this case, decreasing the amount of methanol in the mobile phase would increase the retention factors of the four parabens in the mixture. The portable and benchtop systems are comparable in terms of the retention factors.

Selectivity factors

The selectivity factor between two peaks, is the ratio of the retention factors of the two peaks in question. A selectivity factor of 1 would indicate co-eluting peaks with the same retention factor. Table 5.11 summarises the selectivity factors for each system between the first two peaks and final two peaks.

Table 5.12 – Separation selectivity factors of the benchtop and portable systems.

Analyte	***Benchtop Selectivity Factor***	***Portable Selectivity Factor***
Methyl paraben	1.836	1.854
Ethyl paraben		
Propyl paraben	2.038	2.046
Butyl paraben		

Again, though the composition of the sample is known, it is interesting to observe the difference in selectivity factor and how it looks on the chromatograms in figures 5.11 and 5.12. Again both systems give comparable results.

Peak efficiency

Efficiency is a measurement of the diffusion of an analyte band as is passes through the separation column. With the separation column divided into theoretical plates, the higher the number of plates, the better separating power the column has. The average theoretical plate values presented in table 5.12 for the benchtop system are taken from Chromeleon software which uses the European Pharmacopoeia method of calculating peak efficiency represented in equation 5.2:

$$Theoretical\ Plates = 5.54 \times \left(\frac{t_R}{W_{50\%}}\right)^2 \quad (5.2)$$

The width at half height and retention time data for the portable system separations was extracted with Unichrom software and used in equation 5.2 inside Microsoft Excel. The calculations were performed to generate the average number of plates for each peak with the results shown in table 5.12. Both systems show a comparable peak efficiencies for all four analytes, which is to be expected given the same chromatographic conditions.

Table 5.13 – Separation retention factors of the benchtop and portable systems.

Analyte	***Theoretical Plates Benchtop***	***Theoretical Plates Portable***
Methyl paraben	5543	5923
Ethyl paraben	6056	5183
Propyl paraben	6971	6570
Butyl paraben	8263	8191

Although the sensitivity of the detector has impacted the performance of the portable HPLC, with similar separation parameters of void time, retention factor, selectivity factor and efficiency between the benchtop and portable systems observed, the fluidic system performs to a comparable level with a benchtop HPLC.

5.3 Chapter 5 conclusion

Chapter 5 detailed the characterisation and performance of the portable system. First by characterising the portable detector developed and comparing it to a benchtop HPLC detector. Second, the fully assembled portable system was compared to the benchtop HPLC in a laboratory setting. The portable detector noise and drift was assessed as well as the linearity of response. Detector noise and drift assessments were carried out using the ASTM

685-93 protocol, reporting noise levels up to 80 times higher than commercially available benchtop HPLC detectors and drift up to 4 times higher. The linearity study showed similar performance at concentrations above 250 ppm Toluene at 254 nm. Linearity at lower concentrations was less than that of the benchtop detector. A comparison of the portable and a benchtop HPLC detectors revealed lower sensitivity as seen in reduced peak heights and peak areas. Finally, comparing the fully assembled portable HPLC to the benchtop HPLC using a Paraben mixture revealed similar peak retention times, system void volume, peak retention factors, peak selectivity factors and similar peak efficiency. Once again, peak areas reported were smaller due to the lower sensitivity of the portable detector.

Chapter 6 Conclusions and future work

6.1 Achievements

This thesis presents the development and testing of a novel, portable high-pressure pump, and demonstration of its use in a portable application through the development of a portable high performance liquid chromatography system. Through the development of a novel control algorithm coupled with the use of a swash plate mechanism, pulsations due to the reciprocating motion of pistons were reduced, and a lightweight, compact, robust pump was realised. The pump design was tailored for ease of manufacture through 3D printing and all chassis components were printed in-house. The upgraded chassis design delivered a more robust pump compared to the mark one design, capable of long run times at high pressures. Control electronics and firmware were developed to enable the pump to operate as a standalone pump as well as integrated into a portable system.

The pump was characterised through assessment of power consumption and piston displacement profiles were compared to the ideal profile Flow rate attributes of accuracy, drift and precision were assessed along with pressure ripple and a leak test. The mark two pump is capable of operating at flow rates up to 2250 µL/min and operating pressures up to 300 bar with flow accuracy, precision, and noise comparable to benchtop HPLC pumps. A second pump was built and is currently being used with success in a portable ion chromatograph with a microbore analytical column operation at sub 500µL/min flow rates.

The portable HPLC was developed as a platform to demonstrate the pump's capabilities. A robust design was assembled in CAD software to assess layout configurations prior to 3D printing of components and assembly. The portable platform developed, incorporated previously field-deployed hardware onto which the components were mounted. The design of the portable system allows easy access to all components housed within. A custom design automated injection valve was developed with control electronics to enable independent operation as demonstrated in the repeatability assessment. The injection valve can be operated with a switch or through a 5 Volt on/off signal from an external controller. A detection system combining an off the shelf z-cell coupled with a UV-LED and photodiode was built to perform data acquisition and system control of the portable HPLC.

Combined with the mark two swash plate pump, the automated injection valve, and the detection system, the portable HPLC is capable of performing isocratic separations with UV photometric detection with over 100 hours of run time. Separations with two reverse phase C18 separation columns were demonstrated. First, a 250 mm long, 4.6 mm inner diameter

column was used to assess the pump's precision and compare the portable detector to a benchtop detector. Second, a 150 mm long, 3.9 mm inner diameter column was used for the separation of a mixture of parabens. These separations were conducted to compare the portable HPLC to a benchtop HPLC. The portable system reported similar retention factors, selectivity factors, and peak efficiencies over 5 back to back separations. A summary of specifications for the pump and portable HPLC system is available in appendix A.

6.2 Limitations of designs and future work

Swash Plate Pump

While the pump's flow rate range within the context of this work is suitable for the use of analytical scale columns of which typically require flow rates of 1 to 1.5 ml/min, the main limitation of the pump is the restriction of the flow rate range from 0.1 to 2 ml/min. This is in comparison to the Dionex GP50 pump from which the heads used have an operating range from 0.04 to 10 ml/min. This limit is due to four factors. The first factor is the material the pump chassis is constructed with. A nylon/carbon fibre composite 3D printer filament was used to create robust components with a high-quality surface finish. While the material is quite strong, striking the balance between a serviceable pump design while keeping material use to a minimum was challenging. As the fluidic back pressure increases and increasing loads are transferred from the pistons to the swash plate, the distribution of forces through the material causes the pump head and motor plates to flex.

The second issue is that of fluid compressibility. For each bar increase in pressure, the volume of water will decrease by approximately 47 parts per million. A loss in volume displaced due to the compression of water inside the pump head at a flow rate of 1 ml/min at 100 bar of back pressure would result in an actual flow rate 995.42 µL/min or 99.54% accuracy. This reduces to 99.1 % at 200 bar of pressure. However coupled with the movement in the chassis, the pump reported lower accuracy figures.

The third issue is swash plate velocity. As discussed, as piston displacement due to the swash plate angle increases, the power consumption of the motor increases. As presented, a low angle swash plate is selected for use. However, increasing the rotational velocity of the swash plate results in higher side loading of the piston plunger seals which is added to as back pressures increase and chassis movement occurs.

The fourth issue lies in the flow rate sensor used, which deliver a full scale flow rate up to 2000 µL/min, but can output values up to 3000 µL/min. The combination of design revisions and the use of a flow sensor helped mitigate the pumping losses due to increased chassis movement. While not utilising the full potential of the pump heads, the 0.1 to 2

ml/min flow rate range is suitable for use with a wide range of analytical scale separation columns and analytical methods.

Within the employment partner's research and development department, work is being carried out through European funded projects to develop the next generation of portable analysers based on liquid chromatography. As part of this, work is ongoing to develop a metal pump chassis using elements of the design presented in this thesis, as well as custom design pump heads.

Portable HPLC

The main issue with the portable HPLC developed is the detector noise. The detector setup is unsuitable for the detection of low level analytes in field samples, due to the high noise levels seen in the chromatogram baselines. The physical setup, using fibre optic cables to pass light through the detection channel is a robust design suitable for field applications. However, three areas for improvement have been identified.

Firstly, correct coupling of light from the LED to the fibre optic cable should be considered. The current setup consists of butt-coupling of the fibre end to the LED and PD surfaces. While effective in terms of transmitting light through the detection channel, higher sensitivity may be achieved through the correct coupling of the fibres to the optical components with the use of ball lenses. Secondly, the constant current driver used is suitable for high power LEDS such as the 255 nm one used in the detector system. However, the intensity of the LED was never increased above 35% during the course of the research as the PD was easily saturated. As the LED intensity is controlled through a PWM signal, the lower the PWM signal the increase in baseline noise. An LED constant current driver capable of operating at low power levels should be considered.

Finally, the implementation of robust filtering algorithms needs to be examined. The current system uses a running average to reduce the detector baseline noise levels. More complex smoothing functions such as Savitsky-Golay are used on benchtop detectors to smooth baseline noise while keeping peak shapes and areas intact. A combination of the three outlined noise reduction solutions should result in a detector system that could potentially detect low level analytes in surface and ground waters.

Future work

During this research, 3D printing technology was utilised to rapidly develop a pump chassis capable of operating at high back pressures. Work was carried out to improve the strength of the 3D printed chassis around the pump head plate and to stabilise the stepper motor during operation. This was achieved by increasing the cross-sectional area of the pump

head plate as well as the addition of a support piece around the stepper motor. These changes helped stabilise the pump heads during operation and helped to reduce piston sideloading. While no failures of the chassis occurred during this research, little is known about the long-term effects of the stresses on the carbon fibre nylon composite filament used in the 3D printer that would be induced by pumping at high back pressures. Future work should utilise finite element analysis (FEA) which can simulate real-world forces on 3D models of components. By investigating FEA of the pump chassis, the main stress points in the chassis during operation would be identified. This will help to predict the maximum forces than can be sustained and the lifespan of the developed pump. Based on the results of the investigation, alternative designs and materials should be tested before component manufacture and assembly. By carrying out FEA, improvements to the chassis design will aid in the development of a stronger and lighter frame leading to increased robustness, reduced cost and weight along with further reducing pressure pulsations and improving flow stability.

With the signing of a licence agreement for the pump technology developed during this research project and in addition to second pump built, a third will be commissioned for a second portable LC system using ion exchange chromatography. Along with the recommendations outlined for the portable detector, issues with the pump design will be addressed to increase the flow rate range for use with microbore columns and the transition of the pump design from the R&D department into New Product Development department will begin.

References

[1] Environmental Protection Agency (2021) Ireland's national Water Framework Directive Monitoring Programme, 2019-2021 [online], Available: https://www.epa.ie/publications/monitoring--assessment/freshwater--marine/irelands-national-water-framework-directive-monitoring-programme-2019-2021.php [Accessed: 02 August 2022].

[2] RTE News (2022, July 30) 'Significant' fish kill investigated on River Erkina, https://www.rte.ie/news/leinster/2022/0730/1313127-river-erkina-fish-kill/ [Accessed: 03 August 2022].

[3] TheJournal.ie (2022, July 26) Investigation launched after fish kill in Cavan river, https://www.thejournal.ie/fish-kill-cavan-inland-fisheries-investigation-5826311-Jul2022 [Accessed: 03 August 2022].

[4] TheJournal.ie (2022, August 03) Temporary swim ban enacted for Dollymount and Sandymount Strands https://www.thejournal.ie/sandymount-dollymount-ban-swimming-e-coli-5831888-Aug2022 [Accessed: 03 August 2022].

[5] Directive 2013/39/EU of the European Parliament and of the Council.

[6] Persson L., Carney Almroth B.M., Collins C.D., Cornell S., de Wit C.A., Diamond M.L., Fantke P., Hassellöv M., MacLeod M., Ryberg M.W., Søgaard Jørgensen P., Villarrubia-Gómez P., Wang Z., and Zwicky Hauschild M. (2022), Outside the Safe Operating Space of the Planetary Boundary for Novel Entities, Environmental Science & Technology, 56(3), 1510-1521.

[7] Cousins I.T., Johansson J.H., Salter M.E., Sha B., and Scheringer M. (2022), Outside the Safe Operating Space of a New Planetary Boundary for Per- and Polyfluoroalkyl Substances (PFAS), Environmental Science & Technology 2022 56 (16), 11172-11179..

[8] Farradane, J. (1951), History of Chromatography. Nature 167, 120.

[9] Heines S.V. (1969), Three who pioneered in chromatography, Journal of Chemical Education 46 (5), 315.

[10] Ettre, L.S., Sakodynskii, K.I. (1993), M.S. Tswett and the discovery of chromatography I: Early work (1899–1903), Chromatographia 35, 223–231.

[11] Ettre L.S. (2007), The Rebirth of Chromatography 75 Years Ago, LCGC North America, LCGC North America-07-01-2007, Volume 25, Issue 7 Pages: 640–655.

[12] https://chem.libretexts.org/Bookshelves/Analytical_Chemistry/Analytical_Chemistry_2.1_%28Harvey%29/12%3A_Chromatographic_and_Electrophoretic_Methods/12.02%3A_General_Theory_of_Column_Chromatography [Accessed: 07 August 2022].

[13] https://cen.acs.org/articles/94/i24/50-years-HPLC.html [Accessed: 18 September 2022].

[14] Horvath C.G., Preiss B.A., and Lipsky S.R., (1967) Fast liquid chromatography. Investigation of operating parameters and the separation of nucleotides on pellicular ion exchangers, Analytical Chemistry 39 (12), 1422-1428.

[15] https://www.waters.com/nextgen/ie/en/library/application-notes/2021/the-importance-of-column-compartment-thermostatting-and-preheating-for-temperature-sensitive-separations-in-liquid-chromatography.html [Accessed: 18 September 2022].

[16] http://tools.thermofisher.com/content/sfs/brochures/WP-71499-LC-Temperature-Column-Thermostatting-WP71499-EN.pdf accessed 09/09/2022 [Accessed: 18 September 2022].

[17] https://www.knauer.net/en/Systems-Solutions/Column-tempering [Accessed: 18 September 2022].

[18] Vervoort N., Daemen D., Török G., (2008), Performance evaluation of evaporative light scattering detection and charged aerosol detection in reversed phase liquid chromatography,

[19] https://edu.rsc.org/download?ac=11391 [Accessed: 18 September 2022].

[20] https://www.shimadzu.com/an/service-support/technical-support/analysis-basics/basic/what_is_hplc.html [Accessed: 18 September 2022].

[21] Donald A. Wellings D.A., (2005) Modes of chromatographic separation. In Wellings D.A., (editor) A Practical Handbook of Preparative HPLC. Elsevier Science. 29-56.

[22] García-Alvarez-Coque M.C., Baeza-Baeza J.J. and Ramis-Ramos, G. (2015). Reversed Phase Liquid Chromatography. In Pino V., Anderson J.L., Berthod A. and Stalcup A.M., (editors) Analytical Separation Science. Wiley-VCH.

[23] Snyder, L.R., Kirkland, J.J. (1979), Introduction to Modern Liquid Chromatography (Second ed.). Wiley-Interscience. 90-92.

[24] https://www.waters.com/nextgen/ie/en/education/primers/beginner-s-guide-to-liquid-chromatography.html [Accessed: 18 September 2022].

[25] Shoykhet K., Broeckhoven K., and Dong M.W., (2019), Modern HPLC Pumps: Perspectives, Principles, and Practices, LCGC North America, LCGC North America-06-01-2019, Volume 37, Issue 6 Pages: 374–384.

[26] https://www.waters.com/webassets/cms/library/docs/WA63950.pdf [Accessed: 18 September 2022].

[27] https://www.crawfordscientific.com/chromatography-blog/post/building-your-hplc [Accessed: 18 September 2022].

[28] Sonika Sharma, Luke T. Tolley, H. Dennis Tolley, Alex Plistil, Stanley D. Stearns, Milton L. Lee, Hand-portable liquid chromatographic instrumentation, Journal of Chromatography A, Volume 1421,2015, Pages 38-47

[29] Baram, G. I., Grachev, M. A., Komarova, N. I., Perelroyzen, M. P., Bolvanov, Y. A., Kuzmin, S. V., Kargaltsev, V. V., & Kuper, E. A. (1983). Micro-column liquid chromatography with multi-wave-length photometric detection. I. The OB-4 micro-column liquid chromatograph. Journal of Chromatography A, 264(C).

[30] Baram, G. I. (1996). Portable liquid chromatograph for mobile laboratories: I. Aims. Journal of Chromatography A, 728(1–2), 387–399.

[31] Sharma, S., Plistil, A., Barnett, H. E., Tolley, H. D., Farnsworth, P. B., Stearns, S. D., & Lee, M. L. (2015). Hand-Portable Gradient Capillary Liquid Chromatography Pumping System. Analytical Chemistry, 87(20), 10457–10461.

[32] [Lam, S. C., Coates, L. J., Hemida, M., Gupta, V., Haddad, P. R., Macka, M., & Paull, B. (2020). Miniature and fully portable gradient capillary liquid chromatograph. Analytica Chimica Acta, 1101, 199–210.

[33] https://patents.google.com/patent/US4888295A/en [Accessed 20 September 2022].

[34] Rahimi, F., Chatzimichail, S., Saifuddin, A., Surman, A. J., Taylor-Robinson, S. D., & Salehi-Reyhani, A. (2020). A Review of Portable High-Performance Liquid Chromatography: The Future of the Field? In Chromatographia (Vol. 83, Issue 10). Springer Berlin Heidelberg.

[35] Takaaki Otagawa, Joseph R. Stetter, Solomon Zaromb, Portable liquid chromatograph for analysis of primary aromatic amines in coal-derived materials, Journal of Chromatography A, Volume 360,1986Pages 252-259.

[36] Tulchinsky, V. M., & Angelo, D. E. S. (1998). A Practical Portable HPLC System - MINICHROM, a New Generation for Field HPLC. Field Analytical Chemistry and Technology, 2(5), 281–285.

[37] Ishida, A., Fujii, M., Fujimoto, T., Sasaki, S., Yanagisawa, I., Tani, H., & Tokeshi, M. (2015). A portable liquid chromatograph with a battery-operated compact electroosmotic pump and a microfluidic chip device with a reversed phase packed column. Analytical Sciences, 31(11), 1163–1169.

[38] Li, Y., Dvo, M. S., Nesterenko, P. N., Stanley, R., Nuchtavorn, N., Kujovsk, L., Cmov, K., Aufartov, J., & Macka, M. (2015). Miniaturised medium pressure capillary liquid chromatography system with flexible open platform design using off-the-shelf microfluidic components.

[39] Lynch KB, Chen A, Yang Y *et al* (2017) High-performance liquid chromatographic cartridge with gradient elution capability coupled with UV absorbance detector and mass spectrometer for peptide and protein analysis. J Sep Sci 40:2752–2758.

[40] Chatzimichail S, Casey D, Salehi-Reyhani A (2019) Zero electrical power pump for portable high-performance liquid chromatography. Analyst.

[41] Chatzimichail, S., Rahimi, F., Saifuddin, A. *et al*. Hand-portable HPLC with broadband spectral detection enables analysis of complex polycyclic aromatic hydrocarbon mixtures. Commun Chem 4, 17 (2021).

[42] Sharma, S., Plistil, A., Simpson, R. S., Liu, K., Farnsworth, P. B., Stearns, S. D., & Lee, M. L. (2014). Instrumentation for hand-portable liquid chromatography. Journal of Chromatography A, 1327, 80–89.

[43] Zhao, X., Xie, X., Sharma, S., Tolley, L. T., Plistil, A., Barnett, H. E., Brisbin, M. P., Swensen, A. C., Price, J. C., Farnsworth, P. B., Tolley, H. D., Stearns, S. D., & Lee, M. L. (2017). Compact Ultrahigh-Pressure Nano flow Capillary Liquid Chromatograph.

[44] Foster, S. W., Xie, X., Pham, M., Peaden, P. A., Patil, L. M., Tolley, L. T., Farnsworth, P. B., Tolley, H. D., Lee, M. L., & Grinias, J. P. (2020). Portable capillary liquid chromatography for pharmaceutical and illicit drug analysis. Journal of Separation Science, 43(9–10), 1623–1627.

[45] https://axcendcorp.com/app-notes [Accessed: 21 September 2022].

[46] https://axcendcorp.com/wp-content/uploads/2020/02/Axcend-Focus-LC-v2-Spec-Sheet-Final-02-29-20.pdf [Accessed: 21 September 2022].

[47] Murray, E., Roche, P., Harrington, K., McCaul, M., Moore, B., Morrin, A., Diamond, D., & Paull, B. (2019). Low cost 235 nm ultra-violet light-emitting diode-based absorbance detector for application in a portable ion chromatography system for nitrite and nitrate monitoring. Journal of Chromatography A, 1603, 8–14.

[48] Murray, E., Roche, P., Briet, M., Moore, B., Morrin, A., Diamond, D., & Paull, B. (2020). Fully automated, low-cost ion chromatography system for in-situ analysis of nitrite and nitrate in natural waters. Talanta, 216(March), 120955.

[49] Fitzhenry, C., Jowett, L., Roche, P., Harrington, K., Moore, B., Paull, B., & Murray, E. (2021). Portable analyser using two-dimensional ion chromatography with ultra-violet light-emitting diode-based absorbance detection for nitrate monitoring within both saline and freshwaters. Journal of Chromatography A, 1652, 462368.

[50] Lace, A., Byrne, A., Bluett, S., Malaquin, L., Raimbault, V., Courson, R., Hayat, Z., Moore, B., & Murray, E. (2022). Ion chromatograph with three-dimensional printed absorbance detector for indirect ultraviolet absorbance detection of phosphate in effluent and natural waters. Journal of Separation Science, 45(5), 1042–1050.

[51] https://polylc.com/Downloads/Smart_LifeLC_Product_Data_Sheet-PolyLC_415nm.pdf [Accessed: 21 September 2022]

[52] https://www.thermofisher.com/order/catalog/product/ICS6000-015 [Accessed: 21 September 2022].

[53] https://www.prnewswire.com/news-releases/the-axcend-focus-lc-is-now-shipping--axcends-shoebox-sized-high-performance-liquid-chromatograph-transforms-hplc-science-for-analytical-chemists-worldwide-300797690.html [Accessed: 21 September 2022].

[54] Grinias J.P., Godinho J.M., Gritti F., Schug K.A., Bell D.S., Dasgupta P.K., (2020) State-of-the-Art in Capillary Liquid Chromatography (LC): Now, Next, and How?, LCGC North America, LCGC North America-02-01-2020, Volume 38, Issue 2.

[55] Neubauer K., (2009) Advantages and Disadvantages of Different Column Types for Speciation Analysis by LC-ICP-MS, Spectroscopy, Spectroscopy-11-01-2009, Volume 24, Issue 11.

[56] "Axial piston pump labeled" by Michael Fray CC BY SA 3.0

[57] https://www.thomasnet.com/articles/pumps-valves-accessories/all-about-axial-piston-pumps/ [Accessed: 18 September 2022].

[58] Apostol, T.M., and Mnatsakanian M.A. (2007), Unwrapping curves from cylinders and cones, American Mathematical Monthly 114(May):388-416.

[59] https://www.knauer.net/Application/Tech%20notes/VTN0022_PEEK-Pulsedamper_P2.1L_Final.pdf [Accessed: 18 September 2022].

[60] https://www.phys.uconn.edu/~gibson/Notes/Section5_2/Sec5_2.htm [Accessed: 18 September 2022].

[61] https://www.balseal.com/breaking-the-barrier/ [Accessed: 18 September 2022].

[62] https://www.pumpsandsystems.com/reciprocating-pumps-vs-multi-stage-centrifugal-pumps [Accessed: 18 September 2022].

[63] https://tovatech.com/flow-meters [Accessed: 18 September 2022].

[64] https://www.biotechfluidics.com/products-sensors-flowmeter/ [Accessed: 18 September 2022].

[65] Farooq Wahab M., Dasgupta P.K., Kadjo A.F., Armstrong D.W., (2016) Sampling frequency, response times and embedded signal filtration in fast, high efficiency liquid chromatography: A tutorial, Analytica Chimica Acta, 907:31-44.

[66] https://www.agilent.com/cs/library/support/documents/FAQ_Approved_PDF_Template_enough_datapoints.pdf [Accessed: 14 September 2022].

[67] https://www.edinst.com/blog/the-beer-lambert-law/ [Accessed: 16 September 2022].

[68] Lam H. (2004), Performance Verification of HPLC. In Chan C.C., Lam H., Lee Y.C. and Zhang X. (editors) Analytical Method Validation and Instrument Performance Verification. Wiley-Interscience. 174-177

[69] https://www.agilent.com/cs/library/usermanuals/public/G7110-G7111-G5654-Iso-Quat-Pumps_UseMa-en-SD-29000225.pdf p39 [Accessed: 19 September 2022].

[70] http://www.speciation.net/Database/Instruments/Dionex-Corporation/GP50IP25-Pump-Series-;i719 [Accessed: 19 September 2022].

[71] https://assets.thermofisher.com/TFS-Assets/CMD/Specification-Sheets/PS-70108-LC-Dionex-UltiMate-3000-Pumps-PS70108-EN.pdf p7 [Accessed: 19 September 2022].

[72] https://www.waters.com/webassets/cms/library/docs/720000336en.pdf [Accessed: 19 September 2022].

[73] https://www.uv.es/coque/Mechanism_of_retention_Amsterdam/Slides_Amsterdam_5.pdf [Accessed: 18 September 2022].

[74] https://www.oiml.org/en/files/pdf_r/r112-e94.pdf [Accessed: 02 October 2022].

Appendix A - Swash plate pump and Portable HPLC technical specification.

Table A1 – Swash plate pump specifications

Type	***Specification***	***Comments***
Dimensions	175 x 74 x 50 mm (L x W x H)	Excluding outlet manifold.
Weight	979 g	
Hydraulic System	Frequency modulated dual piston in parallel	
Wetted Materials	PTFE, PEEK, sapphire, ruby, UHMW-PE	
Flow Range	0.1 - 2 ml/min	Tested range.
Flow Precision	≤ 0.08 % RSD	Based on retention time at constant room temperature.
Flow Accuracy	0.9% typical; up to 1.7 %	
Pressure Range	Up to 200 bar	Tested range.
Pressure Ripple	< 1.5 % amplitude	

Table A2 – Portable HPLC specifications

Type	***Specification***	***Comments***
Dimensions	560 x 350 x 230 mm (H x W x L)	
Weight	< 15 kg	Including pump and mobile phase.
Compatible Separation Modes	Isocratic separations using normal and reverse phase, ion pair and ion exchange modes.	Reverse phase demonstrated.
Detector		
Wavelength	255 nm	Tested range.
Drift	≤ 3.97×10^{-4} AU/h	
Noise	ST: ≤ 203×10^{-6} LT: ≤ 43.8×10^{-6}	Tested range.
Upper linear absorbance limit	1.3 AU	Based on Toluene.

Appendix B – Swash plate pump and Portable HPLC serial commands.

Table B1 – Swash plate pump serial commands.

Command	***Description***
ponn	Start pumping
poff	Stop pumping
home	Move swash plate to home position
finc	Increase flow rate by 10µL/min
fdec	Decrease flow rate by 10 µL/min
reboot	Reboot pump control board
#m	Swash plate velocity mode (#ms sinusoidal; #mc constant)
#f	Direct flow rate adjustment (#f1500 for 1.5 ml/min)
#t	Step time on adjustment (#t100 for 100 µs time on)

Table B2 – Portable HPLC serial commands.

Command	***Description***
init	Turn on LED and start pump
stop	Turn off LED and stop pump
run	Performs inject command and starts data acquisition.
end	Stops data acquisition and returns to initial state.
acqon	Manually start data acquisition
acqoff	Manually stop data acquisition
acqdisp	Toggle serial output of live data
#a	Set acquisition time in minutes (e.g. #a12)
#i	Inject command sent to injection valve
#z	Zeroes the detector when using absorbance
?t	Returns system time
Will also directly accept pump commands such as *ponn* and *poff* and *#f*	

Appendix C - Benchtop HPLC separations.

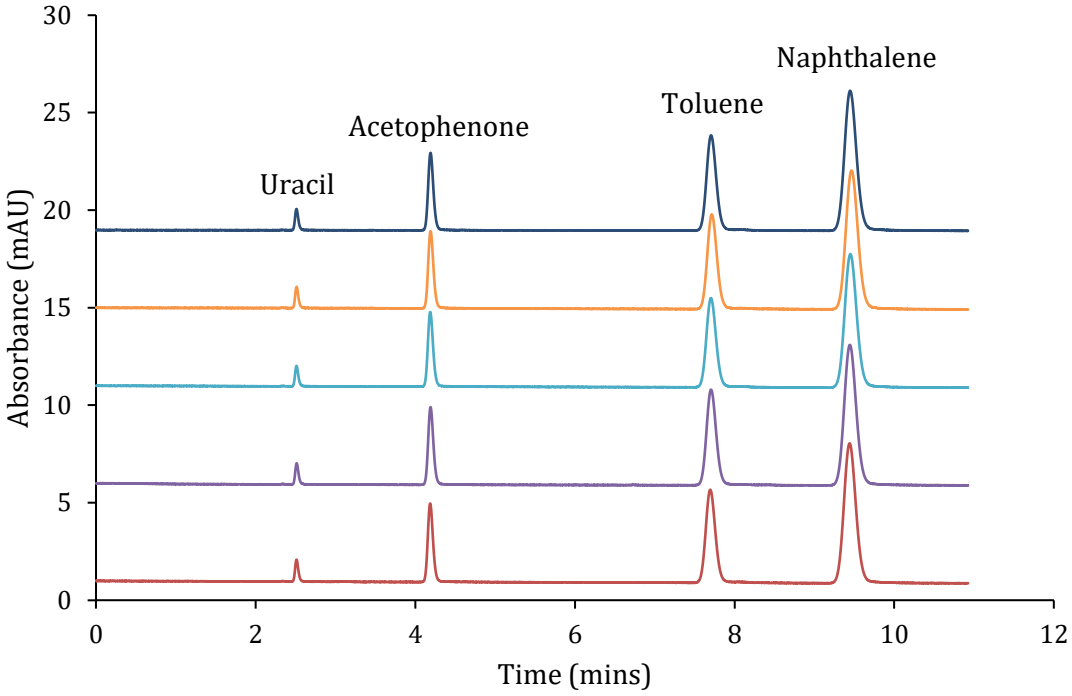

Figure C1 – An example of early separations carried out on a Dionex Ultimate 3000 benchtop HPLC consisting of an LPG-3400M pump and VWD-3400RS detector. Separation conditions: Column C18 250 x 4.6 5µm particle size, Isocratic 60:40 Acetonitrile:DI Water Flow rate 1 ml/min, Injection volume 1µL, Detection UV at 255 nm.

Average baseline noise was taken from the first 10 seconds of the chromatograms above was calculated to be 2.04×10^{-5} AU.

Appendix D - Swash plate pump assembly.

An exploded view of the swash plate pump assembly.

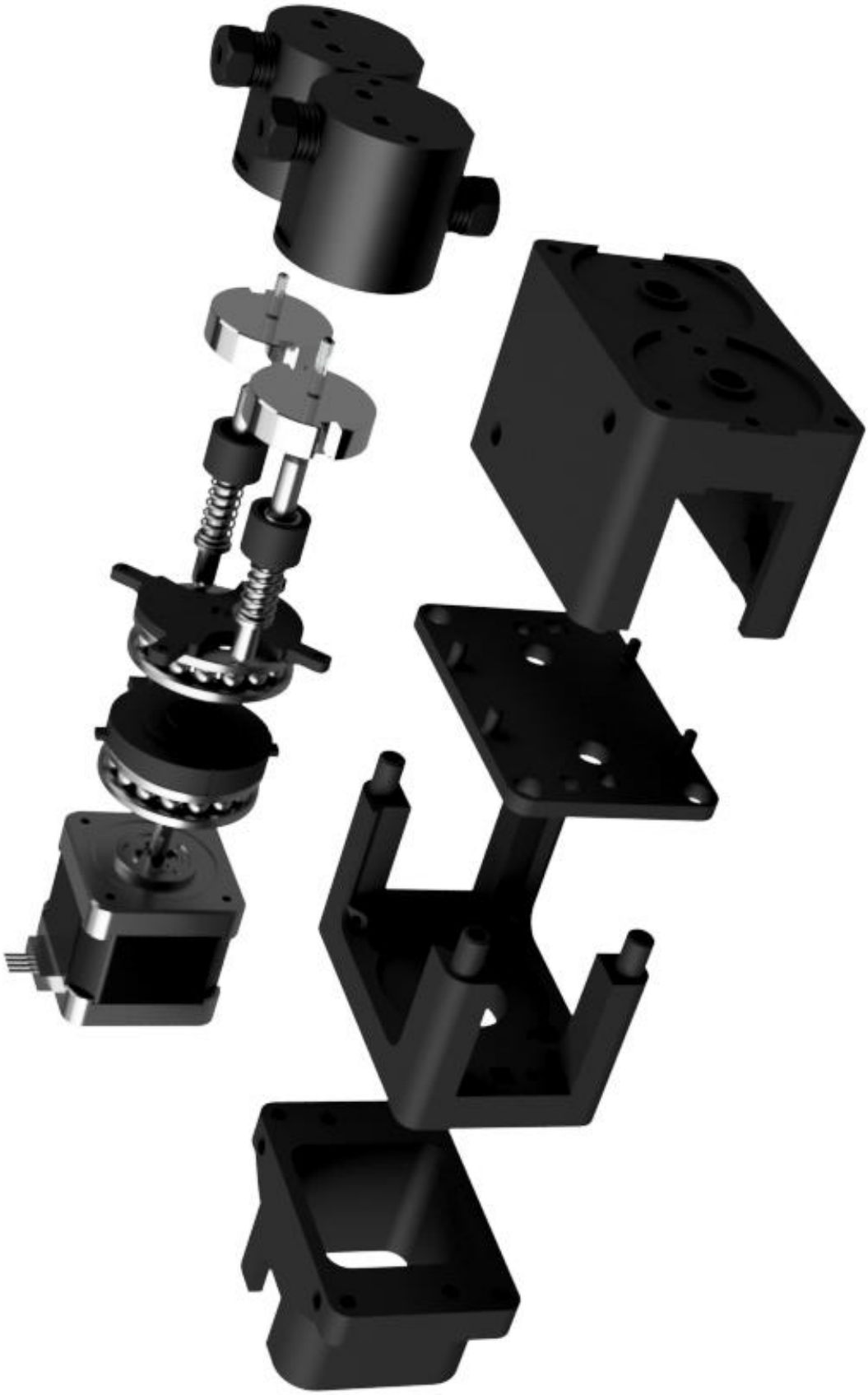

Appendix E - Control circuit schematics.

Control circuit schematic index:

a. Schematic 1 – Swash plate pump control board schematic
b. Schematic 2 – Injection valve control board schematic
c. Schematic 3 – Detector control board schematic

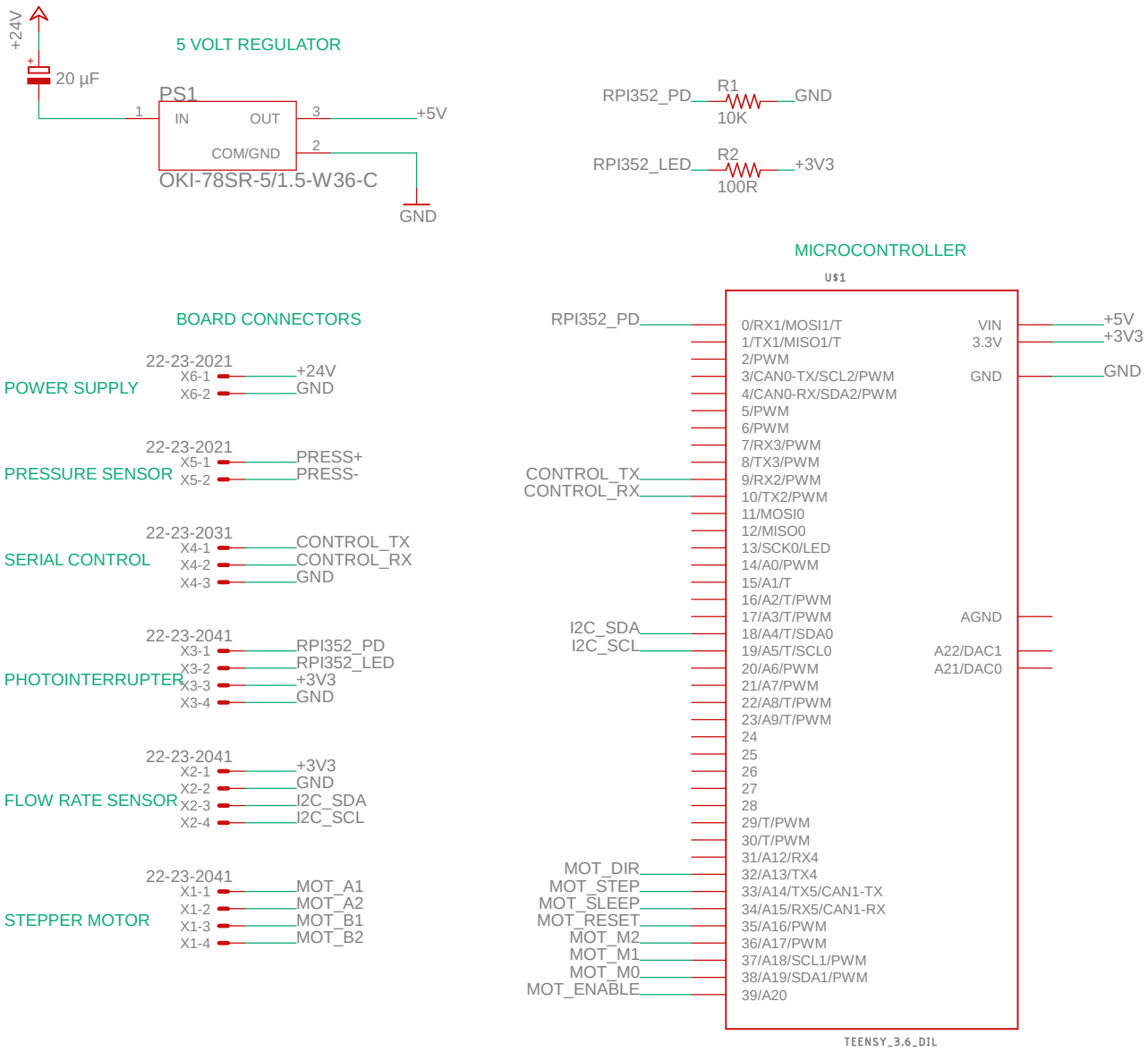

Author: Patrick Roche	
TITLE: Pump_Board_V3	
Document Number:	REV:
Date: 11/10/2022 23:50	Sheet: 1/1

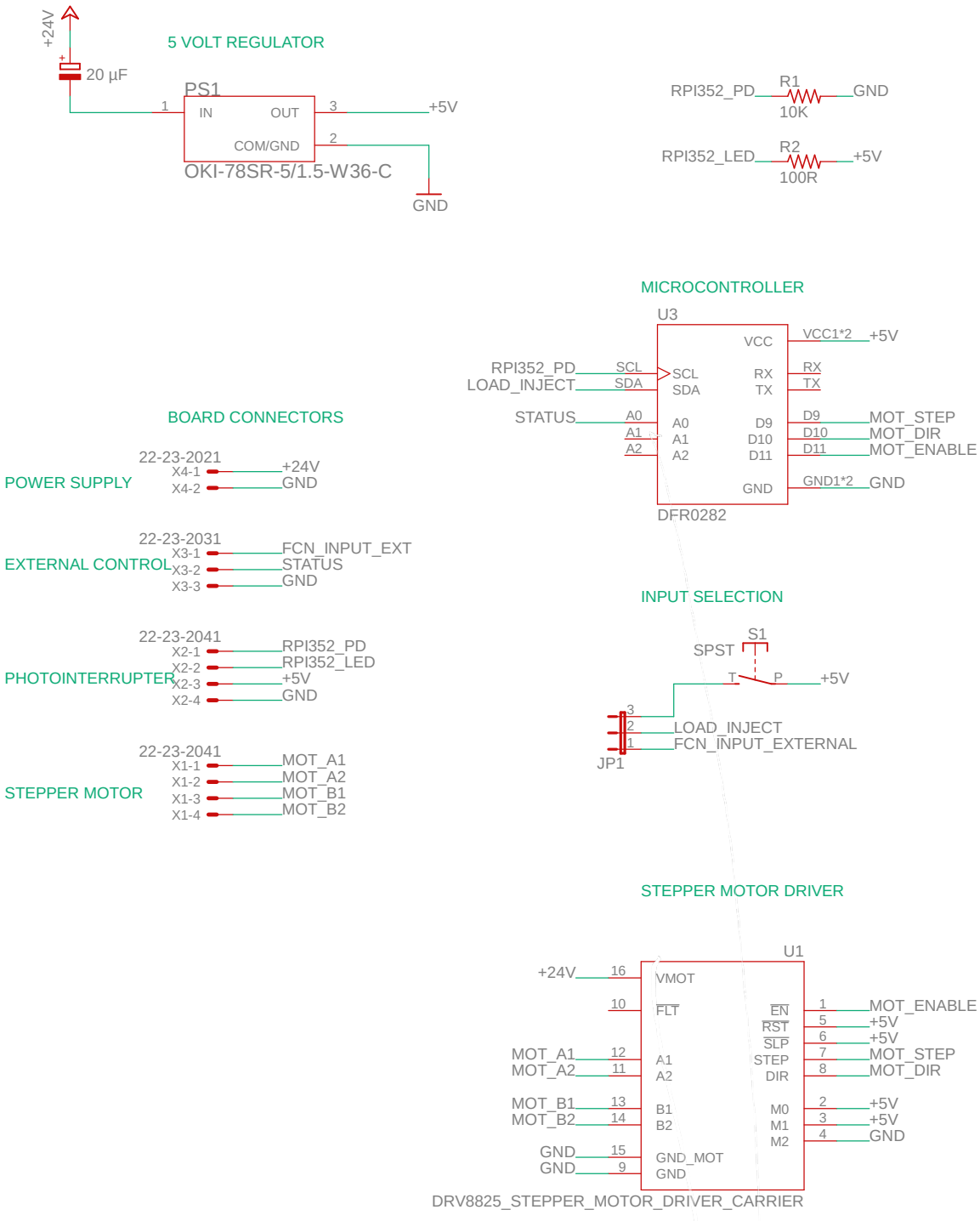

Author: Patrick Roche		
TITLE: Injector_Board_V1		
Document Number:		REV:
Date: 11/10/2022 21:54	Sheet: 1/1	

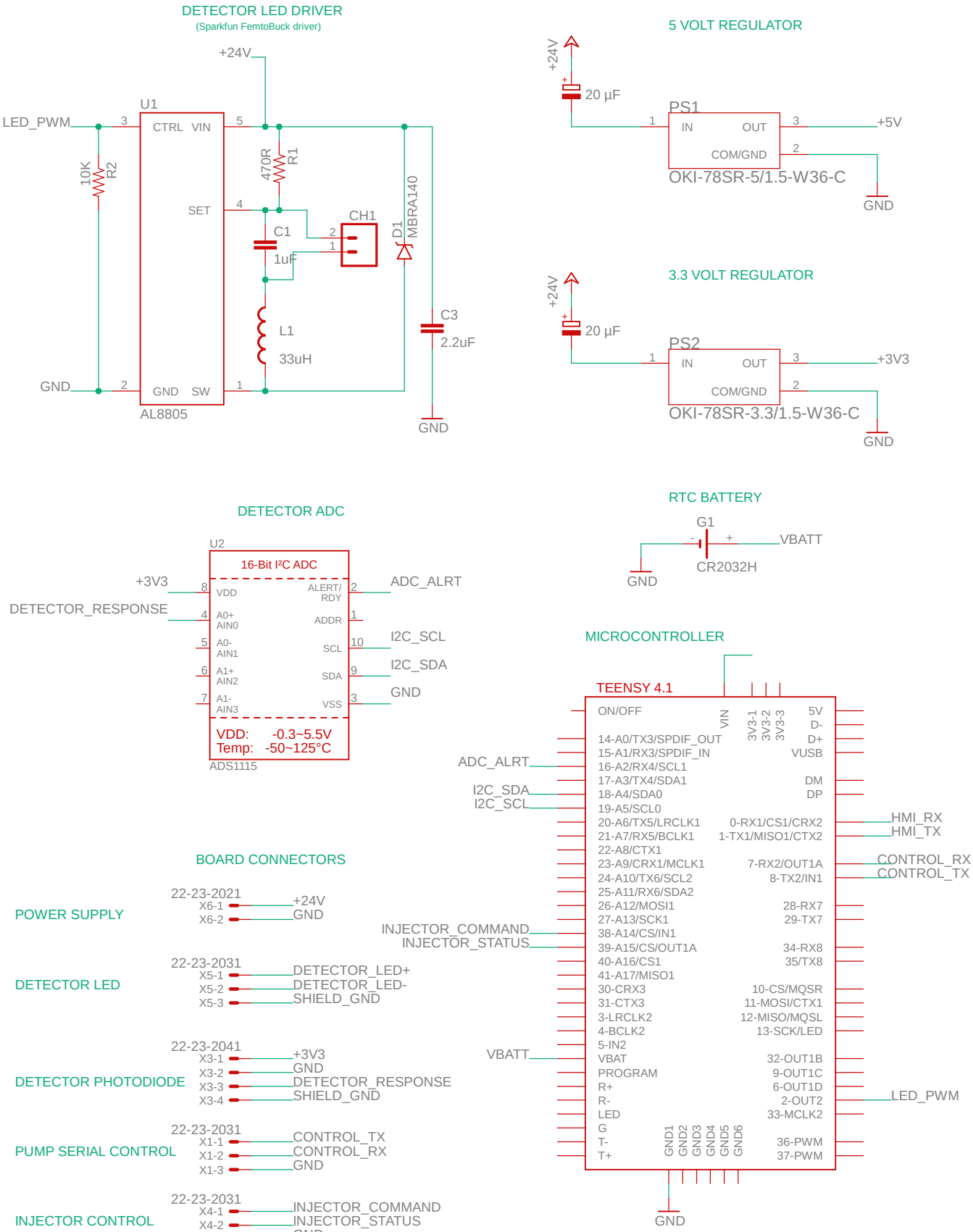

Author: Patrick Roche

TITLE: Detector_Board_V2

Document Number:

REV:

Date: 11/10/2022 23:48

Sheet: 1/1